CORE
Metadata, citation and similar papers at core.ac.uk
Provided by University of Central Florida (UCF): STARS (Showcase of Text, Archives, Research & Scholarship)

University of Central Florida
STARS

Electronic Theses and Dissertations, 2004-2019

2010

Nonlinear Absorption And Free Carrier Recombination In Direct Gap Semiconductors

Peter D. Olszak
University of Central Florida

 Part of the Electromagnetics and Photonics Commons, and the Optics Commons
Find similar works at: https://stars.library.ucf.edu/etd
University of Central Florida Libraries http://library.ucf.edu

This Doctoral Dissertation (Open Access) is brought to you for free and open access by STARS. It has been accepted for inclusion in Electronic Theses and Dissertations, 2004-2019 by an authorized administrator of STARS. For more information, please contact STARS@ucf.edu.

STARS Citation
Olszak, Peter D., "Nonlinear Absorption And Free Carrier Recombination In Direct Gap Semiconductors" (2010). *Electronic Theses and Dissertations, 2004-2019*. 1654.
https://stars.library.ucf.edu/etd/1654

NONLINEAR ABSORPTION AND FREE CARRIER RECOMBINATION IN DIRECT GAP SEMICONDUCTORS

by

PETER D. OLSZAK
B.S. Worcester Polytechnic Institute, 2001
M.S. University of Central Florida, 2003

A dissertation submitted in partial fulfillment of the requirements
for the degree of the Doctor of Philosophy
in the College of Optics and Photonics
at the University of Central Florida
Orlando, Florida

Fall Term
2010

Major Professor: David J. Hagan
Major Professor: Eric W. Van Stryland

© 2010 Peter D. Olszak

This dissertation is dedicated to my family

who has given me patience, support and love throughout these years.

ABSTRACT

Nonlinear absorption of Indium Antimonide (InSb) has been studied for many years, yet due to the complexity of absorption mechanisms and experimental difficulties in the infrared, this is still a subject of research. Although measurements have been made in the past, a consistent model that worked for both picosecond and nanosecond pulse widths had not been demonstrated. In this project, temperature dependent two-photon (2PA) and free carrier absorption (FCA) spectra of InSb are measured using femtosecond, picosecond, and nanosecond IR sources. The 2PA spectrum is measured at room temperature with femtosecond pulses, and the temperature dependence of 2PA and FCA is measured at 10.6μm using a nanosecond CO_2 laser giving results consistent with the temperature dependent measurements at several wavelengths made with a tunable picosecond system. Measurements over this substantial range of pulse widths give results for FCA and 2PA consistent with a recent theoretical model for FCA. While the FCA cross section has been generally accepted in the past to be a constant for the temperatures and wavelengths used in this study, this model predicts that it varies significantly with temperature as well as wavelength. Additionally, the results for 2PA are consistent with the band gap scaling (Eg^{-3}) predicted by a simple two parabolic band model. Using nanosecond pulses from a CO_2 laser enables the recombination rates to be determined through nonlinear transmittance measurements. Three-photon absorption is also observed in InSb for photon energies below the 2PA band edge. Prior to this work, data on three-photon absorption (3PA) in semiconductors was scarce and most experiments were performed over narrow spectral ranges,

making comparison to the available theoretical models difficult. There was also disagreement between the theoretical results generated by different models, primarily in the spectral behavior. Therefore, we studied the band gap scaling and spectra of 3PA in several semiconductors by the Z-scan technique. The 3PA coefficient is found to vary as (Eg^{-7}), as predicted by the scaling rules of simple two parabolic band models. The spectral behavior, which is considerably more complex than for 2PA, is found to agree well with a recently published theory based on a four-band model.

ACKNOWLEDGMENTS

Thanks to my advisors, it has been a privilege to work with you. Thank you for your steady guidance and insightful suggestions, your advice has been invaluable to my education.

"If I have seen further it is only by standing on the shoulders of giants."- Isaac Newton

Thanks to all my professors for everything you have taught me. My education has been a wonderful mosaic created by many skilled artists to whom I owe great gratitude.

"Teaching should be such that what is offered is perceived as a valuable gift and not as a hard duty."- Albert Einstein

Thanks to my classmates for all the late night study sessions and pleasant arguments over homework problems.

"Thus the duty of the man who investigates the writings of scientists, if learning the truth is his goal, is to make himself an enemy of all that he reads, and, applying his mind to the core and margins of its content, attack it from every side. He should also suspect himself as he performs his critical examination of it, so that he may avoid falling into either prejudice or leniency."- Alhazen

Thanks to my friends and family for being there when I have needed a kind word or a helping hand. Life is not easy but it is easier when you have good friends. My fondest memories are of the times I have shared with the ones I love.

"Dost thou love life? Then do not squander time for that is the stuff life is made of."- Benjamin Franklin

Thanks to the One. "Let there be Light"- Genesis 1:3

TABLE OF CONTENTS

LIST OF FIGURES

LIST OF TABLES

CHAPTER 1. INTRODUCTION

1.1 Motivation and Background

The general motivation of this research and objective of the subsequent experiments is to improve upon the understanding of nonlinear optical effects in semiconductors. More specifically, the purpose of this dissertation is to investigate the spectral and thermal dependence of nonlinear absorption and carrier recombination in the narrow band gap semiconductor Indium Antimonide (InSb) as well as the spectral and band gap dependence of three-photon absorption in a series of direct band gap semiconductors. This can only be achieved through the collection of more accurate and comprehensive data than was obtained previously by experiment. Current theoretical models can then be compared to the experimental results through numerical simulation of the data to confirm or to gain further insight for improving these models.

The magnitude of nonlinear absorption [1] and nonlinear refraction [2] in InSb and other narrow band gap semiconductors is of particular interest for passive optical limiting [3]. Optical limiting can be used for many applications such as laser power stabilization or sensor protection [4]. The goal of optical limiting when applied to sensor protection is to prevent transmission of hazardous irradiance or fluence levels while maintaining high transparency at lower input levels [5]. In this way, the sensor is protected from damage without significant reduction in responsivity.

Optical limiting can be achieved through nonlinear absorption, nonlinear refraction, or nonlinear scattering as shown in Fig. 1.1 [6]. Nonlinear absorption includes multiphoton absorption such as two-photon absorption (2PA) which is proportional to the inverse of the band

gap cubed [7-11] or three-photon absorption which is proportional to the inverse of the band gap to the seventh power [9-11], free carrier absorption (FCA for semiconductors) [12, 13], or excited state absorption (ESA for organic molecules) [14]. Nonlinear refraction includes bound electronic nonlinear refraction which is proportional to the inverse of the band gap to the fourth power [8] and free carrier refraction [12].

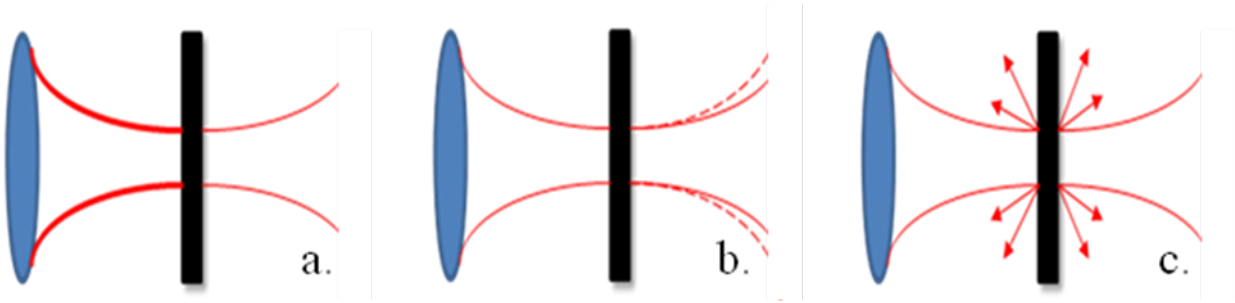

Figure 1.1 Examples of passive optical limiting, where the beam is being focused from left to right, achieved by nonlinear (a) absorption, (b) refraction, and (c) scattering [6].

Nonlinear scattering can include any photoinduced scattering processes, such as stimulated Raman scattering [15] or catastrophic processes, like plasma generation and optical breakdown [16]. It is desirable for a limiting device to maintain its linear properties after exposure to high irradiance. Therefore, nonlinear scattering is more useful for the performance of liquid limiters; however, the damage threshold of a solid limiter is sometimes determined through observation of an abrupt increase in scattering loss, resulting in a permanent change in transmittance [3, 16, 17]. The scattering induced by damage can also be observed by using a Helium-Neon (HeNe) laser or diode laser focused on the same spot on the sample. Laser induced damage in dielectrics is sometimes assisted through self focusing in materials with a positive nonlinear refractive index [18]. The sign of nonlinear refraction is determined by the

dispersion of the bound electronic nonlinear refraction, which is related to the two-photon absorption (2PA) and other 3rd-order "instantaneous" nonlinear absorption mechanisms (electronic Raman and AC Stark) through Kramers-Kronig relations [15]. The spectral function of two-photon absorption (F_2 ($\hbar\omega/E_g$)) and refraction (G_2 ($\hbar\omega/E_g$)) can be isolated so that experimental data for different materials can be collectively compared to theory. Both 2PA and nonlinear refraction in semiconductors have been thoroughly investigated as shown in Fig. 1.2 [8].

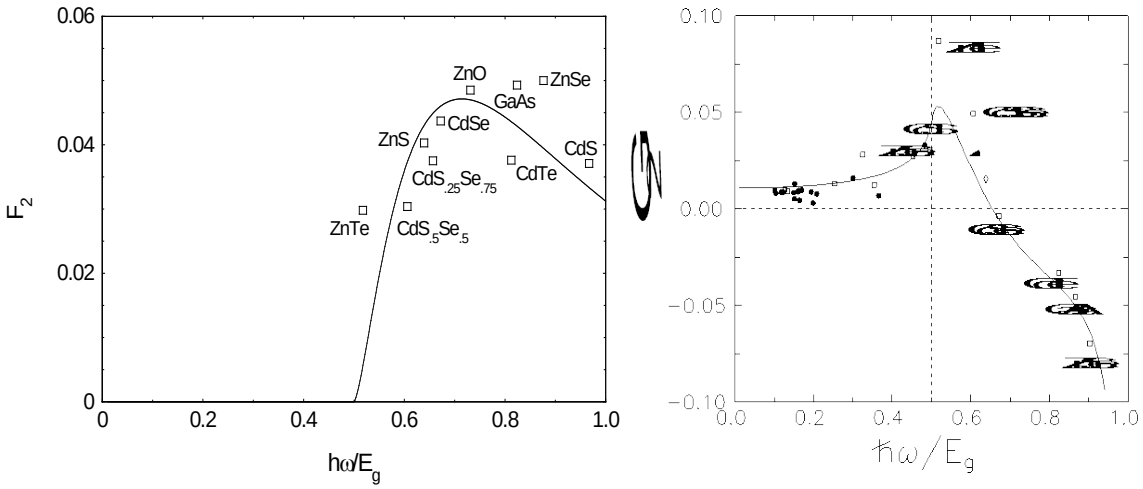

Figure 1.2 (a) Two-photon absorption spectral function, and (b) Dispersion of nonlinear refraction The spectral functions F2 and G2 are unitless functions that depend on the ratio of the photon and bandgap energy. [8].

Self-protecting semiconductor optical limiters have been demonstrated where nonlinear refraction prevents bulk damage so that surface damage is observed before bulk damage [20]. The front surface can be moved further from focus to help prevent surface damage. Since the thickness of a sample can be arbitrarily large, the damage threshold can be increased using

thicker samples. It has also been shown that for negative nonlinear refraction, the best performance or lowest limiting threshold is achieved when focusing on the back surface [16]. Another approach for preventing laser damage of the optical limiter is to use more than one limiter in tandem where each one of increasing optical density protects the following limiter from damage and all the elements are positioned so that they reach the damage fluence simultaneously as shown in Fig 1.3.a [24].

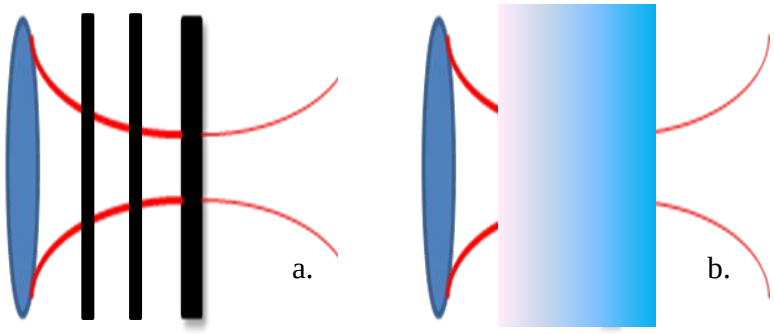

Figure 1.3 a. Cascaded optical limiter geometry, b. gradient density optical limiting

An infinite number of tandem limiters is equivalent to a single thick limiter with a graded optical density as shown in Fig 1.3.b [25]. Since the damage threshold is usually defined by the maximum fluence [J/cm^2], a graded density limiter is optimized when the increase in fluence due to focusing balances the decrease in fluence due to absorption (neglecting nonlinear refraction) [26].

The band gap energy of a semiconductor determines the 2PA edge. The performance of an ideal optical limiter has been compared to the theoretical transmittance of a two-photon absorber as shown in Fig. 1.4 [4]. The spectral region between the band gap $E_g/2$ and E_g allows for high linear transmittance (especially if the material is intrinsic and AR coated) while 2PA and nonlinear refraction can be utilized for optical limiting. Therefore, a semiconductor can be matched to a particular spectral range; for example, InSb is well suited for sensor protection in the mid-infrared spectral region from 7 to 14 microns [2, 5]. In practice, 2PA is not usually the dominant limiting process for InSb with pulses longer than a nanosecond [2, 19]. Free carriers produced through 2PA contribute to and often dominate the nonlinear absorption and refraction, depending on the pulse width [2, 19, 20]. The model is further complicated when the recombination lifetime of the free carriers is comparable to the lifetime of the pulse [2, 19].

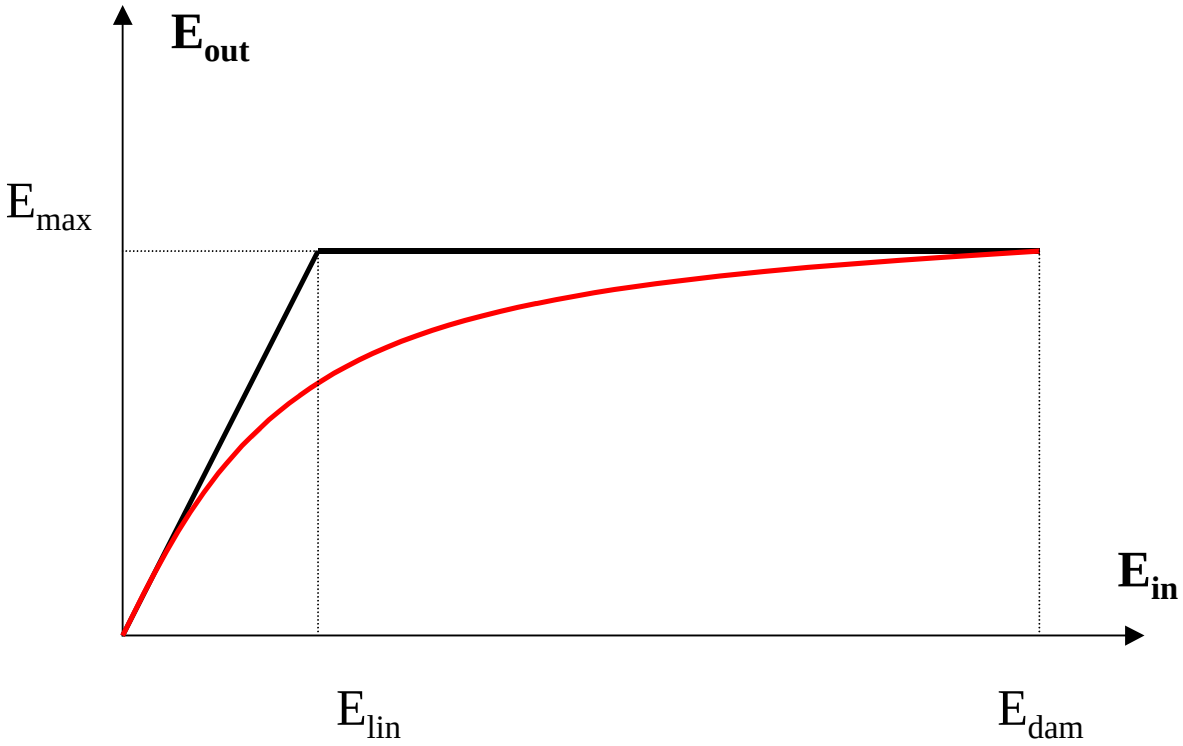

Figure 1.4 Output vs. input energy for an ideal (black) and a realistic (red) optical limiter [4].

The room temperature value of the 2PA coefficient for InSb has been the subject of controversy and the reported values have varied by almost two orders of magnitude [1]. A plot of these reported values as a function of year published in the literature is shown in Fig. 1.5. The mean of these reported values is 6.3 cm/MW and standard deviation 5.3 cm/MW, although if the outlier (point C = 0.2 cm/MW) is ignored the range of values is one order of magnitude with a mean of 6.9 cm/MW and standard deviation 5.2 cm/MW. This large variance in values is presumably due to significant effects from free carrier absorption and refraction [2]. For example, it is possible for the detector to slightly aperture the beam and loss due to nonlinear refraction can be mistakenly attributed to nonlinear absorption. Other difficulties associated with these measurements in the mid-infrared wavelength regime include the availability of detectors

with high sensitivities and low noise, alignment issues, and beam quality, both spatially and temporally. Recent advances such as tunable infrared ultrafast sources and the development of pyroelectric cameras for alignment have enabled more recent work in this area [3].

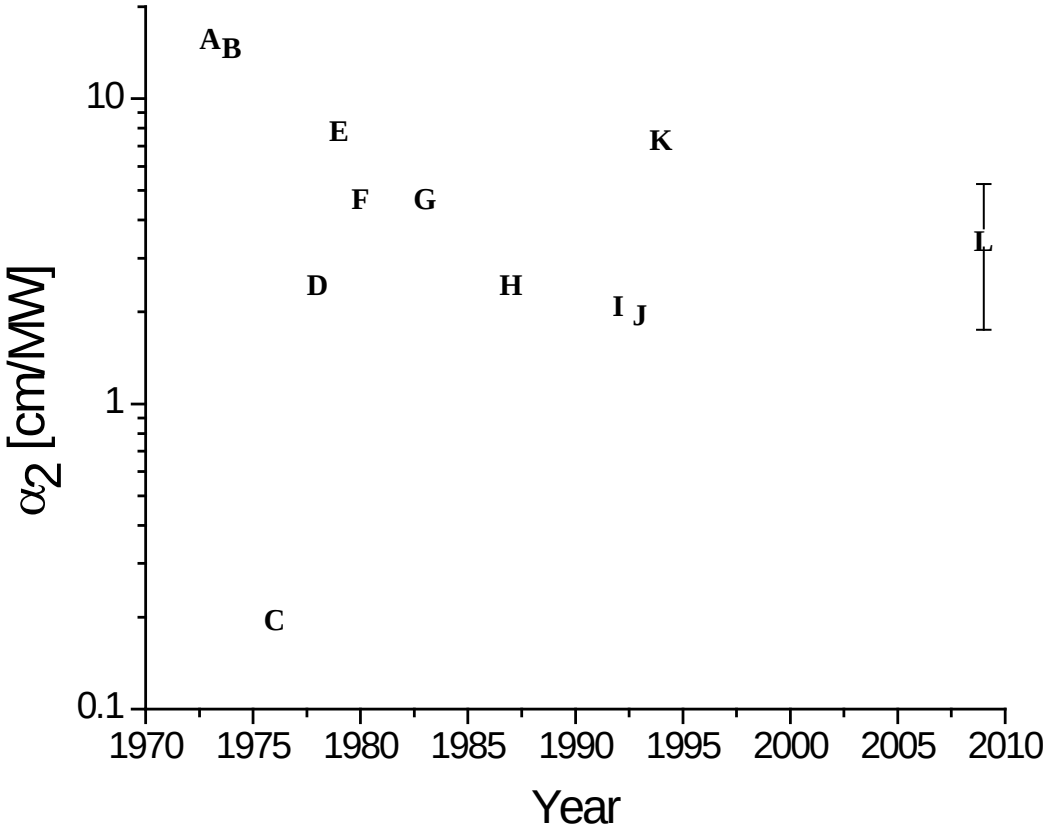

Figure 1.5 Reported values for the 2PA rate at 10.6 μm in InSb at 300K vs. year reported (A) Doviak [27], (B) Lee [28], (C) Gibson [29], (D) Dempsey [30], (E) Miller [31], (F) Johnson [32], (G) Kar [33], (H) Sheik-Bahae [34], (I) Kang [35], J Murdin [36], (K) Smith [37], (L) Olszak [38].

While 2PA has been studied extensively in semiconductors, much less is known about 3PA. Three-photon absorption is less well understood partly due to the increased level of difficulty in measuring, and partly because the process is theoretically more complex [9, 10, 21].

Although 3PA in InSb has been previously reported, a strongly n-type doped sample was used so that the band gap was Burstein-shifted to be larger than the 2PA energy [1]. In this work the band gap of an undoped InSb sample is controlled by cooling the sample and measurements are made at various wavelengths with different pulse widths. In order to compare these results with theory, it was first necessary to test existing theory through femtosecond measurements of 3PA in a number of direct gap semiconductors as was done for 2PA [7] to verify the predicted band gap and wavelength scaling. These measurements verify the predicted band gap scaling but raise some questions about the spectral scaling [22]. The existing theory was then adapted by including four bands in the model instead of only two leading to improved agreement with data for the 3PA spectrum [23].

1.2 Dissertation Statement

In this work the temperature and spectral dependence of nonlinear absorption and recombination in InSb are investigated. The irradiance is varied while the sample temperature is controlled in order to explore the temperature dependant nonlinear transmission. The 2PA and FCA spectrum is measured at room temperature, and the temperature dependence of 2PA and FCA is also investigated. A complementary investigation of three photon absorption (3PA) in a range of direct gap semiconductors confirms theoretical predictions, and 3PA measurements in InSb are compared to this theory. 3PA is measured at wavelengths and temperatures beyond the two-photon band edge where 2PA is not allowed due to energy conservation. Since the fitting parameters depend on temperature, knowing the temperature dependence of each parameter is crucial when modeling absorption and/or recombination at different temperatures. A more complete understanding of nonlinear optical effects in semiconductors can therefore be obtained

by comparing experimental transmission data taken at various temperatures with propagation simulations including the interdependence and temperature dependence of fitting parameters. With high incident laser energy, the absorption and recombination coefficients will determine the change in sample temperature. This last effect is outside the scope of this work; however, as will be discussed in the conclusion of this work, a complete model including laser heating would first require accurate knowledge of the temperature dependent coefficients.

1.3 Dissertation Outline

This dissertation is structured according to the following format. This chapter provides the motivation for this work and introduces the background information necessary for understanding the historical context and applications for this work. In particular, the use of semiconductors (specifically InSb) for the application of infrared optical limiting is explained.

Chapter 2 includes a review of the relevant physics and conceptual foundations for nonlinear absorption and carrier recombination in semiconductors. Examples of previous work on InSb in this area are highlighted. This chapter also describes the experimental apparatus and experimental techniques used in this work.

Chapter 3 describes an experimental investigation of nonlinear absorption and recombination in InSb. Two-photon absorption and free carrier absorption in InSb have been the topic of research for many years, yet a study of the full 2PA spectrum at room temperature has not been presented, nor has the temperature dependence of 2PA been thoroughly investigated. In this paper, the nonlinear absorption spectrum of InSb is measured using a combination of tunable ~160 femtosecond, ~10 picosecond, and ~150 nanosecond IR sources along with a cryostat for

controlling the sample temperature, which varies the band gap energy from 0.17 eV to 0.23 eV. Measurements over this substantial range of pulse widths give results that are consistent with the model used to predict the nonlinear optical properties of InSb. Processes included in the model are 2PA followed by free carrier nonlinearities and various recombination mechanisms. Temperature controlled Z-scan and nonlinear transmission measurements yield information on the temperature and spectral dependence of 2PA, FCA, and carrier recombination processes of Shockley Read Hall, spontaneous emission, and Auger. The observation of a temperature dependence of the FCA as recently predicted is important in our analysis. Only by taking this into account, do we find a quantitative agreement for the nonlinear response. Additionally, results for 2PA are consistent with the scaling rules of a simple two parabolic band model. Nonlinear transmittance measurements using nanosecond pulses from a CO_2 laser are modeled including 2PA, FCA and carrier recombination. Three-photon absorption (coefficient of 0.025 cm^3/GW^2) is also observed in InSb for photon energies below the 2PA band edge using picosecond pulses.

Chapter 4 discusses multiphoton absorption and describes an experimental investigation of three-photon absorption in direct band gap semiconductors using a tunable femtosecond laser system. During the nonlinear absorption measurements of InSb (discussed in Ch.3) 3PA was observed. By studying three-photon absorption in a large range of band gaps, existing scaling theories can be verified and properly extrapolated to InSb for comparison to experimental results. Another student in our group, Claudiu Cirloganu, recently calculated the degenerate 3PA spectrum of ZnSe using third-order perturbation theory based on a Kane 4-band structure consisting of three valence bands (heavy-hole, light-hole, and split-off) and one conduction band

[23]. This model for zincblende structures accounts for the non-parabolicity of the bands and non-zone-center wave functions. Our experimental 3PA results for ZnSe matched the calculated spectral shape although the predicted values were a factor of ~3.2 smaller than the experimental data for ZnSe. Three photon absorption is shown to be an accurate method of determining the split off energy. Our theoretical value for InSb at 80 K using E_g=0.228 eV is $\alpha_3 \approx 0.012$ cm^3/MW^2 at 12 μm is approximately a factor of 2 smaller than the experimental value of 0.025 cm^3/MW^2.

Chapter 5 concludes the dissertation with a short summary of the work presented and few suggestions for further research.

Chapter References

1. Sheikbahaei, M., P. Mukherjee, and H.S. Kwok, *2-PHOTON AND 3-PHOTON ABSORPTION-COEFFICIENTS OF INSB.* Journal of the Optical Society of America B-Optical Physics, 1986. **3**(3): p. 379-385.

2. Dubikovskiy, V., D.J. Hagan, and E.W. Van Stryland, *Large nonlinear refraction in InSb at 10 mu m and the effects of Auger recombination.* Journal of the Optical Society of America B-Optical Physics, 2008. **25**(2): p. 223-235.

3. Vanstryland, E.W., et al., *OPTICAL LIMITING WITH SEMICONDUCTORS.* Journal of the Optical Society of America B-Optical Physics, 1988. **5**(9): p. 1980-1989.

4. Dubikovskiy, V., *Optical Limiting Numerical Modeling and Experiment*, in *Department of Physics*. 2003, University of Central Florida: Orlando.

5. Sheikbahae, M. and E. Van Stryland, *Optical Nonlinearities in the Transparency Region of Bulk Semiconductors: VII. Applications*, in *Semiconductors and Semimetals*. 1999, Academic Press. p. 307-311.

6. Hagan, D., *Optical Limiting*, in *Handbook of Optics*, M. Bass, Editor. 2001, McGraw-Hill: New York.

7. Vanstryland, E.W., et al., *ENERGY BAND-GAP DEPENDENCE OF 2-PHOTON ABSORPTION.* Optics Letters, 1985. **10**(10): p. 490-492.

8. Sheikbahae, M. and E. Van Stryland, *Optical Nonlinearities in the Transparency Region of Bulk Semiconductors: III. Theory of Bound Electronic Nonlinearities - Two Band Model*, in *Semiconductors and Semimetals*. 1999, Academic Press. p. 271-284.

9. Wherrett, B.S., *SCALING RULES FOR MULTIPHOTON INTERBAND ABSORPTION IN SEMICONDUCTORS.* Journal of the Optical Society of America B-Optical Physics, 1984. **1**(1): p. 67-72.

10. Brandi, H.S. and C.B. Dearaujo, *MULTIPHOTON ABSORPTION-COEFFICIENTS IN SOLIDS - A UNIVERSAL CURVE.* Journal of Physics C-Solid State Physics, 1983. **16**(30): p. 5929-5936.

11. Woodall, M.A., *Nonlinear Absorption Techniques and Measurements in Semiconductors*, in *Department of Physics*. 1985, North Texas State University.

12. Sheikbahae, M. and E. Van Stryland, *Optical Nonlinearities in the Transparency Region of Bulk Semiconductors: V. Free carrier Nonlinearities*, in *Semiconductors and Semimetals*. 1999, Academic Press p. 287-293

13. James, R.B. and D.L. Smith, *THEORY OF NON-LINEAR OPTICAL-ABSORPTION ASSOCIATED WITH FREE CARRIERS IN SEMICONDUCTORS.* Ieee Journal of Quantum Electronics, 1982. **18**(11): p. 1841-1864.

14. Pawlicki, M., et al., *Two-Photon Absorption and the Design of Two-Photon Dyes*. Angewandte Chemie-International Edition, 2009. **48**(18): p. 3244-3266.

15. Butcher, P.N. and D. Cotter, *The Elements of Nonlinear Optics*. Cambridge Studies in Modern Optics. Vol. 9. 1990, Cambridge: University Press

16. Sheikbahae, M., et al., *NONLINEAR REFRACTION AND OPTICAL LIMITING IN THICK MEDIA.* Optical Engineering, 1991. **30**(8): p. 1228-1235.

17. Bartoli, F., et al., *IRREVERSIBLE LASER DAMAGE IN IR DETECTOR MATERIALS.* Journal of the Optical Society of America, 1977. **67**(2): p. 254-254.

18. Soileau, M.J., et al., *LASER-INDUCED DAMAGE AND THE ROLE OF SELF-FOCUSING.* Optical Engineering, 1989. **28**(10): p. 1133-1144.

19. Kang, K., S. Guha, and W. Chen, *Nonlinear absorption and nonlinear refraction in InSb and Hg1-xCdxTe.* SPIE, 1992. **1692**: p. 178-190.

20. Hagan, D.J., et al., *SELF-PROTECTING SEMICONDUCTOR OPTICAL LIMITERS.* Optics Letters, 1988. **13**(4): p. 315-317.

21. Yee, J.H., *3-PHOTON ABSORPTION IN SEMICONDUCTORS.* Physical Review B, 1972. **5**(2): p. 449-&.

22. Olszak, P.D. *Energy band-gap dependence of three-photon absorption in semiconductors*. in *Nonlinear Optics Topical Meeting* 2007. Hawaii: Optical Society od America.

23. Cirloganu, C.M., et al., *Three-photon absorption spectra of zinc blende semiconductors: theory and experiment.* Optics Letters, 2008. **33**(22): p. 2626-2628.

24. Hagan, D.J., *High dynamic range passive optical limiters.* International Journal of Nonlinear Optical Physics, 1993. **2**: p. 483-501.

25. Miles, P.A., *BOTTLENECK OPTICAL LIMITERS - THE OPTIMAL USE OF EXCITED-STATE ABSORBERS.* Applied Optics, 1994. **33**(30): p. 6965-6979.

26. Xia, T.J., et al., *Optimization of optical limiting devices based on excited-state absorption.* Applied Optics, 1997. **36**(18): p. 4110-4122.

27. J. M. Doviak, A. F. Gibson, M. F. Kimitt, A. C. Walker, “Two photon absorption in InSb at 10.6 μm,” J. Phys. C **6**, 593-600 (1973).

28. C. C. Lee, H. Y. Fan, “Two photon absorption and exciton effect for degenerate valence bands,” Phys. Rev. B **9**, 3502-3516 (1974).

29. A. F. Gibson, C. B. Hatch, P. N. Maggs, D. R. Tilley, A. C. Walker, “Two photon absorption in InSb and Ge,” J. Phys. C **9**, 3259-3275 (1976).

30. J. Dempsey, J. Smith, G. D. Holah, A. Miller, “Nonlinear absorption and pulse shaping in InSb,” Opt. Commun. **26**, 265-268 (1978).

31. A. Miller, A. Johnson, J. Dempsey, J. Smith, C.R. Pidgeon, G. D. Holah, “Two photon absorption in InSb and $Hg_{1-x}Cd_xTe$,” J. Phys. C **12**, 4839-4849 (1979).

32. A. M. Johnson, C. R. Pidgeon, J. Dempsey, “Frequency dependence of two photon absorption in InSb and $Hg_{1-x}Cd_xTe$,” Phys. Rev. B **22**, 825-831 (1980).

33. A. K. Kar, J. G. H. Mathew, S. D. Smith, B. Davis, W. Prettl, “Optical bistability in InSb at room temperature with two photon excitation,” Appl. Phys. Lett. **42**, 334-336 (1983).

34. M. Sheik-bahae, T. Rossi, H. S. Kwok, “Frequency dependence of the two-photon absorption coefficient in InSb: tunneling effects,” J. Opt. Soc. Am. B **4**, 1964-1969 (1987).

35. Kang, K., S. Guha, and W. Chen, *Nonlinear absorption and nonlinear refraction in InSb and Hg1-xCdxTe.* SPIE. **1692**: p. 178-190 (1992).

36. B. N. Murdin, C. Merveille, A. K. Kar, C. R. Pidgeon, D. A. Jaroszynski, J. M. Ortega, R. Prazeres, F. Glotin, “Infrared free-electron laser measurement of power limiting by two-photon absorption in InSb,” Opt. Quantun Electron **25**, 171-175 (1993).

37. A. E. Smith, R. G. McDuff, N. R. Heckenberg, “Nonlinear optical parameters for InSb at 10.6 and 9.6 μm with microsecond pulses,” J. Opt. Soc. Am. B **12**, 393-400 (1995).

38. P. D. Olszak, et al., “Spectral and temperature dependence of nonlinear absorption in InSb,” submitted to PRB 2010 to be published.

CHAPTER 2. FUNDAMENTALS OF NONLINEAR ABSORPTION

2.1 Fundamentals of Nonlinear Optics in Semiconductors

The theory of optical properties of semiconductors is based on the foundations of solid-state physics. Since the early 1950's, the details of eigenstates in semiconductors have been elucidated and include energy bands, excitonic levels, impurity and defect levels, densities of states, lifetimes, and symmetries. The dependence of these characteristics on the sample conditions such as temperature and pressure has also been researched. The resulting optical properties of semiconductors can be studied by measuring absorption, reflection, photoconductivity, emission, and photon scattering to name a few techniques [1]. The temperature dependence of the optical properties is due to the linear parameters such as free carrier density, free carrier lifetime, refractive index and band gap energy which are all functions of temperature. Nonlinear coefficients that are dependent on these linear parameters are therefore also dependent on temperature.

Semiconductors are crystalline materials (or sometimes amorphous) with an energy band gap where electron energies are forbidden, although this is true of all solid matter. Electrons with energies above the energy band gap are in the conduction band and electrons below the energy gap are in the valence band. The energy band gap for semiconductors is less than 4 electron Volts (eV), and not significantly greater than the thermal energy 0.0256 eV, so that at room temperature the conductivity increases with temperature. Materials with a larger band gap are called dielectrics or insulators. Metallic conductors have zero band gap and indirect gap materials with a "negative energy gap" where the bottom of the conduction band is below the top

of the valence band are sometimes called semimetals, an example of this is mercury telluride (HgTe) [2].

These bands can usually be approximated as parabolic in k-space and the energy of a carrier in the band $E(k) = \frac{\hbar^2 k^2}{2m^*}$ is related to an effective mass m^*. A simple model includes a single parabolic conduction band and a single parabolic valence band. A more detailed model may include more bands and nonparabolicity of those bands. For example, the Kane model includes four nonparabolic bands including one conduction band and three valence bands given by [3]:

$$\text{conduction band} \qquad E_c = E_g + \frac{\hbar^2 k^2}{2m} + \frac{P^2 k^2}{3}\left(\frac{2}{E_g} + \frac{1}{E_g + \Delta}\right),$$

$$\text{heavy-hole band} \qquad E_{v1} = \frac{\hbar^2 k^2}{2m},$$

$$\text{light-hole band} \qquad E_{v2} = \frac{\hbar^2 k^2}{2m} - \frac{2P^2 k^2}{3E_g},$$

$$\text{and split-off band} \qquad E_c = -\Delta + \frac{\hbar^2 k^2}{2m} - \frac{P^2 k^2}{3(E_g + \Delta)}. \qquad \text{[2-1]}$$

All of which can be approximated by parabolic bands of different effective masses. The band structure of InSb [4] is shown in Figure 2.1.

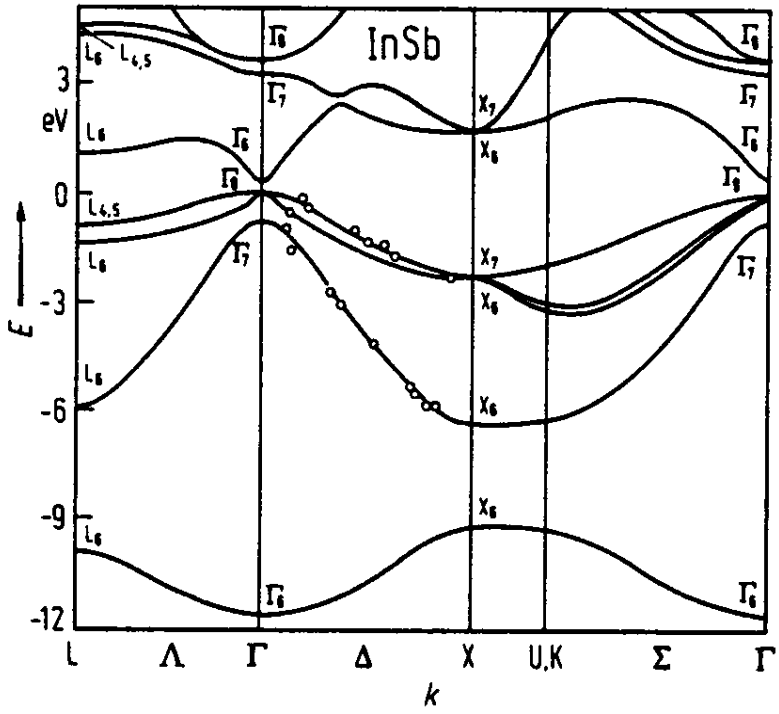

Figure 2.1 Band structure of InSb showing four Kane model bands near the direct gap at the Γ point.

Semiconductors are categorized as direct or indirect gap materials depending on the location of the minimum of the conduction band. If the minimum of the conduction band is directly above the maximum of the valence band then the lowest energy transition is vertical, i.e. direct and therefore not phonon assisted or indirect.

Photons with energy greater than the band gap can excite an electron from the valence band into the conduction band leaving a mobile empty state called a hole in the valence band. Through the generation of phonons, the electron will quickly decay to the lowest available state in the conduction band. The electron can then return to the valence band through stimulated or spontaneous emission of a photon, known as radiative recombination. The electron can also recombine with a hole through simultaneous generation of many phonons or through carrier collisions, resulting in nonradiative recombination where no photons are generated. The

probability of nonradiative recombination is increased by energy levels associated with crystal defects and impurities. Every recombination process is characterized by a recombination rate or its inverse, called carrier lifetime, although sometimes this lifetime depends on the population density.

The density of electrons within an energy interval is given by the product of the density of states with the distribution function that describes the probablility of occupation of electron states. The density of states is defined as the number of states per unit volume in momentum space that results from the volume per state determined by the Uncertainty Principle. Electrons and holes are fermions which are particles that have half integer spin and obey the Pauli Exclusion Principle. The distribution function must satisfy this Pauli Exclusion Principle and therefore the Fermi distribution function is used. For the conduction band, there are few electrons present and it is simpler to consider the occupied states; however, it is simpler to consider the holes (unoccupied states) for the valence band. Electrons in the valence band have a negative charge, but holes have a positive charge. Holes are legitimate particles with real momentum and kinetic energy and can collide with electrons in the valence band and excite them into the valence band through a process called impact ionization [5].

Semiconductor compounds and alloys are formed by the combination of elements with the correct number of valence electrons for chemical bonding. For example, binary semiconductor alloys can be made by combining a group III element with a group V element to make a III-V compound, or group II elements combined with a group VI element make II-VI compounds. Ternary alloys, containing three elements, and quaternary alloys, containing four elements, can be formed from mixtures of binary alloys [6].

The intentional introduction of impurities into a semiconductor is called doping. These impurities can create energy states between the conduction and valence bands. Donors are impurities that have one valence electron more than necessary for chemical bonding with neighboring atoms. The extra electron is weakly bound to the donor atom and creates a donor impurity state below the conduction band. An acceptor is an impurity that has one valence electron less than is necessary with neighboring atoms. The energy of the electron that fills the acceptor state exists slightly above the edge of the valence band, or equivalently holes are weakly bound to acceptors and are easily donated to the valence band. Impurities with electron energies in the middle of the band gap create mid-gap states which increase interband recombination rates. Typical doping concentrations are in the range 10^{15} cm^{-3} to 10^{19} cm^{-3}, which is small compared to the typical atomic density of 10^{22} cm^{-3} [7]. In an undoped (intrinsic) semiconductor, all of the electrons in the conduction band come from the valence band.

The absorption of light in semiconductors is the fundamental mechanism in many optoelectronic applications and devices such as energy measurement in detectors and photovoltaic energy conversion in solar cells. The interaction of light with a semiconductor can involve atomic and lattice properties. Most of the transitions that contribute to the optical properties of semiconductors can be explained by considering that an electron moves through a periodic potential which is the sum of the atomic core potentials. This model describes the conduction and valence bands as well as the band gap. The electron's response to an optical field is described by the simple harmonic oscillator model. This leads to the classical model for electromagnetic polarization response of a material shown in Equation [2-2], for bound electrons this is called the Lorentz model and for free electrons is called the Drude model. When bound electrons are driven by an external field with amplitude E_0 much smaller than the atomic field,

the consequent deviations in position are small and the restoring force is accurately described by Hooks' Law [8]. This is the linear case of low intensity radiation and the potential is assumed to be parabolic with a polarization response $P(\omega)$ described by the linear optical susceptibility $\chi(\omega)$,

$$P(\omega) = \frac{1}{2}\varepsilon_0 \chi(\omega) E_0 \exp^{(-i\omega t)} + C.C. \quad \chi(\omega) = \frac{Ne^2}{\varepsilon_0 m} \cdot \frac{1}{\Omega^2 - 2i\Gamma\omega - \omega^2}, \qquad [2\text{-}2]$$

where ω is the driving frequency, Ω is the resonance frequency, Γ is the damping term, e is the electron charge, N is the number of electrons, m is the electron mass, and ε_0 is the permittivity of free space. This approach works well for obtaining the absorption and refraction in dielectrics and metals; however, the linear absorption of semiconductors are found by the density of states model described earlier also known as the Fermi Golden Rule.

Nonlinear optics pertains to the study of high intensity radiation with matter. For high intensity laser radiation, the displacements are larger and eventually become anharmonic while the potential becomes non-parabolic. The susceptibility may then be expanded in a power series of the electric field in the frequency domain and the polarization takes on an expanded form

$$P = \varepsilon_0 (\chi^{(1)} E + \chi^{(2)} E^2 + \chi^{(3)} E^3 + ...) . \qquad [2\text{-}3]$$

This anharmonic oscillator model was used by Bloembergen in 1965 and Garrett and Robinson in 1966 to estimate the second and third order nonlinear susceptibilities of dielectrics [8]. The second order susceptibility is responsible for the difference frequency generation used in parametric amplification, second harmonic generation, and the well-known Pockels effect used in electro-optic devices. The second order susceptibility is zero in materials with inversion symmetry as are all terms in the expansion that are proportional to even powers of the field. This becomes obvious when one considers that if a material is completely identical in opposite directions then the polarization only changes in sign as the direction of the optical field is

reversed. Therefore, the first nonlinear term in the expansion for materials with inversion symmetry is the third order susceptibility [8]. The third order term in the polarization expansion is responsible for third harmonic generation, optical Kerr effect (intensity-dependent refractive index), stimulated Raman effect, and two-photon absorption, which is the transition that is most central to this research.

2.2 Multi-Photon Absorption

2.2.1 Two-Photon Absorption

The two-photon absorption (2PA) coefficient α_2 (frequently called β in the literature) was shown to be inversely proportional to the third power of the band gap energy E_g as predicted by theory for semiconductors with various band gap energies [9]. This demonstrated that the macroscopic nonlinear coefficients could be determined for other materials at a specific wavelength. The two-photon absorption coefficient dependence on fundamental microscopic material properties is given by the following equation in the two-parabolic-band model

$$\alpha_2 = K\sqrt{E_p}\cdot\frac{1}{n^2 E_g^3}\cdot F_2(2\hbar\omega/E_g). \qquad [2\text{-}4]$$

For the two-parabolic-band model K_{pb}=1940 cm/GW(eV)$^{5/2}$ [10]; however, fitting this material-independent constant to experimental data has given a value of 3100 cm/GW(eV)$^{5/2}$ [11]. The Kane momentum parameter P defines the energy $E_p = 2P^2 m_e/\hbar^2$, which is approximately 21eV for most semiconductors, n is the linear refractive index at frequency ω and the F_2 function for the two-parabolic-band model is given by, $F_2(2\hbar\omega/E_g) = (2\hbar\omega/E_g - 1)^{3/2}/(2\hbar\omega/E_g)^5$ and more complicated spectral functions include the four nonparabolic bands from Kane's model

[10,12]. Previous data for InSb agrees with the predicted band gap scaling within an order of magnitude as shown in Figure 2.1 [13].

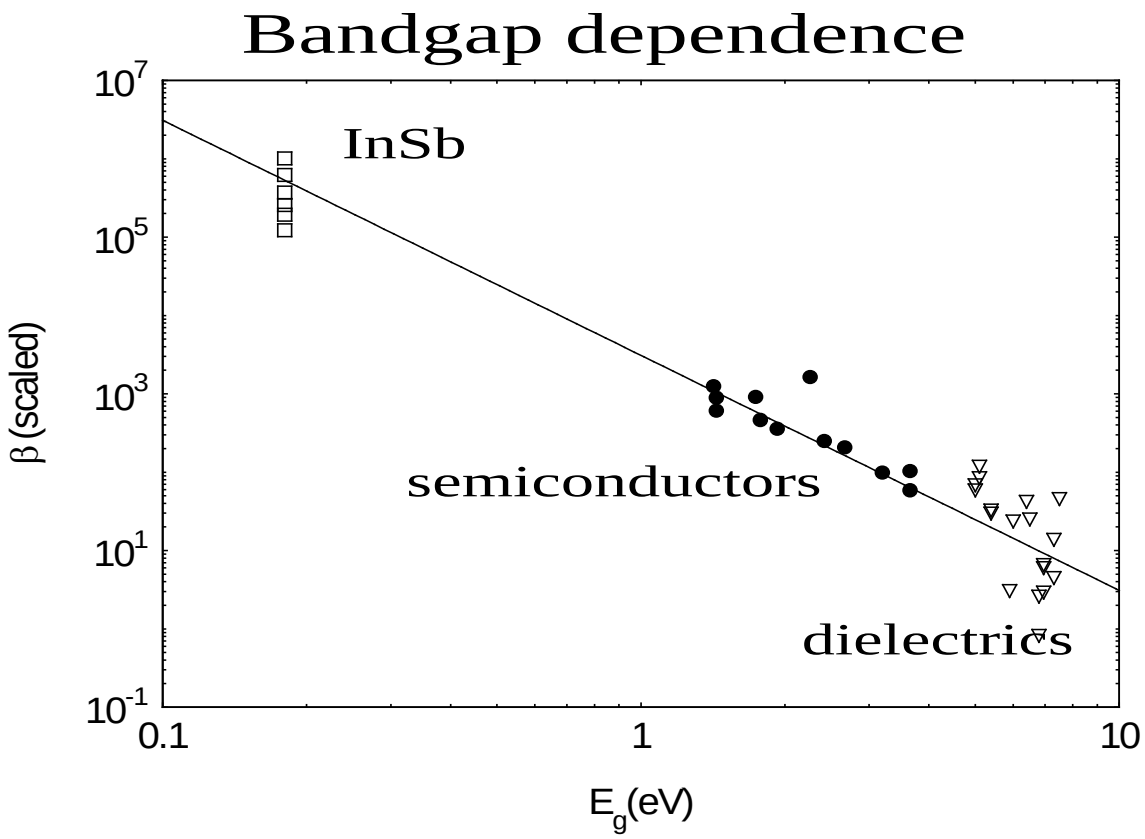

Figure 2.2 Comparison of scaled 2PA theory with reported values vs. Eg [13].

More accurate and comprehensive data and a more detailed model are desired to confirm the agreement of 2PA in InSb with the predicted band gap scaling. The F_2 function has also been defined including nonparabolic bands with spin-orbit splitting being smaller or larger than the band gap and can also be multiplied by an exciton enhancement factor, which becomes most important near the band edge [14]. Multi-photon absorption scaling rules can also be derived for three-photon, four-photon, and the general case of n-photon absorption [15].

In the linear regime, when the absorption as a function of frequency is known, if the interband absorption in a semiconductor is measured, then the corresponding contribution to the refractive index can be calculated using the Kramers-Kronig dispersion relations. These relations are also extremely important to the study of nonlinear spectroscopy. Nonlinear absorption is an induced change in the absorption spectrum, so the refractive index must undergo an induced change from the linear value. The following relation (where c is the speed of light and ω is the optical frequency) can therefore be used to deduce the change in refraction $\Delta n(\omega',I)$ from measured values of the change in absorption spectrum $\Delta\alpha(\omega,I)$:

$$\Delta n(\omega', I) = \frac{c}{\pi}\int_0^\infty d\omega \frac{\Delta\alpha(\omega, I)}{\omega^2 - (\omega')^2}. \qquad [2\text{-}5]$$

It is important to note that these relations are only strictly valid if I(ω) is constant [16]; however, good results can be obtained where the change in absorption (and therefore the integral) is limited to a finite spectral region [17].

Linear absorption can be observed in semiconductors due to interband or intraband absorption. In InSb, the absorption cross section for holes and electrons (σ_p=8.65x10^{-16} cm^2 and σ_n=0.23x10^{-16} cm^2 respectively) was obtained by transmission measurements within a spectral range of 5 to 10 microns at 298K and 78K [18]. Nonlinear free carrier absorption (FCA) due to photogenerated carriers also contributes to the absorption. Free carriers are created through interband absorption in semiconductors and then absorb proportionately to their cross section. For the case of pure 2PA, the change in irradiance is described by the equation:

$$\frac{dI}{dz} = -\beta I^2. \qquad [2\text{-}6]$$

If we consider that the rate of change in the carrier density due to 2PA is described by $\frac{d\Delta N}{dt} = \frac{d\Delta P}{dt} = \frac{\beta I^2}{2\hbar\omega}$, then the former differential equation for the irradiance becomes

$$\frac{dI}{dz} = -\beta I^2 - (\sigma_e N + \sigma_H P) I \,. \qquad [2\text{-}7]$$

This equation describes the nonlinear absorption including 2PA and FCA [19].

The carrier density also changes in time due to radiative and nonradiative recombination of the carriers. After including radiative recombination, we obtain

$$\frac{dN}{dt} = \frac{\alpha_2 I^2}{2\hbar\omega} - B_{rad}(N^2 - N_0^2) \,. \qquad [2\text{-}8]$$

The radiative lifetime has been reported as τ =143 ns for InSb at a temperature of 77K [20]. Linear nonradiative recombination involving collision of carriers with impurities is called Shockley Read Hall recombination and depends on trap density but has been reported to be between 0.1 and 1 microsecond. Nonlinear nonradiative recombination involving the collisional process of creating hot carriers known as Auger recombination can also be observed. After including the Auger process we obtain,

$$\frac{dN}{dt} = \frac{\alpha_2 I^2}{2\hbar\omega} - A_{SRH}(N - N_0) - B_{rad}(N^2 - N_0^2) - C_{Auger} N (N^2 - N_0^2) \,. \qquad [2\text{-}9]$$

The value of N_0, the initial carrier density, is a function of temperature and is described by Fermi-Dirac statistics since the conduction electrons and the valence holes are fermions. The population is often calculated using the Boltzmann approximation

$$f(E) = \frac{1}{1+\exp\left(\frac{E-E_f}{k_B T}\right)} \approx \exp^{-\left(\frac{E-E_f}{k_B T}\right)}. \qquad [2\text{-}10]$$

This approximation works well when the band gap is much larger than the thermal energy. For an intrinsic semiconductor, the concentration is approximately (where k_B is the Boltzmann constant, m_c and m_v are the effective mass of the conduction and valence band) given by

$$N_0(T) = 2\left(\frac{k_B T}{2\pi\hbar^2}\right)^{1.5} (m_c \cdot m_v)^{3/4} e^{\left(\frac{-E_g}{2k_B T}\right)}. \qquad [2\text{-}11]$$

For the specific case of undoped InSb at room temperature (E_g=0.1675 eV), this approximation gives a slightly larger population density $N_0(300K) = 2.12\times10^{16}\,cm^{-3}$ than the exact result $N_0(300K) = 1.95\times10^{16}\,cm^{-3}$ obtained using a Fermi-Dirac distribution. Using a slightly different value for the band gap (E_g=0.18 eV) will lead to a different population density $N_0(300K) = 1.7\times10^{16}\,cm^{-3}$.

The energy band gap is a function of temperature. The band gap energy for InSb is given by an empirical formula known as the Varshni equation (where a, b, and $E_{gap}(0)$ are fitting parameters) having the following form:

$$E_g(T) = E_g(0) - \frac{aT^2}{b+T}. \qquad [2\text{-}12]$$

The value for $E_g(0)$ is generally accepted to be 0.235 eV [21,22]. The most recent fitted values of these coefficients from infrared transmission measurements were $E_g(0)$ =0.235 eV, a=0.00027 eV/K, and b=106 K [21]. Earlier fitted values of these coefficients shown in Fig 2.3 measured

using the two-photon photo-Hall effect were consistent with the empirical relationship of Varshni with $E_g(0)$ =0.235 eV, a=0.0006 eV/K, and b=500 K [22]. When taking into account the effects of the temperature on the sample properties, it becomes important to ensure the beam does not significantly heat the sample enough to change its measured properties.

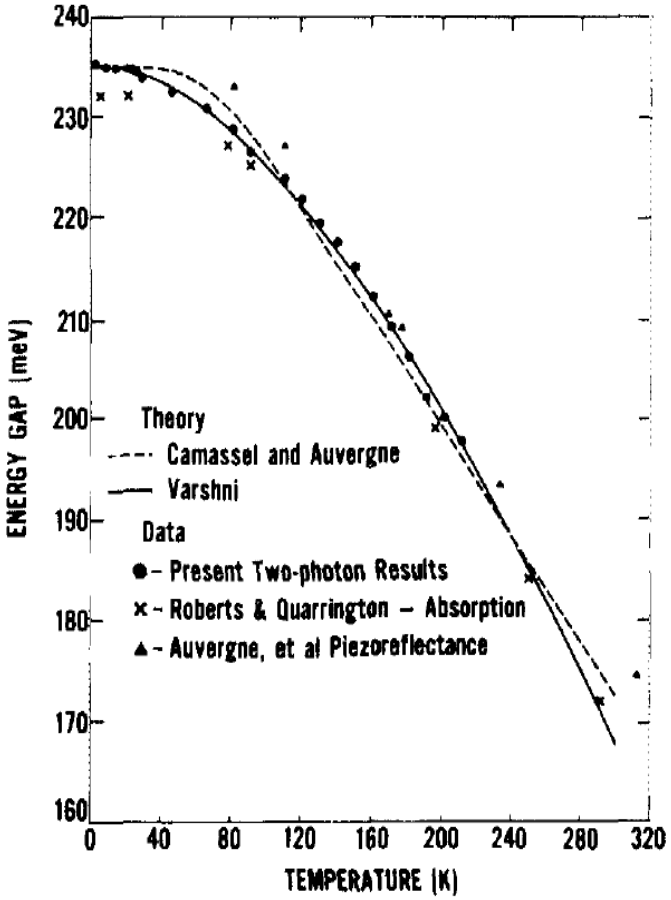

Figure 2.3 Band gap energy vs. temperature for InSb [22].

A diagram of these transitions is shown in Fig. 2.4. The room temperature value of the 2PA coefficient for InSb has been the subject of controversy because the reported values have ranged over two orders of magnitude. In this work the 2PA spectrum of InSb is studied between 80 K and 320 K.

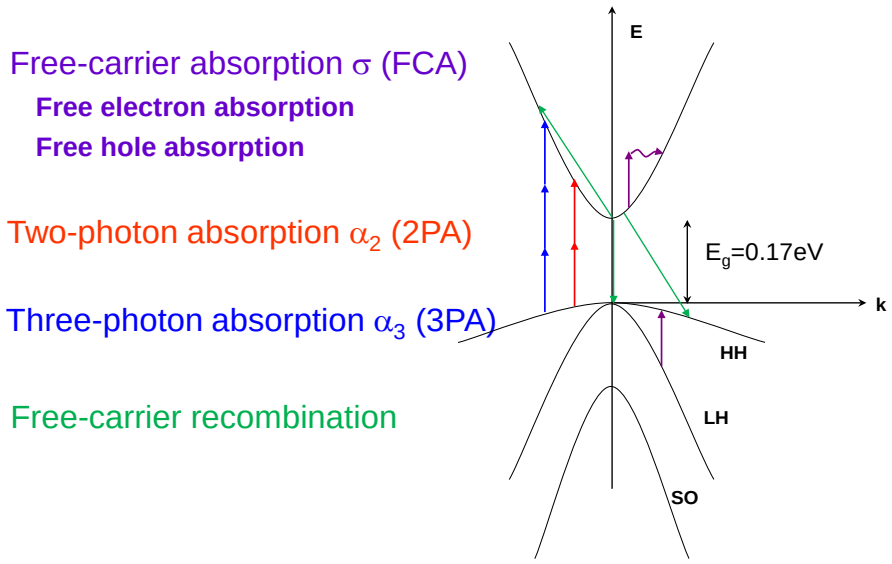

Figure 2.4 Nonlinear transitions between the conduction, heavy-hole, and light-hole bands.

2.2.2 Three-Photon Absorption

The three-photon absorption (3PA) coefficient of InSb was reported as 0.2 cm^3/MW^2 [23]. 2PA has been the subject of research since the 1930's [24] and has been extensively studied in semiconductors, but much less is known about 3PA [25-29]. Three-photon absorption is less understood partly due to its increased level of difficulty to measure in experiments [29] and partly because the process is theoretically more complex [31,32]. Three-photon absorption is expected to scale with E_g^{-7} as predicted by Wherrett's theory with α_3 given by:

$$\alpha_3 = K_3 \frac{\sqrt{E_p^3}}{n^3 E_g^7} \left[\frac{((3\hbar\omega / E_g) - 1)^{1/2}}{(3\hbar\omega / E_g)^9} \right], \qquad [2\text{-}13]$$

where K_3 is a constant, n is the refractive index, and $E_p \approx 21$eV is the Kane momentum parameter.

In order to study 3PA in semiconductors, it is important to use wavelengths corresponding to $E_g/3 < \hbar\omega < E_g/2$, therefore allowing 3PA and not 2PA. The values measured at 1064 nm on other samples were obtained more than twenty years ago but were not previously published due to concerns about the effects of carrier nonlinearities [33]. The spectral function F_3 (given by the bracketed portion of Eq. 2) suggested by Wherrett is different from the F_3 suggested by Brandi and de Araujo [16, 26]. (The essential difference between these two theories will be explained in Chapter 4.) Without data on the spectrum of 3PA, it is difficult to verify any particular theory. It is important to note that although most of the literature on 3PA refers to Wherrett's theory, each use a different arbitrary scaling constant to obtain a theoretical value. Sometimes, a theoretical value is obtained by taking an experimental value and applying the scaling rules to estimate a value for another material, which is essentially applying an

arbitrary scaling factor [27]. For example, InAs was determined to have a theoretical 3PA value of α_3 = 1,800 cm^3/GW^2 [34], but the value predicted by the present work is 11,000 cm^3/GW^2. It was suggested recently that the spectral function of Brandi and de Araujo might show better agreement for "wide" band gap materials [28], but for AlGaAs, the trend of the data from 1500 nm to 1650 nm shows agreement with Wherrett's theory [29]. CdSe was determined to have a theoretical 3PA value of α_3 = 0.05 cm^3/GW^2 [35], but the value predicted by the present work is 0.10 cm^3/GW^2. It should also be noted that in the conclusion of Hasselbeck's work [36], the absorption at 15K observed in InSb was due to leakage 2PA instead of 3PA was partially based on the large magnitude of the value obtained by fitting the data.

Part of the approach of this work was to use many materials to determine a reasonable empirical constant or average scaling factor for 3PA theory. We have measured 3PA in ten binary semiconductors including narrow band gap and wide band gap samples. To the best of the author's knowledge, this work includes the first reported experimental values for 3PA in bulk ZnSe, ZnTe, and CdTe [37]. The scaled 3PA coefficients obtained from experiments are plotted versus band gap energy. The band gap scaling of the 3PA coefficient is found to vary as Eg^{-7} as predicted by Wherrett's theory.

It was previously known that it is likely that transition schemes including other additional factors such as self transitions and additional bands could "easily introduce a factor of four" [15] and thus influence the wavelength dependence of 3PA. Finding the agreement between existing theory and measured 3PA spectrum, our group was motivated to develop a more detailed theory to explain our data. This theory predicts the spectrum of three-photon absorption (3PA) in zincblende semiconductors using Kane's 4-band model. We obtained excellent agreement by

applying this theory to ZnSe and comparing to the 3PA spectrum measured using femtosecond pulses from an optical parametric generator/amplifier system. The spectrum shows the onset of 3PA from the split-off band and also shows quantum interference between the several possible evolution pathways when exciting carriers from valence to conduction band [38]. This will be presented in chapter 4.

2.3 Measurement Techniques

2.3.1 Spectroscopic Ellipsometry

The study of the interaction of light with matter employs a multitude of useful measurement techniques, only a few of which are discussed here. Changes in the intensity of light can be understood by measuring reflectance, transmittance, absorbance, and scattering. Changes in the polarization of light can be studied using polarimetry or ellipsometry. One of the most useful techniques used to measure the linear optical properties of materials is spectroscopic ellipsometry. The optical constants and the Fresnel coefficients can be determined by measuring the change in polarization of light reflected from the sample, which can be generally defined as elliptical. Making this measurement at several angles of incidence close to Brewster's angle to maximize penetration allows the best sensitivity and increases the confidence in values obtained from modeling the data [39]. Spectroscopic ellipsometry is a technique where ellipsometry measurements are made over a broad spectrum, allowing the measured refraction and absorption to be related by the application of Kramers-Kronig relations when modeling the data.

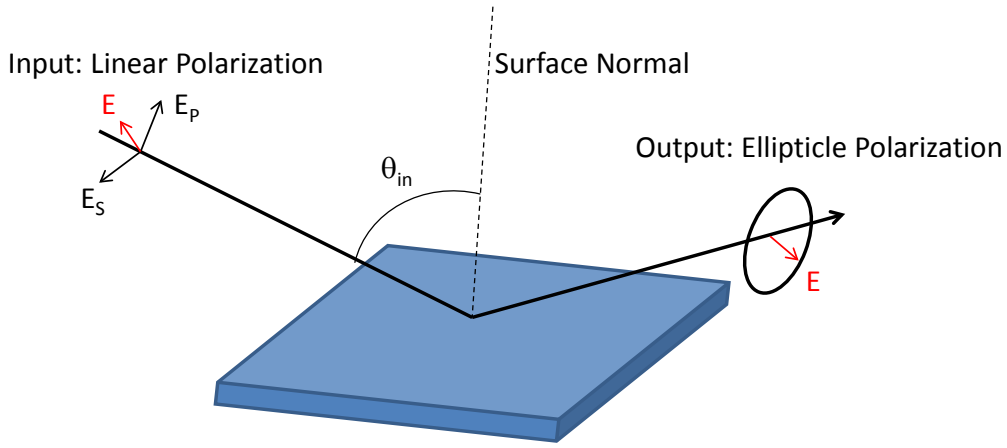

Figure 2.5 Concept of ellipsometric measurement [39].

2.3.2 Nonlinear Transmission

Nonlinear transmission of a sample in the focus of a laser as shown in Fig 2.4 is a very basic way to study nonlinear absorption coefficients. Knowing the spatial and temporal profiles of the input laser pulse in the focus of a lens and the average energy per pulse allows calculation of the irradiance as a function of space and time *I(r,t)*. The absorption of a sample placed in focus can be modeled and compared to the measured transmission of the sample as a function of incident irradiance. An energy detector must be placed behind the sample and a collection lens can be used to help ensure collection of all transmitted energy. A calibrated beam splitter and energy meter is used as a reference to measure the incident energy and a collection lens can be used to help collect all the reflected energy. The sample in focus can be anti-reflection (AR)

coated to reduce or eliminate reflection losses at the front and back surfaces of the sample. The sample can also be mounted in a cryostat to control the sample temperature during a nonlinear transmission measurement. Instead of monitoring only the transmitted energy, it is also useful to measure the transmitted spatial and temporal profiles when possible [40]. For ultrafast pulses, it becomes more difficult to measure the temporal profile after the sample, compared to using a fast detector and oscilloscope with nanosecond pulses. It should be stressed that accurate calibration and excellent collection efficiency are required when doing this experiment.

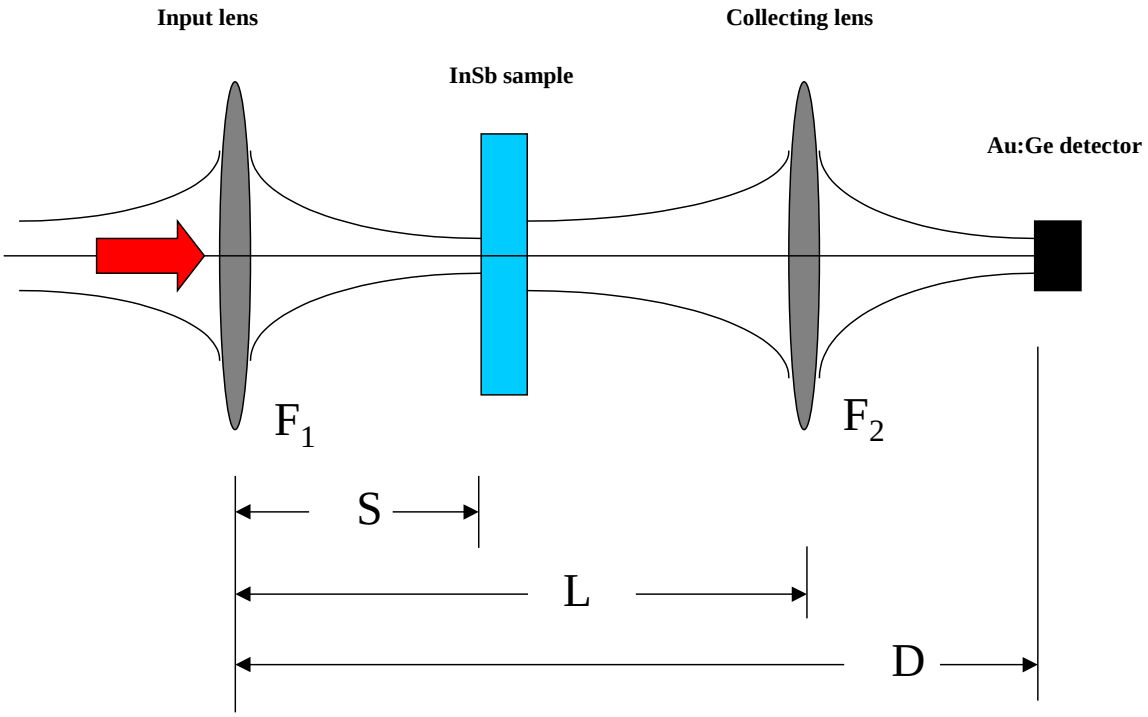

Figure 2.6 Transmission measurement setup with sample fixed at focus [40].

2.3.3 Z-Scan Technique

The Z-scan technique was introduced in 1989 as a simple yet sensitive experiment for measuring nonlinear optical absorption and refraction [41]. Scanning a thin nonlinear sample through the focus of a Gaussian beam, instead of leaving it fixed as in the transmission measurement, allows a variation of incident irradiance without varying the incident energy. When all of the transmitted energy is collected, an open aperture Z-scan is produced and the nonlinear absorption coefficients can be extracted. When an aperture is placed after the sample, a closed aperture Z-scan is produced. The sensitivity to nonlinear phase changes has been demonstrated to be better than $\lambda/100$ (actually nearer to $\lambda/1000$ for a S/N ~1). For semiconductor samples, where nonlinear absorption and refraction are present, the closed aperture data can be divided by the open aperture data to separate and extract the nonlinear refraction. This technique is most accurate when the change in transmission is small.

Many useful variations in the Z-scan experiment have been explored since it was introduced. Reflection Z-scan, Eclipsing Z-scan **(**EZ-scan), and the White Light Continuum (WLC) Z-scan have been some of the many variations. EZ-scan is similar to the closed aperture Z-scan except that instead of an iris aperture a disk aperture is used to eclipse the beam. When the nonlinear refraction spreads the beam, there is a peak instead of a valley; and when the sample causes the beam to converge then there is a valley instead of a peak [42]. Reflection Z-scan is used to measure the change in the reflected energy as a sample is scanned through focus [43]. The WLC Z-scan allows for characterization of multiple wavelengths by using a filter wheel to select a wavelength, enabling much faster characterization of the nonlinear absorption spectrum of materials compared to taking Z-scans with a tunable source one wavelength at a

time. Anisotropy of nonlinear refraction and absorption in crystals has also been measured with the Z-scan experiment by simply introducing some polarizers and a half-wave plate into the setup.

2.3.4 Pump-Probe Technique

The pump-probe experiment uses a strong pump laser pulse to create changes in the optical absorption of the sample while a weak probe beam measures the transmission as a function of the temporal delay between the two overlapped beams [44]. If the probe gets to the sample before the pump then there is no nonlinear signal. When the two pulses have a zero delay, a maximum change in transmission is observed and the instantaneous nonlinearity can be extracted. However there are many interference effects (such as transient gratings) near zero delay that often make such extraction difficult. The recombination dynamics can be observed as the delay is increased. For molecules, the excited state absorption can be measured using a pump-probe experiment; for semiconductors, the free carrier absorption can be extracted [45]. When using pump-probe to study the carrier dynamics of free carriers, the pulse width must be much shorter than the recombination lifetime. For this reason, the pump-probe experiment usually requires lasers with ultrafast pulses.

2.3.5 Temperature Controlled Transmission

Temperature controlled transmission experiments with high energy pulses are useful for testing the capability of theoretical models and accuracy of fitting parameters up to the damage threshold of the sample material. The nonlinear absorption and recombination mechanisms in InSb are difficult to separate using long nanosecond and microsecond pulses. Using a cryostat to cool the sample and change the band gap can be helpful to separate 2PA and 3PA. The two-photon absorption is eliminated when the band gap is larger than twice the photon energy. The two-photon coefficient should follow the scaling rules for semiconductors as the band gap is varied by changing the sample temperature. Also, cooling the sample reduces the free carrier population, thus if the photogenerated population is kept small enough, then Auger recombination can be neglected. The experimental setup used is shown below.

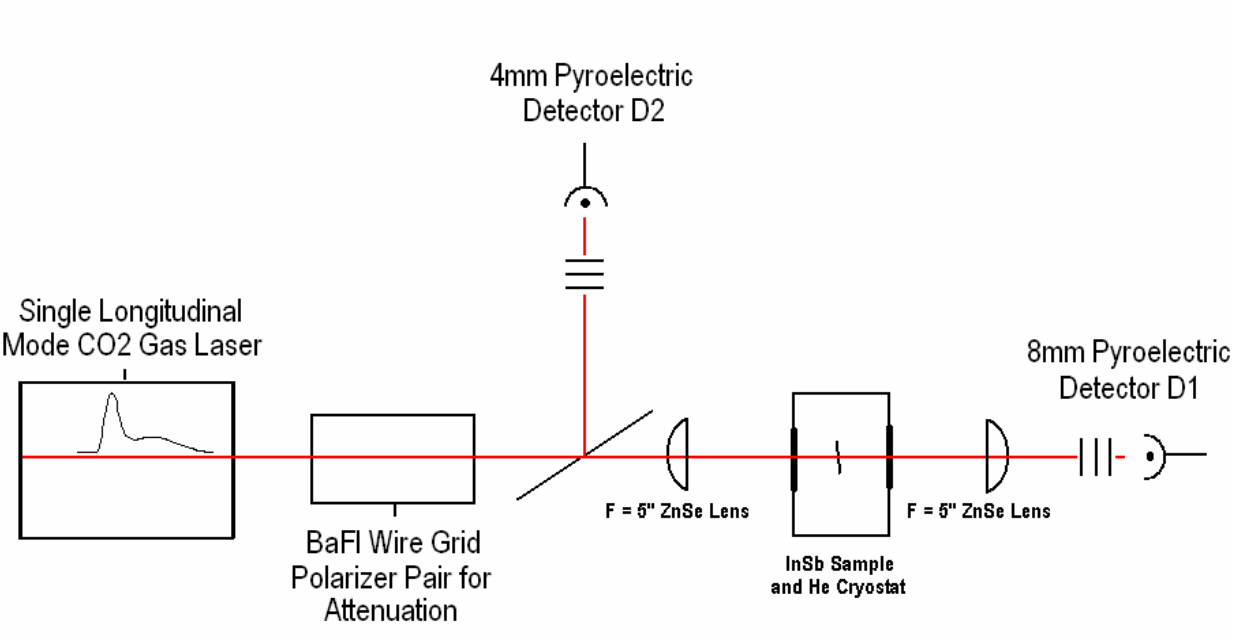

Figure 2.7 Temperature controlled transmission setup using Helium cryostat.

Chapter References

1. Paul M. Amirtharaj and David G. Seiler, “Optical Properties of Semiconductors”, OSA, Handbook of Optics II, 36.1-36.92 (1995).
2. E.L. Dereniak and G.D. Boreman, “Infrared Detectors and Systems”, Ch. 7.7 HgCdTe, John Wiley & Sons, pg. 317 (1996).
3. Evan O. Kane, “Band Structure of Indium Antimonide”, Journal of Physical Chemistry in Solids Vol.1, pg. 249-261 (1957).
4. Vladislav Dubikovskiy, “Optical Limiting: Numerical Modeling and Experiment”, University of Central Florida Ph.D. Dissertation, Ch.4 pg.96 (2003).
5. Peter Wurfel, “Physics of Solar Cells”, Ch. 3.2 Holes, Wiley-VCH Verlag GmbH & Co., pg. 46 (2005).
6. Patrick L. LiKamWa, Optoelectronics Class Notes, CREOL/ UCF 2007.
7. Peter Wurfel, “Physics of Solar Cells”, Ch. 3.3 Doping, Wiley-VCH Verlag GmbH & Co., pg. 50 (2005).
8. P.N. Butcher and D. Cotter, “The Elements of Nonlinear Optics”, Cambridge Studies in Modern Optics Vol. 9, Ch. 1, 8, and Appendix 8 (1990).
9. R. DeSalvo, M. Sheik-bahaei, A.A. Said, D.J. Hagan, and E.W. Van Stryland, “Z-scan measurements of the anisotropy of nonlinear refraction and absorption in crystals”, Optics Letters, Vol.18, No.3, pg.194-196 (1993).
10. M. Sheik-Bahae, D.C. Hutchings, D.J. Hagan, and E.W. VanStryland, “Dispersion of Bound Electronic Nonlinear Refraction in Solids”, IEEE J. Quantum Electron. QE-27, 1296-1309 (1991).

11. Eric W. Van Stryland, Milton A. Woodall, “Energy band-gap dependence of two-photon absorption”, Optics Letters, Vol.10 No.10, pg. 490-492 (1985).
12. D.C. Hutchings and E.W. Van Stryland, “Nondegenerate two-photon absorption in zinc blende semiconductors”, J.O.S.A. B, Vol.9 No.11, pg. 2065-2074 (1992).
13. Vladislav Dubikovskiy, “Optical Limiting: Numerical Modeling and Experiment”, University of Central Florida Ph.D. Dissertation, Ch.3 pg.47-95 (2003).
14. M.H. Weiler, “Nonparabolicity and exciton effects in two-photon absorption in zinc blende semiconductors”, Solid State Communications, Vol. 39, pg. 937-940 (1981).
15. B.S. Wherrett, “Scaling rules for multiphoton interband absorption in semiconductors”, J.O.S.A. B **1**, pg.67-72 (1984).
16. Handbook of Optics IV, Ch.17.4 Kramers-Kronig Dispersion Relations
17. J.S. Weiner, D.A.B. Miller, D. S. Chemla, “Quadratic electro-optic effect due to the quantum-confined Stark effect in quantum wells” Applied Physics Letters **50**, 842 (1987).
18. S.W. Kurnick and J.M. Powell, “Optical Absorption in Pure Single Crystal InSb at 298 and 78K”, Physical Review, Vol.116, No.3, pg. 597-603 (1959).
19. Michael P. Hasselbeck, “High Intensity Laser Interactions with Narrow Gap Semiconductors”, University of Central Florida Ph.D. Dissertation, Ch.6 pg.199-252 (1995).
20. Johnston, A.M., Pidgeon, C.R., Dempsey, "Frequency dependence of two-photon in InSb and HgCdTe", Physical Review B 22 (1980) 825.
21. P. Y. Liu and J.C. Maan, “Optical properties of InSb between 300 and 700K. I. Temperature dependence of the energy gap”, Physical Review B, Vol.47, No.24, pg.16 274-16 278 (1993).

22. C.L. Littler and D.G. Seiler, “Temperature dependence of the energy gap of InSb using nonlinear optical techniques”, Applied Physics Letters, Vol.46, No.10, pg.986-988 (1985).
23. M. Sheik-bahaei, P. Mukerjee, and H.S. Kwok, “Two-photon and three-photon absorption coefficients of InSb”, Journal of Optical Society of America B, Vol. 3, No. 3, pg.379-385 (1986).
24. Goeppert-Mayer, M., Ann. Physik, Uber elementarakte mit zwei quantensprungen, **9**, 273 (1931).
25. Eric W. Van Stryland, Milton A. Woodall, “Energy band-gap dependence of two-photon absorption”, Optics Letters, Vol.10 No.10, pg. 490-492 (1985).
26. C.B. de Araujo, “Multiphoton absorption coefficients in solids: a universal curve,” J. Phys. C, **16**, 5925-5936 (1983).
27. W.C. Hurlbut, Y.-S. Lee, K. L. Vodopyanov, P. S. Kuo, and M. M. Fejer, “Multiphoton absorption and nonlinear refraction of GaAs in the mid-infrared,” Opt. Lett., **32**, 668 (2007).
28. J. He, Y. Qu, H. Li, J. Mi, and W. Ji, “Three-photon absorption in ZnO and ZnS crystals,” Opt. Exp., **13**, 9235, (2005).
29. J.U. Kang, A. Villeneuve, M. Sheik-Bahae, G.I. Stegeman, K. Al-hemyari, J. Stewart Aitchison, C.N. Ironside, “Limitation due to three-photon absorption on the useful spectral range for nonlinear optics in AlGaAs below half band gap,” A.P.L., **65**, 147, (1994).
30. M. Lepore, R. Tommasi, I.M. Catalano, “Spectral behavior of three-photon absorption coefficient in II-VI compounds: ZnO, CdS and ZnSe”, Sol. State. Comm., **84**, 463-468 (1992).

31. S.S. Mitra, N.H.K. Judell, A. Vaidyanathan, A.H. Guenther “Three-photon absorption in direct-gap crystals”, Opt. Lett., **7**, 307 (1982).
32. J.H. Yee, “Three-photon absorption in semiconductors,” Phys. Rev. B, **5**, 449 (1972).
33. Milton A. Woodall, “Nonlinear Absorption Techniques and Measurements in Semiconductors”, North Texas State University Ph.D. Dissertation, Ch.4 pg.100-148 (1985).
34. M.P. Hasselbeck, E.W. Van Stryland, M. Sheik-Bahae, “ Dynamic band unblocking and leakage two-photon absorption in InSb,” Phys. Rev. B, **56**, 7395, (1997).
35. G.M. Schucan, R.G. Ispansoiu, A.M. Fox, J.F. Ryan, “ Ultrafast Two-Photon Nonlinearities in CdSe Near 1.5μm Studied by Interferometric Autocorrelation”, IEEE J.Q.E., **34**, 1374, (1998).
36. M.P. Hasselbeck, E.W. Van Stryland, M. Sheik-Bahae, “ Dynamic band unblocking and leakage two-photon absorption in InSb,” Phys. Rev. B, **56**, 7395, (1997).
37. P.D. Olszak, S. Webster, L. A. Padilha, C.M. Cirloganu, M. Woodall, D.J. Hagan, E.W. Van Stryland, “Energy band-gap dependence of three-photon absorption in semiconductors,” in *Nonlinear Optics: Materials, Fundamentals and Applications*, Topical Meeting (CD) (Optical Society of America, 2007), paper WC5.
38. Cirloganu, C.M., et al., “Three-photon absorption spectra of zinc blende semiconductors: theory and experiment.” Optics Letters, 2008. **33**(22): p. 2626-2628.
39. J.A. Woollam Company, Inc. “Spectroscopic Ellipsometry Short Course”, UCF Orlando FL, 2/28-3/3/2005.
40. Vladislav Dubikovskiy, “Optical Limiting: Numerical Modeling and Experiment”, University of Central Florida Ph.D. Dissertation, Ch.3 pg.47-95 (2003).

41. Mansoor Sheik-Bahae, Ali A. Said, Tai-Huei Wei, David J Hagan, E.W. Van Stryland, "Sensitive Measurement of Optical Nonlinearities Using a Single Beam", Journal of Quantum Electronics, Vol.**26**, No.4, pg.760-769 (1990).

42. T. Xia, D.J. Hagan, M. Sheik-Bahae, and E.W. Van Stryland, "Eclipsing Z-scan measurement of $\lambda/10^4$ wave-front distortion", Optics Letters, Vol.**19**, No.5, pg.317-319 (1994).

43. D.V. Petrov, A.S.L. Gomes, and C.B. de Araujo, "Reflection Z-scan technique for measurements of optical properties of surfaces", Applied Physics Letters, Vol.**65**, pg.1067-1069 (1994).

44. Murdin BN, Pidgeon CR, Jaroszynski DA, Phillips CC, Stradling RA, Ciesla CM, Praseres R, Langerak CJGM, "Picosecond free electron laser studies recombination in InSb and InAsSb systems",Narrow Gap Semiconductors 1995, Institute of Physics Conference Series **144**, pg.267-271 (1995).

45. J. Cheng, JY Zhou, YJ Yan, "Theory of pump-probe propagation in third- and higher-order, nonlinear optical media", Journal of the optical society of America B, Vol. **21**, 364-369 (2004).

CHAPTER 3. SPECTRAL AND TEMPERATURE DEPENDENCE OF NONLINEAR ABSORPTION IN INDIUM ANTIMONIDE

3.1 Theory and Scaling of Two-photon absorption in Semiconductors

The theory for two photon absorption was first introduced by Goeppert-Mayer, and generalized theories for multi-photon absorption in semiconductors were developed over the following decades [1-6]. Keldysh used tunneling theory or scattering matrix approach to determine the multi-photon transition rate [3]. Then Jones and Reiss used both tunneling approach (using Volkov-type wave functions) and perturbation theory assuming circular polarization, showing that the results are similar for the calculated transition rates [4]. The theory for multi-photon interband absorption in semiconductors, assuming linear polarized radiation and two parabolic bands, produced simple scaling rules for N-photon absorption, as done by Brandi and de Araujo using Keldysh's approach in 1983 [5] and by Wherrett in 1984 using perturbation theory [6]. Both theories predict the absorption coefficient to be inversely proportional to the band gap energy as E_g^{4N-5}, leading to E_g^{-3} for 2PA and E_g^{-7} for three-photon absorption (3PA) [5, 6]. These theories are not expected to give exact quantitative agreement with experiment and are typically scaled by an empirical constant when being compared to data.

2PA in semiconductors was experimentally shown in 1985 [7] to scale with E_g^{-3} as predicted, thus demonstrating the utility of a simple two parabolic band approach as used by Wherrett and de Araujo [5, 6]. The 2PA coefficient, α_2, of semiconductors can be estimated by,

$$\alpha_2 = K_2 \frac{\sqrt{E_p}}{n^2 E_g^3} \left[\frac{(2\hbar\omega / E_g - 1)^{3/2}}{(2\hbar\omega / E_g)^5} \right] \qquad [3\text{-}1]$$

using a value for K_2 = 1.94 $eV^{5/2}$ cm/MW calculated from first principles and universal constants or with K_2 = 3.10 $eV^{5/2}$ cm/MW obtained empirically by fitting the 2PA measured using many semiconductors with different band gap energies [7,8]. This empirical constant used in the scaling theory allowed prediction of α_2 in other materials. For example, Ref. 7 employs the scaling function for InSb using E_g = 0.18 eV at 10.6 μm and predicts α_2 = 6.8 cm/MW. Experimentally reported values for the 2PA coefficient of InSb at room temperature have ranged from 0.2 to 20 cm/MW [9]. This inconsistency is presumably due to significant effects from free carrier absorption (FCA) and refraction (FCR) in InSb [10]. Other difficulties associated with these measurements in the mid-infrared wavelength regime include the availability of detectors with high sensitivities and low noise, alignment issues, as well as beam quality and pulse shape.

3.2 Methodology Used to Characterize Indium Antimonide

In this work, we present an investigation of both the temperature and spectral behavior of 2PA and FCA in InSb along with the relevant carrier dynamics. Semiconductor band gap energies are known to vary with temperature, therefore α_2 in InSb is expected to vary accordingly, i.e. with E_g^{-3} [11]. While the FCA cross section has been generally accepted in the past to be roughly constant [12] for the temperatures and wavelengths used in this study, it has been recently predicted, as shown in Fig 3.1, that it varies significantly with wavelength and temperature [13]. We employ a wide range of pulse widths to measure the nonlinear absorption and account for the increasing importance of free carrier effects for longer pulses in the determination of absorption coefficients. The methodology is to study the ultrafast multiphoton absorption spectrum independently and then in combination with free carrier effects with progressively longer pulses adding more parameters to the model as needed.

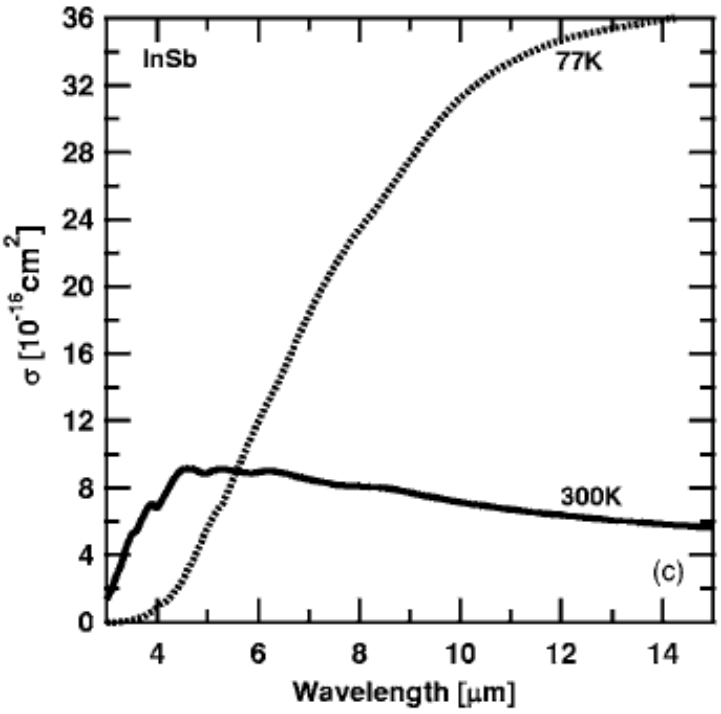

Figure 3.1 Free-carrier absorption spectrum at room temperature and liquid nitrogen temperature, from [13].

Linear and nonlinear transmission measurements are used to characterize the temperature and spectral behavior of FCA. We make use of the known temperature dependence of the band gap and to verify 2PA scaling rules we use a tunable picosecond laser system and a nitrogen cryostat to control the sample temperature. Values of 2PA coefficients obtained at room temperature using a tunable femtosecond laser system are also presented along with an investigation of nonlinear absorption and free carrier recombination using a nanosecond CO_2 transverse excitation atmospheric (TEA) pressure laser system and a helium cryostat to control the sample temperature. Great care was taken to insure that all of the transmitted light was collected, as this may be a significant source of error in previously reported values due to the large free carrier refraction and nonlinear index of refraction.

3.3 Modeling Parameters

The modeling of our data utilizes a propagation equation for the irradiance, *I*, coupled to a rate equation for the free carrier population *N*, as shown in CH.2 and reviewed below;

$$\frac{dI}{dz} = -\alpha_1 I - \alpha_2 I^2 - \alpha_3 I^3 - \sigma_{FCA}(N_0 + N_{pg})I \qquad [3\text{-}2]$$

$$\frac{dN}{dt} = \frac{\alpha_2 I^2}{2\hbar\omega} + \frac{\alpha_3 I^3}{3\hbar\omega} - A(N - N_0) - B(N^2 - N_0^2) - CN(N^2 - N_0^2) \qquad [3\text{-}3]$$

.

Here α_2 is the 2PA coefficient and α_3 the 3PA coefficient. The total free carrier population N is the sum of initial or thermal carriers N_0 and photo-generated carriers N_{pg}. The FCA cross section σ_{FCA} is the sum of the cross sections for electrons and holes. The cross section for holes is about 40 times larger than that for electrons due to the direct (non-phonon-assisted) heavy hole to light hole transition, so FCA is dominated by free hole absorption [12,13]. For the wavelengths used, one-photon absorption (1PA) across the band gap is not energetically possible. Linear absorption from defects and impurities can be included in α_1; however, our FTIR fits well without including such linear losses in our undoped samples with a defect concentration of approximately 9×10^{13} cm^{-3}. Thus, the only linear absorption needed is due to the free carriers. The Shockley-Read-Hall (SRH) recombination rate *A*, spontaneous radiative recombination (RR) rate *B*, and Auger recombination (AR) rate *C* are neglected for sub-nanosecond measurements while FCA and recombination are neglected for sub-picosecond measurements as will be justified later in this paper. Stimulated recombination is neglected in the model because the photon energies used are always less than the band gap energy; however, two-photon gain in

optically pumped InSb has been discussed in the literature [14], but we do not see any evidence for it in this work.

The advantage of using a range of pulse widths to study the nonlinear optical properties of InSb is that we are able to test the model through various simplifying assumptions for short pulse widths and with increasing complexity as the pulse width increases. For example, instantaneous absorption processes such as multi-photon absorption are more easily investigated using ultrashort pulse widths so that large irradiances can be obtained with negligible effects from photogenerated carriers which build up during the pulse. The picosecond range is ideal for studying nonlinear absorption including multi-photon absorption and population dependent FCA since recombination effects are negligible. For nanosecond pulse widths, nonlinear absorption and carrier recombination processes yield effective lifetimes in the nanosecond range and must be considered, further complicating the analysis. Thus, the methodology is to study the material parameters with progressively longer pulses adding more parameters to the model as they become significant.

3.4 Experiments

3.4.1 Linear Spectroscopy Experiments

Measurements of the linear transmittance from 8 to 12 μm at room temperature exhibit FCA due to the thermal population in InSb. The free carrier absorption cross-section can therefore be isolated through linear transmittance measurements. To determine the temperature dependence of the FCA spectrum, the linear transmittance is measured at different temperatures via FTIR using a Thermo model 100 FTIR spectrometer and a micro-miniature refrigerator (MMR model K-77) nitrogen cryostat to control the sample temperature. Our FCA values

compared to theory are shown in Fig. 3.2, demonstrating that the FCA cross section is not constant but has a spectral and temperature dependence [13].

The carrier population is taken to be equal for holes and electrons. This is a valid assumption since our sample (Galaxy Compound Semiconductors Inc. undoped <111> cut single crystal) with a defect concentration of approximately 9×10^{13} cm^{-3}, and this is approximately equal to the thermal population at 160 K. The thermal population at room temperature is approximately 2×10^{16} cm^{-3}. The Boltzmann approximation for carrier concentration leads to an error of almost 10% due to the degenerate population so the more accurate Fermi-Dirac distribution is used. At 80 K, the thermal population is much smaller (5×10^{9} cm^{-3}), and the population is nondegenerate for temperatures below 200 K. The carrier population becomes too small at low temperatures making it difficult to measure the loss with this experiment, as the total linear absorption is less than 5% below 200 K. This leads to large experimental uncertainties below 200 K so that the total experimental error for FCA is estimated to be ±10% at 300 K and ±100% at 180 K. For the low temperature range, we use the FCA cross sections determined from fitting the picosecond Z-scans (to be discussed in the following sections), which agrees with the theoretical values reported in Ref. [13].

Free carrier Absorption

Although the FCA cross section for electrons is known to be dependent on the square of the wavelength and also temperature dependent, FCA is dominated by heavy hole absorption in InSb and this was previously accepted to be roughly constant for the range of temperatures and wavelengths used in our experiments [12]. We have found from FTIR measurements of the linear absorption and picosecond Z-scan measurements (to be discussed in the following sections)

that it is actually temperature dependent. Moreover, the temperature dependence is in agreement with the recent theoretical predictions of Ref. [13] as shown in Fig. 3.3. The FCA is should be expected to be temperature dependent due to the change of the Fermi-Dirac distribution of carriers.

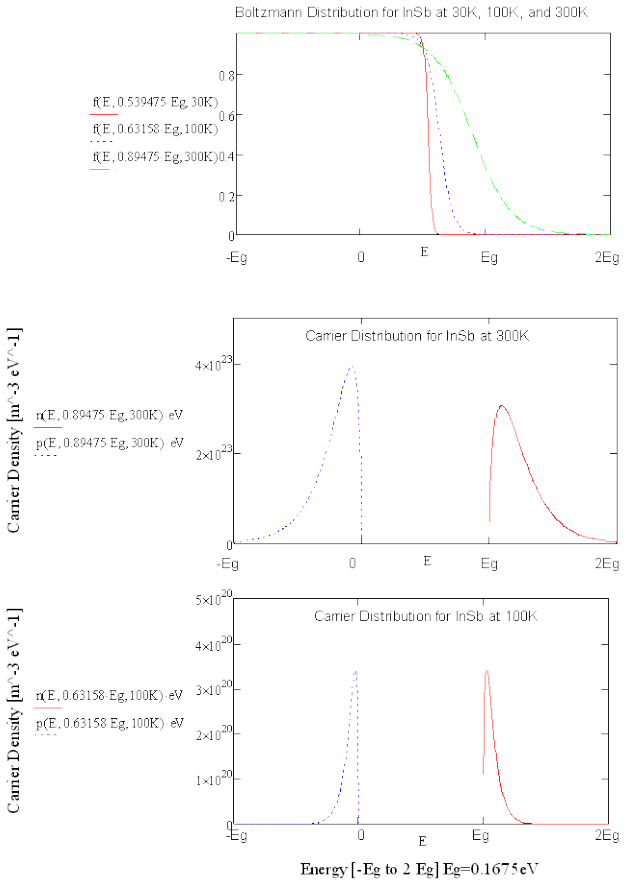

Figure 3.2 Temperature dependence of Fermi-Dirac carrier distribution for InSb.

This distribution is narrower for lower temperatures and a larger fraction of holes are available for absorbing longer wavelength photons due to the constraints for energy and momentum conservation. This results in a larger FCA cross section and a red-shifted absorption edge for low temperature [13].

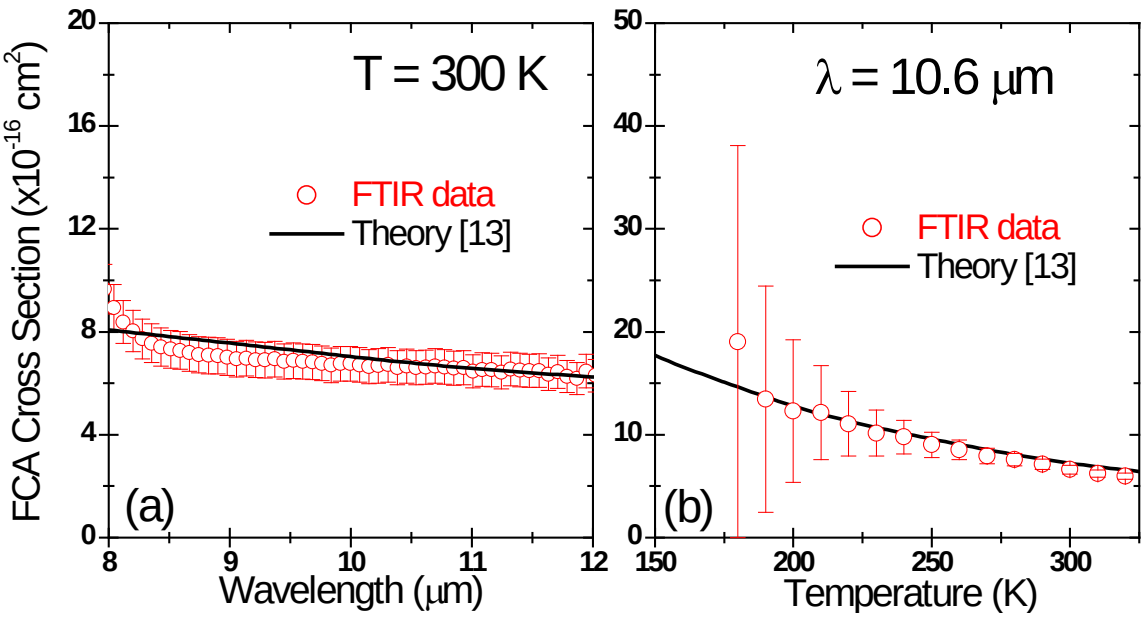

Figure 3.3 Free carrier absorption, FCA spectral theory (solid lines) [13] and data (open circles) from linear absorption measurements at (a) 300 K vs. wavelength and (b) 10.6 um vs. temperature.

3.4.2 Femtosecond Experiments

The instantaneous multiphoton absorption effects can be isolated from FCA by measuring the nonlinear transmittance (in the 2PA or 3PA wavelength range respectively) using focused femtosecond pulses to achieve high irradiance with low energies. The 2PA spectrum of InSb at room temperature is measured by the Z-scan technique [15, 16] using a regeneratively amplified femtosecond Ti:Sapphire laser from Clark at 775 nm, which pumps an optical parametric generator/amplifier (OPG/A) and difference frequency generator (DFG) [a]. Examples of data and fitting (performed by Claudiu Cirloganu) are shown in Fig. 3.4. A beam waist ω_0 of 40 to 60 μm defined as the half width at the one over e squared value of the maximum (HW1/e^2M) is determined from fitting the InSb Z-scan results across the measured spectral range from 8 μm to 12 μm.

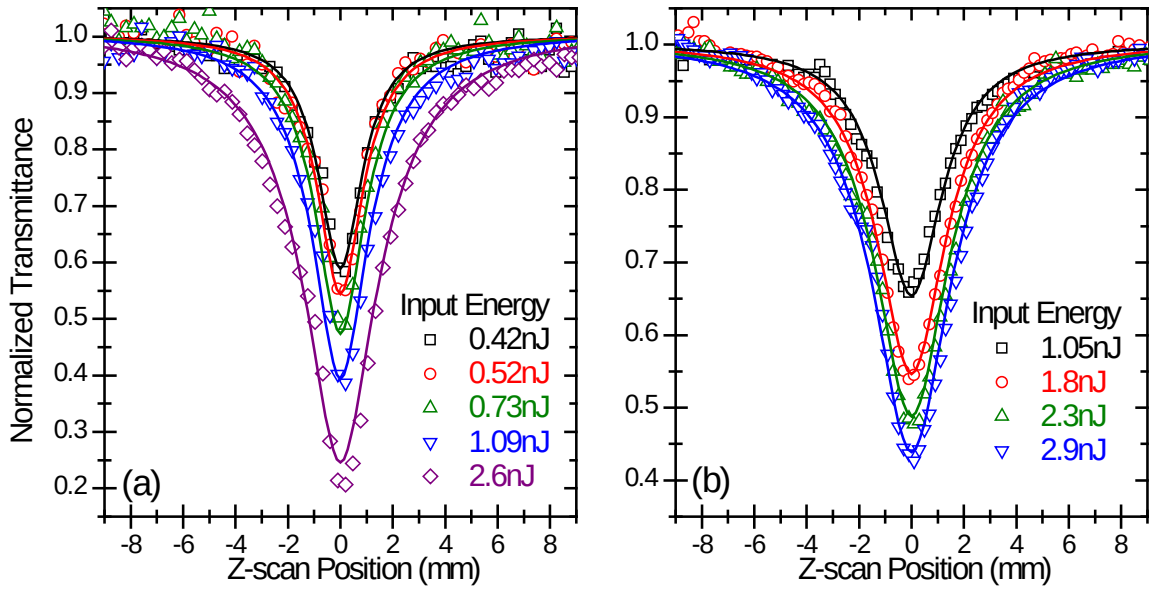

Figure 3.4 Open aperture Z-scan data at several input pulse energies using 300 K InSb at (a) 9 μm fit with τ_{FWHM} = 370 fs, w_0 = 45 μm, α_2 = 2.9 cm/MW and (b) 11.5 μm fit with τ_{FWHM} = 500 fs, ω_0 = 63 μm, α_2 = 2.0 cm/MW.

For Z-scan data that results from pure 2PA, the full width half maximum (FWHM) of the open aperture Z-scan curve is equal to twice the Rayleigh range (assuming a Gaussian beam) and the beam waist is determined with an error of ~ ±5%. In the cases where only 2PA is present this is as accurate as using a knife-edge scan or pinhole scan if the beam is Gaussian. Although these experiments have the advantage of independently measuring multi-photon absorption, the low energies used make it difficult to align the setup and accurately calibrate the energy incident on the sample (errors were estimated to be around ±30% and calibration was performed with a Laser Precision RK-5100 pyroelectric radiometer and a lock-in amplifier). The spectrum of the pulse was measured using a monochrometer (Oriel, Cornerstone 130 M-74000, 150 l/mm Au coated grating) with a Mercury Cadmium Telluride (HgCdTe) detector. We had difficulties in performing autocorrelations on these pulses as the low energies available prevented us from obtaining any useful results. However, we measured the spectral widths for the wavelength range considered (between 8500 nm and 9500 nm). At each wavelength we calculated the

corresponding transform limited Gaussian pulse to be about 160 fs FWHM. The dispersion of the ZnSe and BaF optics was then considered at each wavelength to calculate the pulse width at the sample where the pulse was broadened to a maximum of ~500 fs FWHM. This assumption allowed us to calculate the minimum pulse width possible at the sample and implicitly a lower limit for the 2PA coefficient. Total absolute experimental error for 2PA is estimated to be ±50%. Results for the 2PA spectrum at room temperature from femtosecond data are discussed later together with picosecond data.

3.4.3 Picosecond Experiments

The linear transmittance as a function of temperature is also measured at several wavelengths using the experimental picosecond Z-scan setup with low energy while the sample is kept stationary and out of focus to ensure negligible nonlinear effects. This allows the characterization of FCA dependence on temperature before any nonlinear measurements. It is found that our linear absorption measurements agree within ±25% with the product of the theoretical cross section and the population density (note that both cross section and population are temperature dependent) as suggested in Ref. [13] at room temperature for 9.6 and 10.6 μm as shown in Fig. 3.5. These FCA values also agree with the results from FTIR measurements. As mentioned in the previous section, at temperatures below 180 K where the thermal population is orders of magnitude smaller, the linear absorption is so small that the cross section cannot be determined with useful precision. To determine the FCA cross section at low temperature, we use the nonlinear absorption of photogenerated carriers and compare our experimentally obtained values to those theoretically predicted [13].

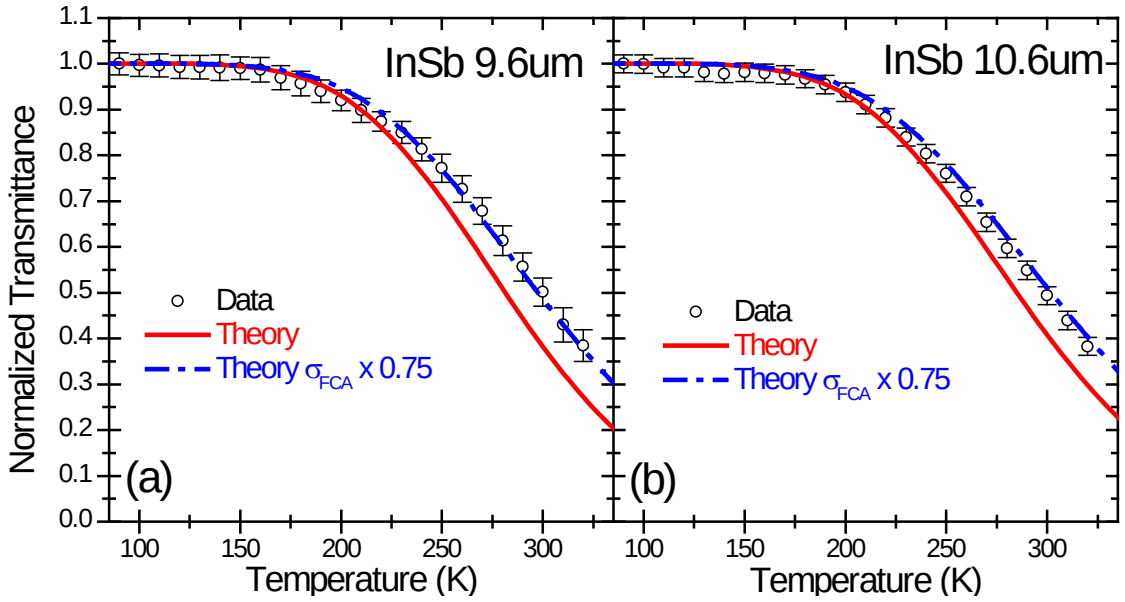

Figure 3.5 Linear transmission data obtained at (a) 9.6 μm and (b) 10.6 μm compared to transmission using theory [13] for free carrier absorption and the same theoretical absorption reduced 25%.

The FCA due to photogenerated population can be measured in combination with 2PA or 3PA by the Z-scan technique using picosecond pulses. The more energy that is absorbed by the sample the more important the contribution from FCA becomes. These measurements are useful for determining the shape of the 2PA and FCA spectrum at different temperatures for comparison to theory and scaling rules. Temperature dependent picosecond Z-scan measurements are performed using a 10 Hz modelocked Nd:YAG laser pumped optical parametric generator/amplifier (OPG/OPA) with tunable difference frequency generation (DFG) system [b]. The temporal pulse width was determined to be 10 ± 1 ps (FWHM) at 10.6 μm from pump probe measurements in InSb discussed later in this section. A beam waist of 120 to 140 μm HW1/e^2M was determined from fitting the InSb Z-scan results across the measured spectral range from 8 to 12 μm. Examples of the Z-scan data and fitting are shown in Fig. 3.6 It is found that for the lowest energy picosecond Z-scans (with small changes in transmittance ~5%); the fitting for 2PA is almost independent of the FCA cross section used allowing for a good

estimation of the beam waist and 2PA absorption coefficient. It is also found through fitting of data taken at higher irradiance levels for the FCA cross section that the values obtained are consistent with the theoretical values of σ_{FCA} (as reported by Krishnamurthy) over the entire temperature range studied. Therefore, theoretical values for FCA are adopted in modeling so that the only fitting parameter is 2PA. Part of the justification for doing this is that the theoretical values for FCA cross section were independently verified by linear absorption except at the lowestst temperatures. The 2PA coefficients are compared to theory and to values determined by femtosecond Z-scans showing agreement between the data and model using the values for the FCA cross sections given by Ref. [13].

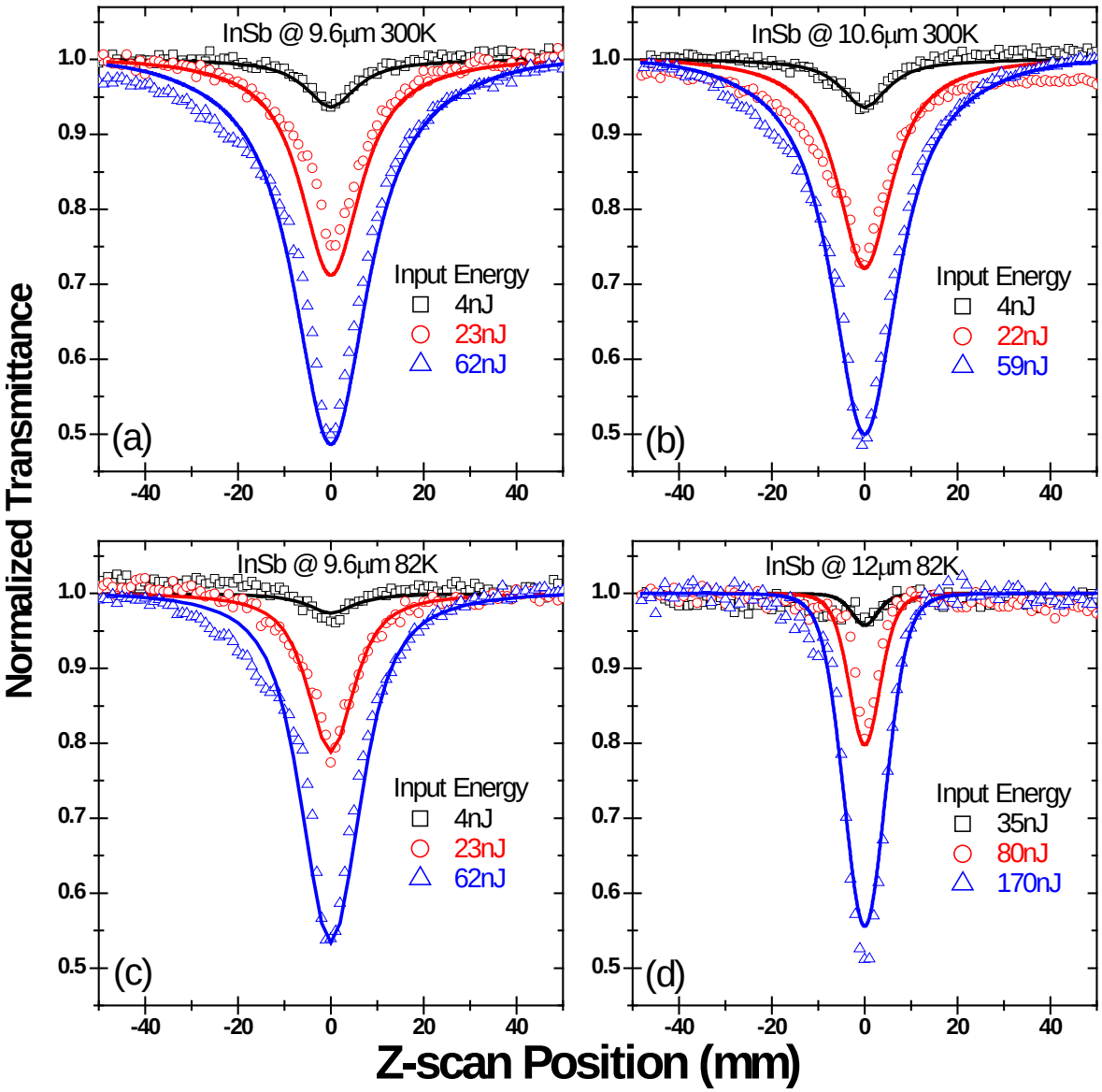

Figure 3.6 Open aperture Z-scan data using 300 K InSb at (a) 9.6 μm fit with $\tau_{HW1/e}$ = 6 ps, w_0 = 140 μm, α_2 = 3.4 cm/MW, (b) 10.6 μm fit with $\tau_{HW1/e}$ = 6 ps, w_0 = 140 μm, α_2 = 3.5 cm/MW, and 82 K InSb (c) 9.6 μm fit with $\tau_{HW1/e}$ = 6 ps, w_0 = 140 μm, α_2 = 1.0 cm/MW, (d) 12 μm fit with $\tau_{HW1/e}$ = 6 ps, w_0 = 140 μm, α_3 = 0.025 cm^3/MW^2.

Since the photogenerated free carrier population increases for the longer pulse widths, the associated refraction is also more significant and potentially problematic. It is important to note that nonlinear refraction can result in collection losses that will inflate the extracted value for

nonlinear absorption. Total experimental error for 2PA is conservatively estimated to be ±50%, and the FCA cross section values were also estimated to be correct within ±50% based on the resulting variation in fitting the highest irradiance Z-scan data. The experimental error is derived by estimating the error in irradiance parameters, sample thickness, and fitting error. The energy error is estimated to be ±30%, the pulse width error is estimated to be ±30%, the spot size error is estimated to be ±10%, and the sample thickness error is estimated to be ±5%. Fitting error is determined by the range of values that can be used to fit spot size and 2PA amplitude. Although the absolute error for 2PA is quite large the relative error is approximately ±10% allowing for accurate comparison of our data to the trend of the calculated spectra. The relative error is estimated by leaving out the systematic error due to pulse width, sample thickness, and energy calibration. Relative error is essentially due to fitting error and determined by the noise in the Z-scan data.

We also performed several degenerate pump-probe experiments at 10 μm on a 0.54 mm thick intrinsic InSb sample (performed by Claudiu Cirloganu). The probe beam was kept at a much smaller irradiance in order to not induce any nonlinear effects by itself and its transmittance was monitored for different delays with respect to the pump beam. We used a standard non-collinear geometry with an angle between the two beams of ~7 degrees, and the polarization of the probe was rotated by 90 degrees with respect to the pump to avoid coherent artifacts. These transient experiments provided a few advantages over the other single beam techniques. They allowed for the estimation of the employed pulse widths directly while effectively decoupling the bound electronic effects from the free carrier ones. The short delay curves (~100 ps) shown in Fig. 3.7a allow for the monitoring of the free carrier population buildup and for the determination of the 2PA coefficients. The data taken with longer delays

shown in Fig. 3.7b (~1 ns) show relaxation on a picosecond time scale due to the Auger recombination which is much faster than the SRH recombination time which is usually on the order of microseconds [24].

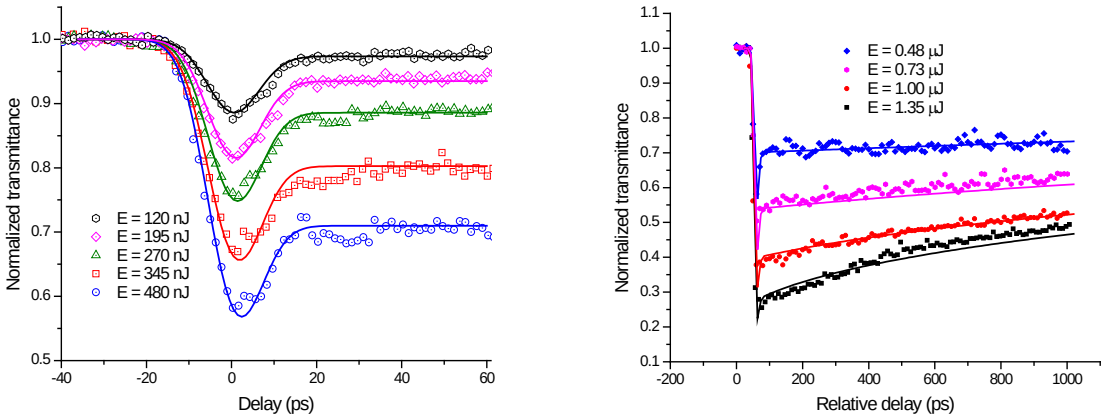

Figure 3.7 Degenerate pump-probe data in InSb at 10 μm with cross-polarized beams; both the (a) short and (b) long delay curves are fit with the same parameters: t = 6 ps, σ_{FC} = 6.8 × 10^{-16} cm^{-2}, w_0 = 500 μm, L = 450 μm, α_{2self} = 1.4 cm/MW, α_{2cross} = 1.9 cm/MW, C = 6.5 × 10^{-26} cm^6/s.

We were able to obtain a consistent fitting for several pumping energies using the same parameters and a fixed value for free carrier absorption as extracted from the linear measurements. These experiments provide a much better indication for the magnitude of the Auger coefficient as the fits suggest a value of $C = 6.5 \times 10^{-26}$ cm^6/s with a relative error of about ±20%. This is possible since at longer delays the only absorption present is due to the free carrier population and by monitoring the transmittance one can monitor directly the evolution of the carrier population. Previous measurements were done mostly employing much larger densities of photogenerated carriers through one photon pumping and yielded numbers spanning more than 1 order of magnitude [20].

Two-Photon Absorption

The 2PA absorption values measured by Z-scan agree well with the spectral shape predicted by the detailed theory of Ref. [13] for both thermal and spectral variation as shown in Fig. 3.8 and Fig. 3.9. The absolute values also agree within a factor of three to the values calculated using the simple parabolic band model of 2PA with an empirical constant (K=3.1 $eV^{5/2}$ cm/MW) previously determined for semiconductors [7]. This level of agreement with Wherrett's theory [6] using an empirical scaling constant demonstrates the utility of a simple two-parabolic band model as well as the accuracy of an extrapolated value based on the scaling rules derived from it. A comparison of all the 2PA data with these scaling functions is shown in Fig. 3.10.

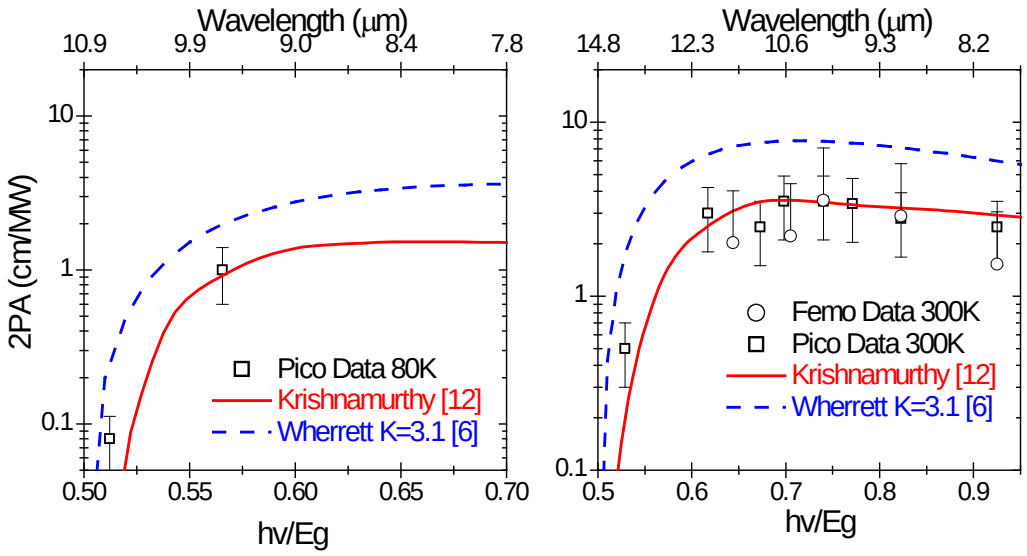

Figure 3.8 Comparison of 2PA values obtained from fitting femtosecond and picosecond Z-scan data with Wherrett's theory [6] scaled by an empirical factor and more recent theory [13] at (a) 80K and (b) 300K.

The thermal variation of 2PA due to the change in band gap energy agrees slightly better with the predictions of Ref. [13] than with that of Ref. [6] and the difference in absolute magnitude between the theory of Ref. [13] and the data is within experimental error, except very

near the band edge. Additionally, the results for femtosecond Z-scans and picosecond Z-scans at 300 K shown in Fig. 3.7 agree well with each other, α_2 ~3 cm/MW. As discussed in Ch.2 there are two values typical used for the material independent constant K. The picosecond values agree with the spectral shape for both theories and the magnitude of the data agrees better with Wherrett's theory if K=1.9 $eV^{5/2}$ cm/MW (α_2 =4.9cm/MW) is used in place of the value of K=3.1 $eV^{5/2}$ cm/MW (α_2 =7.8cm/MW) from Ref. [7] as shown in Fig. 3.11. It is important to note that fitting the femtosecond data gives the lowest possible 2PA value as the error bars in Fig. 3.12 suggest, since the pulse widths used in fitting are calculated assuming the pulse width at the output of the OPG is transform limited and thus the pulses are assumed to have the highest possible irradiance. Picosecond Z-scan data independently confirm the predicted spectral and temperature dependence of 2PA and combined with the femtosecond data is in a good agreement with the predicted magnitude of the 2PA spectrum at room temperature.

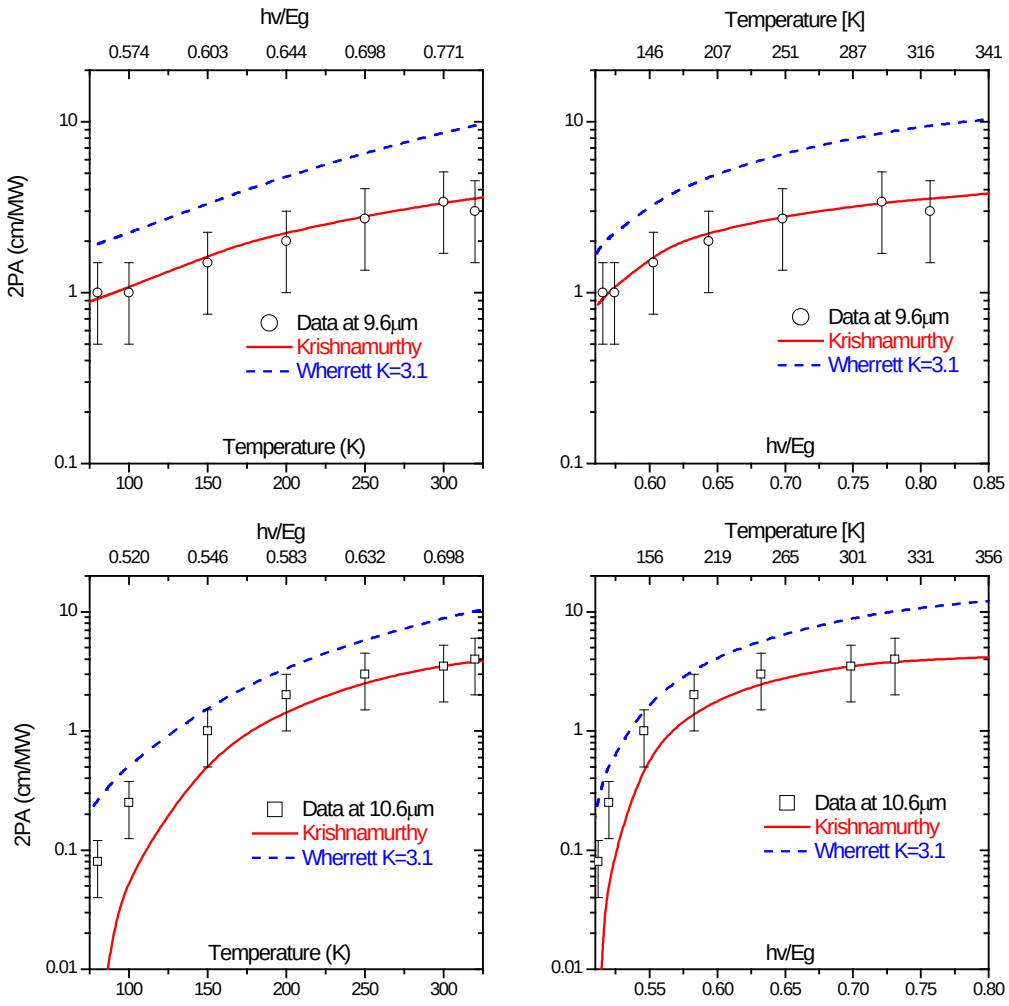

Figure 3.9 Picosecond Z-scan results for 2PA vs. temperature and vs. photon energy normalized to the band gap vs. temperature (a) and energy (b) at 9.6 μm and vs. temperature (c) and energy (d) at 10.6 μm compared to theory.

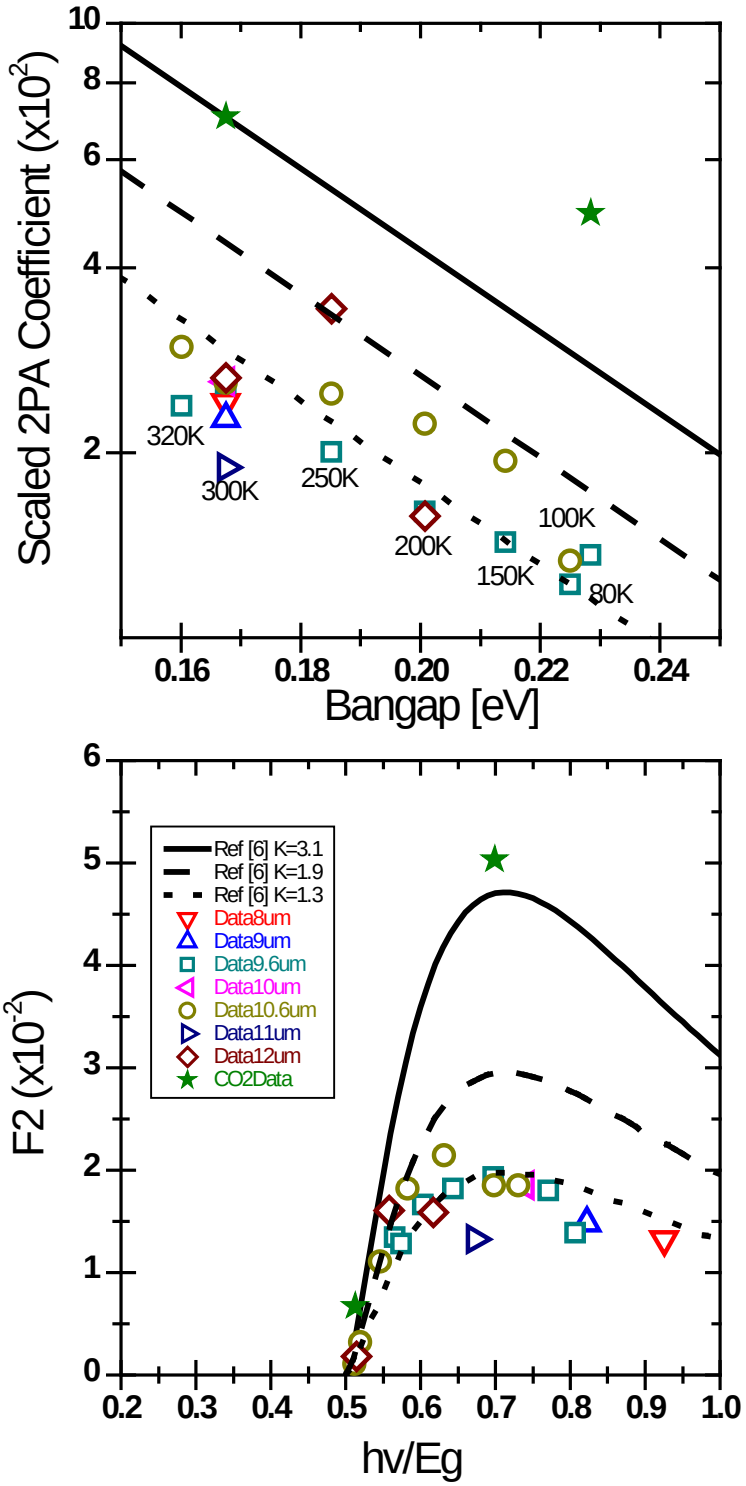

Figure 3.10 Scaled 2PA data from picosecond Z-scan experiments and nanosecond results at 300K and 80K compared to Wherrett's scaling theory from Ref. [6] with K=3.1 (solid line) K=1.9 (dashed line) and K=1.3 (dotted line). The CO_2 data obtained by fitting with different FCA cross sections will be compared again to picosecond data at 10.6 in Fig. 3.11.

Three-photon Absorption

At wavelengths longer than the 2PA band edge, 3PA is the dominant absorption mechanism. This is the case for InSb at 80 K with wavelengths longer than 10.9 μm. In this work, 3PA in InSb at 80 K is determined by fitting picosecond Z-scan data shown in Fig. 3.6 to give $\alpha_3 \approx 0.025 \pm 0.012$ cm^3/MW^2 at 12 μm. It should be noted here the agreement of this data with the 3PA model is achieved using the theory for FCA at low temperature. The observation of 3PA in InSb led to a project focused on 3PA in direct band semiconductors. This project is the topic for the next chapter.

3.4.4 Nanosecond Experiments

Nanosecond experiments are used to test our full model for nonlinear transmission, including the free carrier recombination terms, starting with irradiances showing linear transmittance up to the damage threshold. The sample is held in focus for two reasons: first, it is easier to determine the damage threshold by slowly increasing the energy; second, it proved difficult to scan the sample through focus to perform Z-scan measurements as it was mounted in a large CTI-Cryogenics Model 22 helium cryostat, which was used to enable measurements at temperatures down to 10 K.

A single mode TEA CO_2 laser with a gain-switched pulse width of 150 ns FWHM and a beam waist of 180 μm HW1/e^{2}M (measured by knife-edge scans) is used to obtain data from the linear to nonlinear regime to the laser induced damage threshold (LIDT). The LIDT is reported to be 1-2 J/cm2 [18,19] which is similar to the fluence levels that result in surface damage in this work. The temporal pulse profile is asymmetric and so it is important that the profile is recorded for modeling and monitored during the experiment. It is long enough to be measured using a

digital storage oscilloscope (Tektronix, TDS680C, 1GHz/5Gs) with a fast gold-doped germanium detector. A considerable amount of effort went into getting the laser to run with a high level of stability so that the temporal profile, spatial profile, and energy were stable during the experiments. Also, since there is a large electrical discharge in the gain cells of the laser it is critical that the data acquisition system and detectors be properly shielded, grounded, and isolated. A typical temporal profile and normalized nonlinear transmittance data recorded at 80 K and 300 K, with the corresponding fitting are shown in Fig. 3.11.

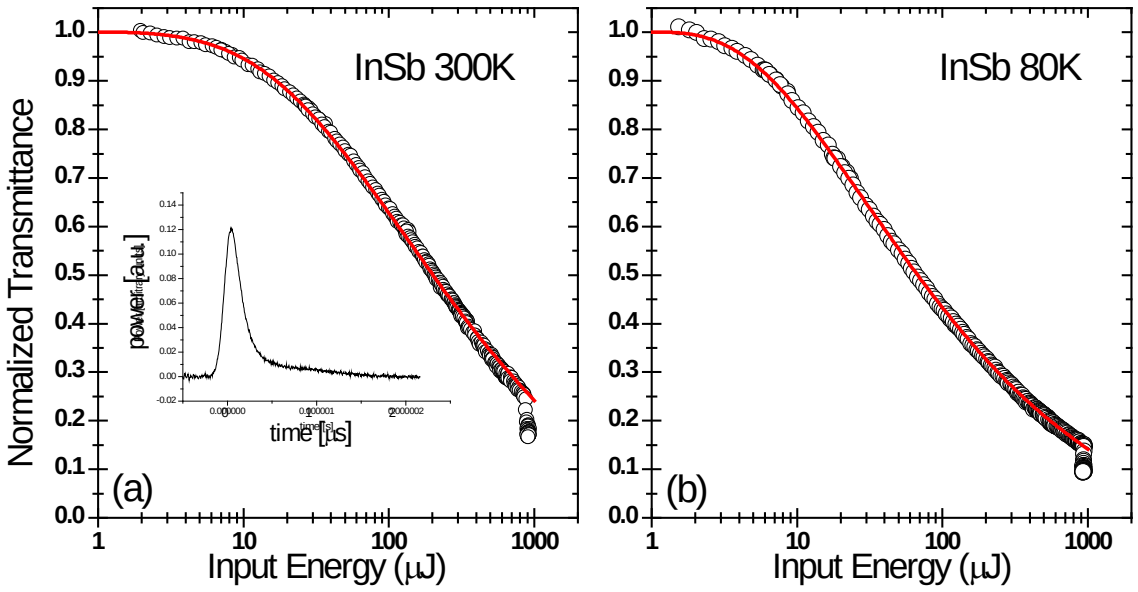

Figure 3.11 Nonlinear transmission data up to the damage threshold at λ=10.6μm of InSb (a) 300 K fit with w_0=180 μm, σ =6.757x10^{-16} cm^2, τ=2x10^{-6} s, B=0.7x10^{-10} cm^3/s, α_2=9.5 cm/MW, C=7x10^{-26} cm^6/s and (b) 80 K fit with w_0=180 μm, σ =32.44x10^{-16} cm^2, τ=2x10^{-6} s, B=3.3x10^{-10} cm^3/s, α_2=0.5 cm/MW, C=30x10^{-26} cm^6/s

The nonlinear transmission data was fit first as independent data as the picosecond and femtosecond experiments had not yet been performed. The same data was later fit with theoretical values for the temperature dependent FCA as confirmed by FTIR and picosecond experiments. This data is fit through iteration of optimizing the different parameters one at a time with initial parameters based on literature values. The importance of taking the temperature

dependence of the FCA cross section into account when modeling nonlinear absorption is demonstrated by the improved agreement obtained for 2PA at low temperature by using the FCA values predicted by theory in Fig 3.12. Attempting to fit the nonlinear transmittance data with a fixed, temperature independent, FCA cross section (with $\sigma = 8.6 \times 10^{-16}$ cm^2) gives best fit values for 2PA which produce a spectrum inconsistent with the temperature dependence of 2PA as predicted by theory and verified by picosecond measurements. Using the temperature dependent values for FCA cross sections (with $\sigma = 3.5 \times 10^{-15}$ cm^2 at 80K and $\sigma = 6.8 \times 10^{-16}$ cm^2 at 300K) allows for more accurate determination of 2PA as shown in Fig. 3.12. The nanosecond data is finally fit using FCA cross sections and 2PA coefficients consistent with theory [13] and obtained from FTIR measurements and picosecond Z-scan data. The data agrees remarkably well with the model using absorption values determined with shorter pulses and recombination rates that are consistent with the accepted range of values at room temperature ($B \approx 1 \times 10^{-11}$ -7×10^{-11} cm^3/s, $C \approx 4 \times 10^{-26}$ - 2×10^{-23} cm^6/s) [20] and previous work at low temperatures ($B \approx 1 \times 10^{-9}$) [21].

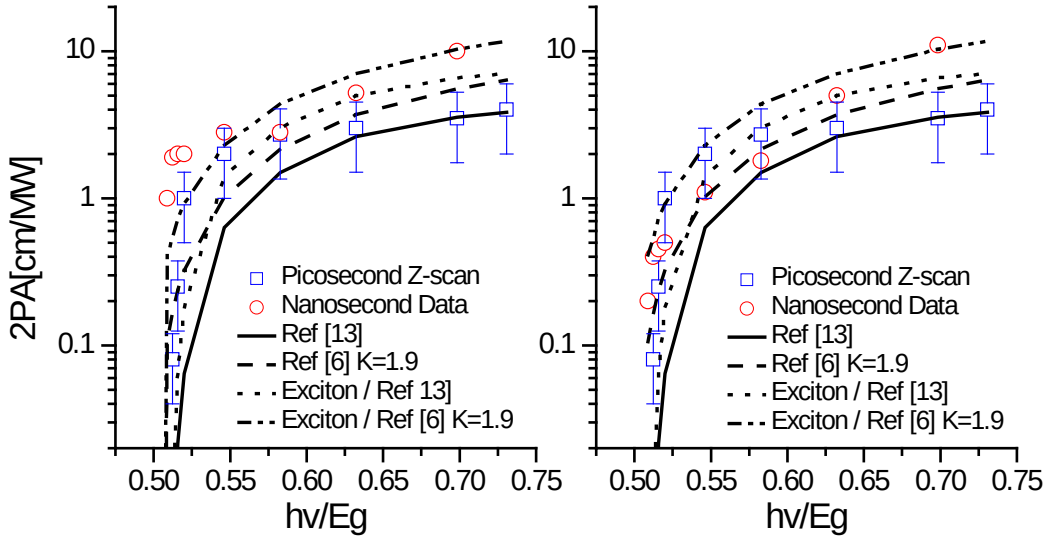

Figure 3.12 Comparison of values obtained from fitting nanosecond data for 2PA at 10.6μm (a) with a constant FCA cross section and (b) with a temperature dependent FCA cross section. Theory of Wherrett [6] (dashed line) and Krishnamurthy [13] (solid line) is shown for comparison. The same theories are multiplied by an exciton enhancement factor [6] (dash dot line) [13] (dotted line) and this will be discussed in the following section.

Exciton Enhancement

It has been suggested that exciton enhancement should be considered in the theoretical calculation of 2PA coefficients [22]. Exciton enhancement is an increase in the absorption rate due to transitions that include energy levels of exciton states near the bottom of the conduction band. The discrepancy between theoretical and measured values observed in this work is larger near the band edge, which is consistent with the predicted spectral behavior of exciton enhancement [23]. The calculated enhancement factor for 2PA due to excitons is shown in Fig 3.13.

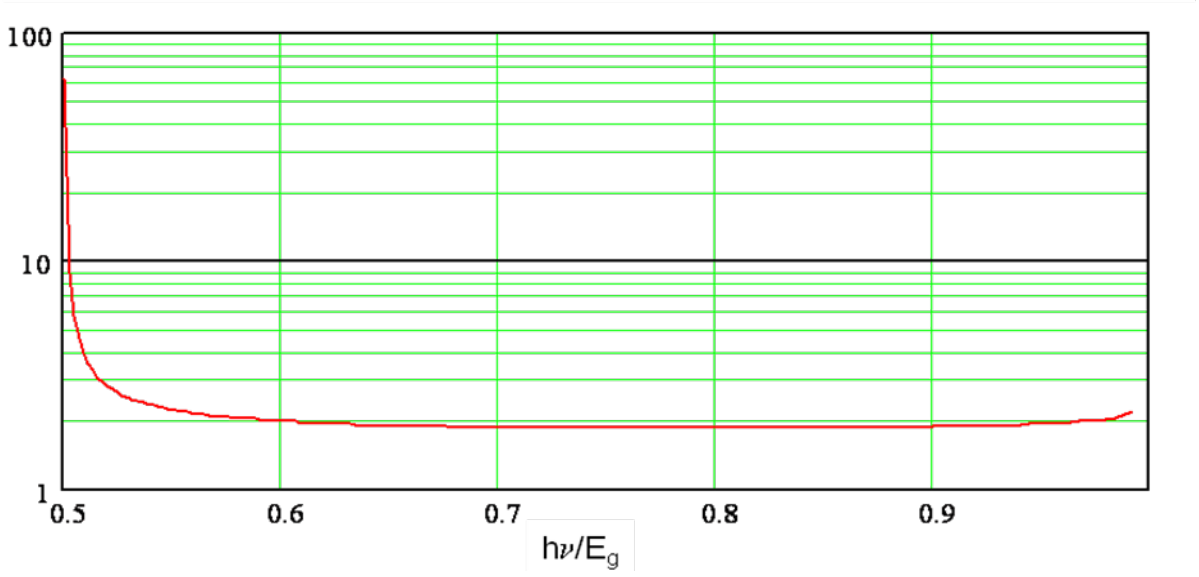

Figure 3.13 Exciton enhancement factor for 2PA calculated from Weiler's theory. [23]

Therefore, a comparison of the picosecond data at 9.6 μm and 10.6 μm to both the theory of Ref. [6] without empirical factors and the theory of Ref. [13] while including exciton enhancement of 2PA is shown in Fig. 3.14, and nanosecond data at 10.6 μm modeled with 2PA as a free parameter is included for the same comparison in Fig. 3.15.

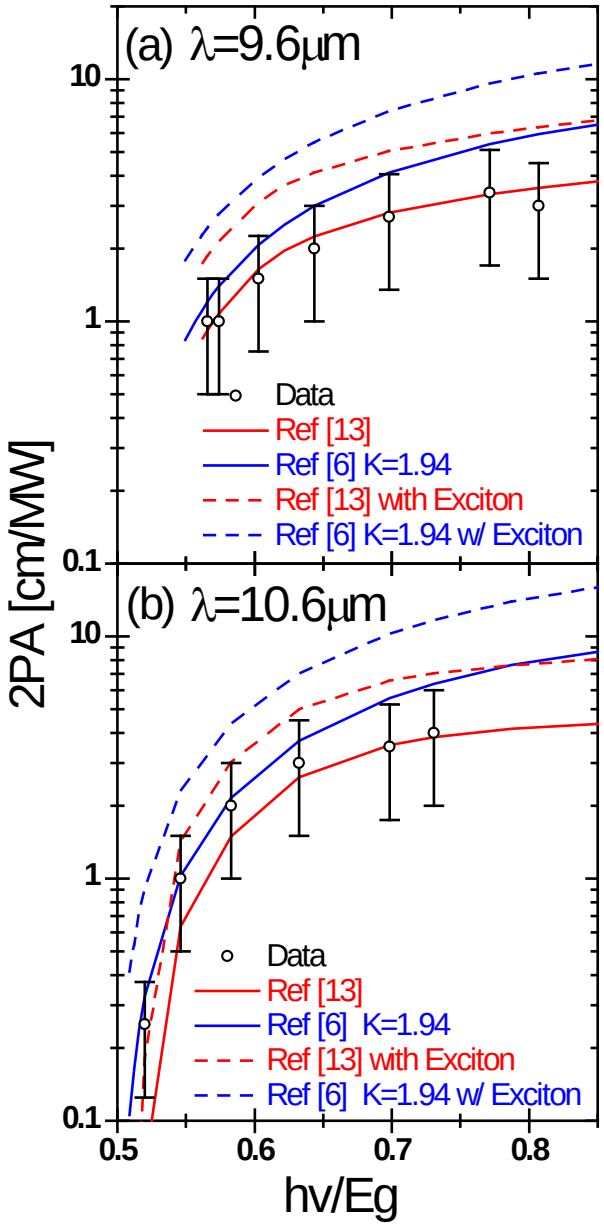

Figure 3.14 2PA picosecond data vs. temperature at 9.6 μm and 10.6 μm with and without exciton enhancement.

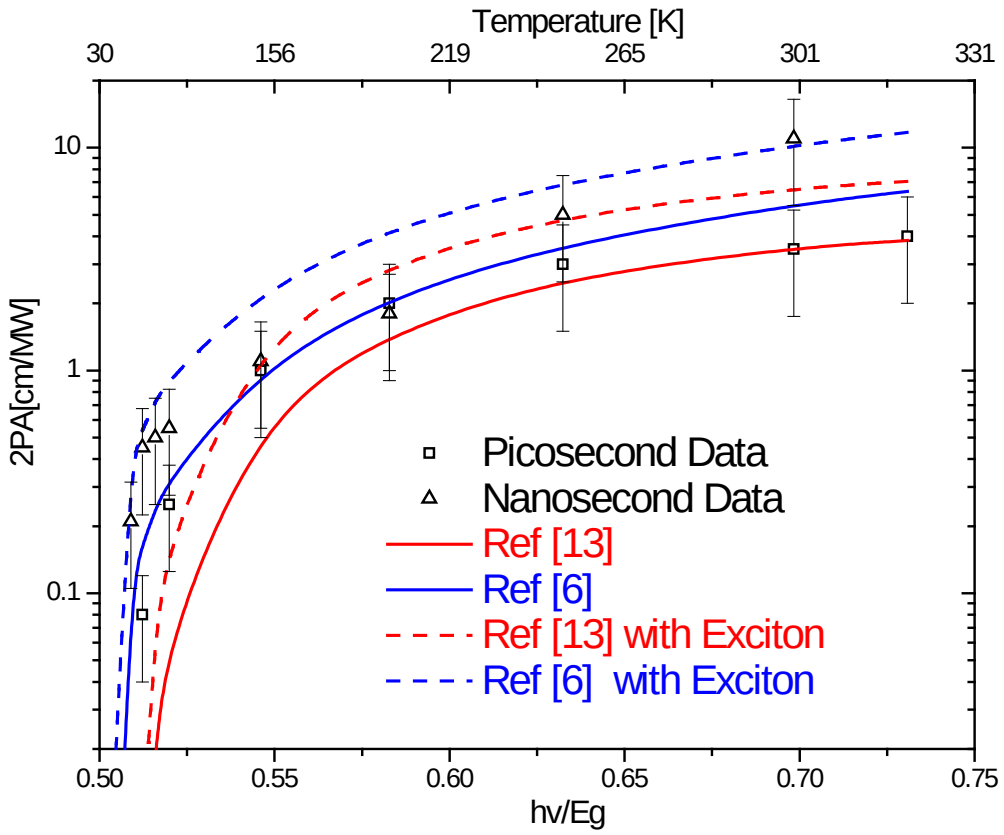

Figure 3.15 2PA vs. temperature at 9.6 μm and 10.6 μm with and without exciton enhancement.

Carrier Recombination Rates

The Shockley-Read-Hall (SRH) recombination involves energy levels related to crystal defects, and is therefore different from sample to sample. The SRH lifetime is taken to be a constant of 2 μs and it is found that this process is negligible for fitting our data and values ranging from 2 μs to 0.5 μs make little difference in the fitting. The parameter B as shown in Fig 3.16 is expected to decrease with increasing temperature [20,24], radiative recombination is therefore varied when fitting the nanosecond nonlinear transmittance data from $B \approx 0.7 \times 10^{-10}$ cm^3/s at 300 K to $B \approx 3.3 \times 10^{-10}$ cm^3/s at 80 K.

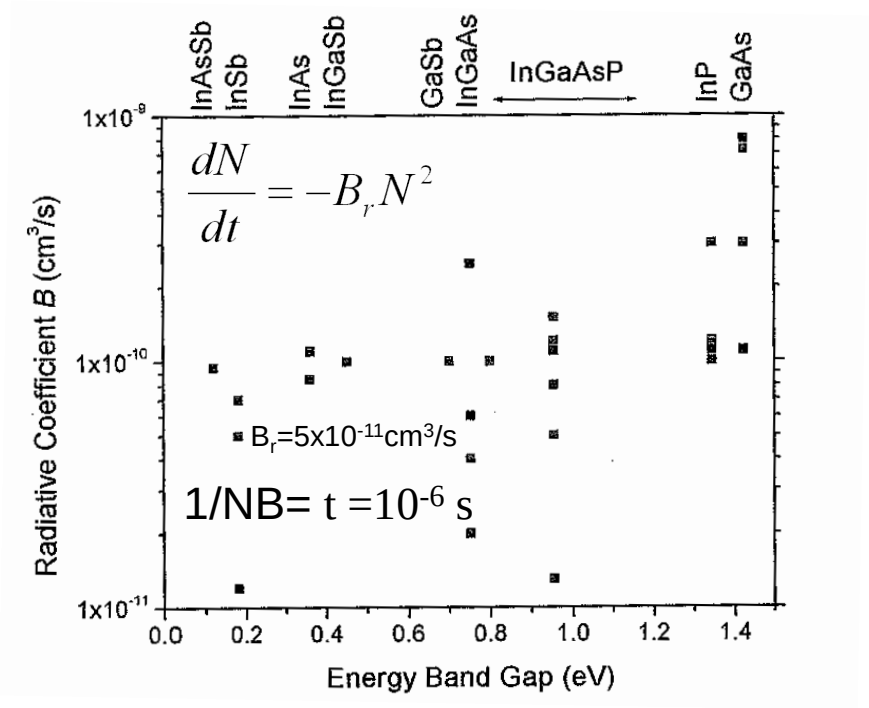

Figure 3.16 Radiative recombination rate for various III-V semiconductors vs. bandgap energy [20].

The Auger rates were determined from picosecond pump probe at room temperature to be $C = 6.5 \times 10^{-26}$ cm^6/s and from fitting the nanosecond nonlinear transmittance data to be $C = 7 \times 10^{-26}$ cm^6/s at 300 K and $C = 30 \times 10^{-26}$ cm^6/s at 80 K. This trend is slightly contradictory with the expected trend since the band gap energy is considerably larger at lower temperature. Auger rates are generally smaller for larger band gap semiconductors as shown in Fig 3.17 [20], and it is predicted by [13] that the Auger coefficient should be approximately four times smaller at 80 K than 300 K. The room temperature value for Auger recombination that we measure is at the lower end but within the range of reported values. [20] Auger recombination is the dominant decay term for modeling the nanosecond data and although literature values for SRH and

radiative were included in the model for nanosecond data they are negligible for fitting picosecond data.

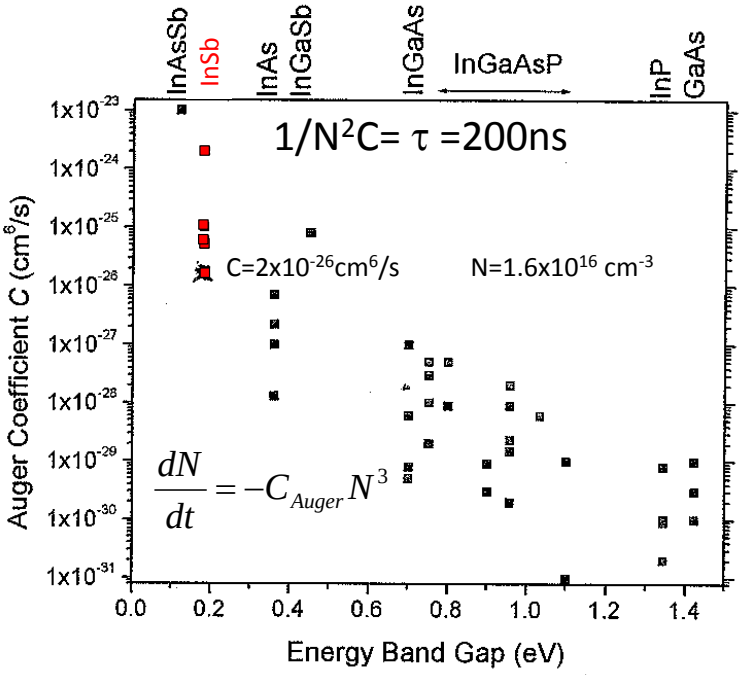

3.17 Auger recombination rates for various III-V semiconductors vs. band gap energy [20].

3.5 Chapter Summary

In this work we present an investigation of both the temperature and spectral behavior of 2PA and FCA in InSb using tunable IR sources with pulse widths spanning 6 orders of magnitude from ~160 fs to ~150 ns. We compare our experimental results to predictions from a simple 2-parabolic band model [6] and to more recent calculations that include a more accurate band structure [13].

The measured 2PA absorption spectrum agrees well with the spectral shape predicted by both theories for thermal variation (80 to 300 K) at fixed wavelengths and for spectral variation (8 to 12 μm) at fixed temperatures. The measured values agree with the new theoretical values for 2PA [13] and 3PA [17] within error; however, the discrepancy between data and theory is

larger near the absorption edge, consistent with exciton enhancement. A comparison of both theories with the picosecond data including exciton enhancement shows improved agreement near the absorption edge. Although the room temperature 2PA values obtained from fitting picosecond and nanosecond data at 10.6μm do not agree within error they are within the range of previously reported values. Also, the picosecond and nanosecond experiments for the temperature dependence of 2PA show good agreement with each other and with theory.

Table 3.1 Two photon absorption coefficient vs. wavelength by fs and ps experiments. NM is not measured.

Wavelength	**hν**	**2PA Coefficient**	
[μm]	**[eV]**	**300K**	
		fs	**ps**
8	0.155	1.5 ± 0.8	2.5 ± 1.2
9	0.138	2.9 ± 1.5	2.8 ± 1.4
9.6	0.129	NM	3.4 ± 1.7
10	0.124	3.6 ± 1.8	NM
10.5	0.118	2.2 ± 1.1	NM
10.6	0.117	NM	3.5 ± 1.8
11	0.113	NM	2.5 ± 1.2
11.5	0.108	2.0 ± 1.0	NM
12	0.103	NM	3.0 ± 1.5
14	0.089	NM	0.5 ± 0.2

Table 3.2 Two photon absorption coefficient versus temperature measured by ps and ns experiments. NM is not measured and NA is not allowed.

Temperature	E_g	2PA Coefficient [cm/MW]			
[K]	[eV]	ps			ns
		9.6 µm	10.6 µm	12 µm	10.6 µm
80	0.228	1.0 ± 0.5	0.08 ± 0.04	NA	0.45
100	0.225	1 ± 0.5	0.25 ± 0.13	NA	0.55
150	0.214	1.5 ± 0.7	1 ± 0.5	NA	1.1
200	0.201	2 ± 1	2 ± 1	0.2	1.8
250	0.185	2.7 ± 1.4	3 ± 1.5	2.25	5
300	0.168	3.4 ± 1.7	3.5 ± 1.8	3.0 ± 1.5	9.5
320	0.160	3 ± 1.5	4 ± 2	NM	NM

FCA cross section values are confirmed through modeling of 1PA, 2PA, and 3PA data. In order to obtain a consistent analysis of the 2PA spectra for nanosecond pulse widths, it is necessary to consider that the FCA cross section as temperature dependent. FCA cross section values were measured at and above 200 K through 1PA via temperature controlled FTIR measurements and temperature controlled linear transmittance measurements of picosecond pulses. This along with FCA values used for the entire temperature range (80 K to 300 K) to fit picosecond Z-scans and nanosecond nonlinear transmittance measurements confirm that the FCA cross section is temperature dependent as recently predicted by theory [13]. Recombination rates are included for modeling nanosecond data and it is found through modeling this data that these rates change with sample temperature. The room temperature values for Auger recombination determined by picosecond pump-probe agree well with values used to fit nanosecond nonlinear transmittance data. The Auger rates were determined from picosecond pump probe at room

temperature to be $C = 6.5 \times 10^{-26}$ cm^6/s $\pm$20% at 300 K and the values used to fit the nanosecond nonlinear transmittance were $C = 7 \times 10^{-26}$ cm^6/s at 300 K and $C = 30 \times 10^{-26}$ cm^6/s at 80 K.

Table 3.3 Free carrier absorption cross section from 180K to 320K at 9.6μm and 10.6μm

Temperature	**Eg**	**σ_{FCA} 9.6μm**	**σ_{FCA} 10.6μm**
[K]	**[eV]**	**($\times 10^{-16}$cm^2)**	**($\times 10^{-16}$cm^2)**
180	0.206	19.0	19.0
190	0.204	15.5	13.4
200	0.201	13.9	12.3
210	0.198	12.4	12.1
220	0.195	12.1	11.1
230	0.192	11.0	10.2
240	0.188	10.2	9.8
250	0.185	9.3	9.0
260	0.182	8.9	8.5
270	0.178	8.3	7.9
280	0.175	7.8	7.6
290	0.171	7.4	7.1
300	0.168	6.9	6.6
310	0.164	6.5	6.2
320	0.160	6.1	6.0

Chapter References

a (Clark-MXR, model 2010) operating at 1 kHz (~ 2 mJ per pulse) at 775 nm, which pumps an optical parametric generator/amplifier and difference frequency generator (OPG/OPA/DFG) Light Conversion Ltd., model TOPAS)

b (EKSPLA, model PL2143) pumping an OPG/OPA/DFG (model: PG401/DFG#80) with tunability from 400nm – 18μm

1 Goeppert-Mayer, "Uber elementarakte mit zwei quantensprungen," M., Ann. Physik, 9, 273 (1931).

2 W. Kaiser and C. G. B. Garrett,"Two-Photon Excitation in CaF_2:Eu^{2+}," Phys. Rev. Lett. **7**, 229 (1961).

3 L.V. Keldysh, Sov. Phys. JETP 20, 1307 (1965).

4 H. D. Jones and H. R. Reiss, Phys. Rev. B 16, 2466 (1977).

5 H.S. Brandi and C.B. de Araujo, "Multiphoton absorption coefficients in solids: a universal curve," Solid State Phys. **16**, 5929 (1983).

6 B.S. Wherrett, "Scaling rules for multiphoton interband absorption in semiconductors," JOSAB **1**, 67 (1984).

7 E.W. Van Stryland, M.A. Woodall, H. Vanherzeele, and M. J. Soileau, "Energy band-gap dependence of two-photon absorption," Opt. Lett., **10**, 490 (1985).

8 M. Sheik-Bahae, D. C. Hutchings, D. J. Hagan, and E.W. Van Stryland, "Dispersion of Bound Electronic Nonlinear Refraction in Solids," IEEE J. Quantum Electron., **27**, 1296 (1991).

9 M. Sheik-bahaei, P. Mukherjee, H. Kwok, “Two-photon and three-photon absorption coefficients of InSb,” JOSAB **3**, 379 (1985).

10 V. Dubikovskiy, D.J. Hagan, and E.W. Van Stryland, “Large nonlinear refraction in InSb at 10μm and the effects of Auger recombination,” JOSAB **25**, 223 (2008).

11 C.L. Littler and D.G. Seiler, “Temperature dependence of the energy gap of InSb using nonlinear optical techniques,” Appl. Phys. Lett. **46**, 987 (1985).

12 S.W. Kurnick and J.M. Powell, “Optical Absorption in Pure Single Crystal InSb at 298 and 78K,” Physical Review **116**, 597 (1959).

13 S. Krishnamurthy, Z. G. Yu, L. P. Gonzalez, S. Guha, “Accurate evaluation of nonlinear absorption coefficients in InAs, InSb, and HgCdTe alloys,” JAP, **101**, 113104 (2007).

14 C. N. Ironside, “Two-Photon Gain Semiconductor Amplifier,” IEEE J. Quantum Electron., **28**, 842 (1992).

15 M. Sheik-Bahae, A. A. Said, T.-H. Wei, D. J. Hagan, and E. W. Van Stryland, “Sensitive measurement of optical nonlinearities using a single beam,” IEEE J. Quantum Electron., **26**, 760 (1990).

16 M. Sheik-Bahae, A. A. Said, and E. W. Van Stryland, “High-sensitivity single-beam n_2 measurements,” Optics Letters, **14**, 955 (1989).

17 C. M. Cirloganu, P. D. Olszak, L. A. Padilha, S. Webster, D. J. Hagan, and E. W. Van Stryland, “Three-photon absorption spectra of zinc blende semiconductors: theory and experiment,” Opt. Lett. **33**, 2626 (2008).

18 A. Garg, et al., “Evolution of laser damage in Indium Antimonide (InSb) at 1.06μm wavelength,” Lasers in Material Processing and Manufacturing II, Proc. of SPIE **5629**, 361 (2005).

19 V. Dubikovskiy, “Optical Limiting: Numerical Modeling and Experiment,” University of Central Florida, CREOL PhD Dissertation Ch.3, 89 (2003).

20 J. Piprek, “Semiconductor Optoelectronic Devices: Introduction to Physics and Simulation” Academic Press, Ch 3.7 (2003).

21 H.J Fossum and B. Ancker-Johnson, “Radiative Recombination of Electron-Hole Pairs Generated by Two-Photon Absorption in Indium Antimonide,” Phys. Rev. B **8**, 2850 (1973).

22 C. C. Lee and H. Y. Fan, “Two-photon absorption with exciton effect for degenerate valence bands,” P.R.B **9**, 3502 (1974).

23 Weiler, “Nonparabolicity and exciton effects in two photon absorption in zinc-blend semiconductors,” Solid State Comm. **39**, 937 (1981).

24 R. D. Grober, H. D. Drew, G. L. Burdge, B. S. Bennett, “Direct measurement of the recombination rates in bulk InSb by time-resolved photoluminescence,” J. Appl. Phys. **71**, 5140 (1992).

CHAPTER 4. THREE PHOTON ABSORPTION IN DIRECT BAND GAP SEMICONDUCTORS

4.1. Introduction

The theory for three-photon absorption (3PA) in semiconductors using different energy-band models was investigated by Yee in 1971 [1]. He considered an anisotropic effective mass and included more than one degenerate valence band in his model. The theory of scaling rules for multiphoton interband absorption assuming an isotropic effective mass and only two parabolic bands was developed for N-photon absorption by Brandi and de Araujo in 1983 [2], and Wherrett in 1984 [3]. These theories used different theoretical approaches, Brandi and de Araujo using Keldysh's tunneling approach and Wherrett using perturbation theory, but both theories predicted the absorption coefficient to be inversely proportional to the band-gap energy as E_g^{4N-5} leading to E_g^{-3} for 2PA and E_g^{-7} for 3PA [2, 3]. The objective was to obtain the relative scaling of the absorption and not necessarily the absolute magnitude of the absorption coefficient. Brandi and de Araujo scaled the calculated two-photon coefficient by an arbitrary factor of six to match data for CdS [2].

As mentioned in the previous chapters, two-photon absorption was shown to scale with E_g^{-3} as predicted by Wherrett [4]. The 2PA of new materials can be predicted by,

$$\alpha_2 = K_2 \frac{\sqrt{E_p}}{n^2 E_g^3}\left[\frac{((2\hbar\omega/E_g)-1)^{3/2}}{(2\hbar\omega/E_g)^5}\right] \qquad [4\text{-}1]$$

with a value K_2=1940 $eV^{5/2}$cm/GW calculated from first principles and universal constants used in the theory and with K_2=3100 in the same units obtained from fitting data from several

semiconductors with different band-gap energies [4]. While 2PA has been extensively studied in semiconductors, much less is known about 3PA. Three-photon absorption is less well understood partly due to increased level of difficulty in the experiment, and partly because the process is theoretically more complex. Three-photon absorption is expected to scale with E_g^{-7} as predicted by Wherrett's theory with α_3 given by:

$$\alpha_3 = K_3 \frac{\sqrt{E_p^3}}{n^3 E_g^7} \left[\frac{((3\hbar\omega / E_g) - 1)^{1/2}}{(3\hbar\omega / E_g)^9} \right], \qquad [4\text{-}2]$$

where K_3 is a constant, n is the refractive index, and $E_p \approx 21$eV is the Kane momentum parameter [4]. Although 3PA in InSb had been previously reported [5], theoretical models had not been verified using a variety of direct gap semiconductors. In this work we have measured 3PA in ten semiconductors, and we report K_3=25.1 $eV^{11/2}cm^3/GW^2$ as calculated by Woodall to be in general agreement with data over two orders of magnitude in band-gap [6].

4.2. Experimental procedure and data

The Z-scan technique introduced in Ch.2 is useful in determining the magnitude of absorptive optical nonlinearities such as multiphoton absorption [7]. A tunable infrared femtosecond source was used in this study to achieve the large irradiances necessary for 3PA and to avoid significant free carrier absorption encountered with longer pulse widths. In order to study 3PA in semiconductors it is important to use wavelengths corresponding to $E_g/3 < \hbar\omega < E_g/2$, therefore allowing 3PA and not 2PA as shown in Fig 4.1.

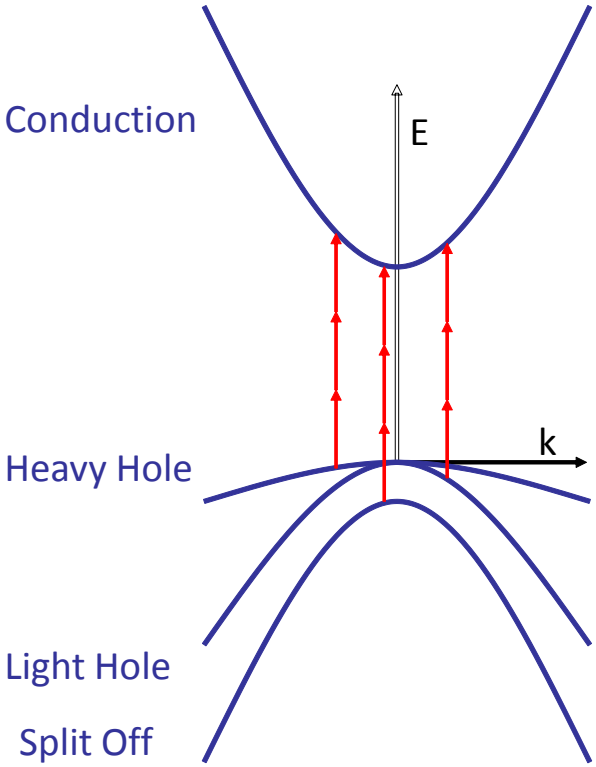
Conduction
E
k
Heavy Hole
Light Hole
Split Off

wavelength range from 1μm to 5μm. An autocorrelator was also built into the setup so that the pulse width could be measured for each wavelength used. The optics for the Z-scan and autocorrelator were chosen so that the beam passed through identical optics in each experiment to ensure that the pulse width measured in the autocorrelator was the same as in the sample. This setup was used to measure 3PA Z-scans in GaAs with wavelengths between 1.9μm to 2.7μm and could be used to measure nonlinear absorption in a variety of IR materials including CdTe, InP, GaSb, InGaSb, and InAs.

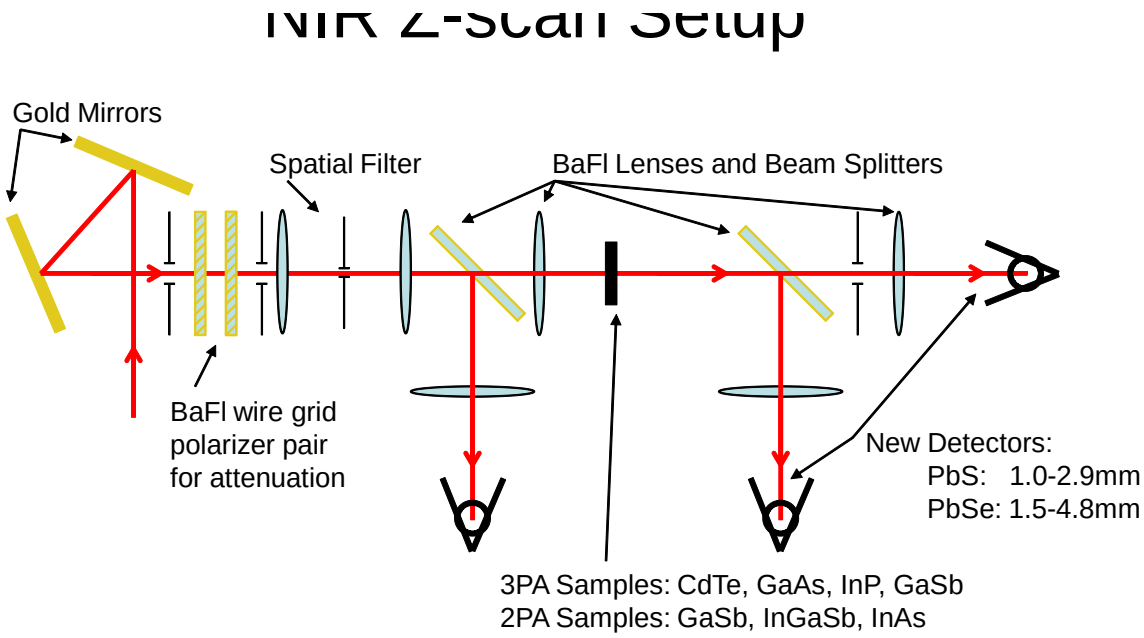

Figure 4.2 Z-scan setup built to allow measurement of the 3PA spectrum of GaAs. This setup also enables the measurement of 3PA spectrum in other samples of interest such as CdTe, InP, and GaSb, as well as 2PA in GaSb, InGaSb, InAs. This setup is aligned with a HeNe that is made collinear with the IR beam.

The Z-scan experiment was repeated for several pulse energies for each sample and each curve was fit independently for the absorption coefficient. For ZnS, ZnSe, and GaAs this

procedure was repeated at many wavelengths to study the spectral dependence of the 3PA. An example of the open aperture Z-scan data and fitting for ZnSe at 1050nm and 1300nm is shown below in Fig 4.3.

4.3. Band gap Scaling of Three Photon Absorption

The values for α_3 obtained from data and material parameters used in calculating the theoretical absorption coefficients are listed in Table 4.1. The scaled 3PA coefficients obtained from experiment are shown in Fig. 4.3 versus band-gap energy. The fit for the data is found to be K_3=25 $eV^{11/2}cm^3/GW^2$, agreeing with the theory from Wherrett and (using f_6/f^3= 5) as estimated by Woodall [6]. These f factors are correction factors that are related to angular averaging in Wherrett's theory and are often omitted in the literature as they are omitted in equation 22 of [3]. Since this theory was only expected to give order-of-magnitude agreement, it is not surprising that factors thought to be on the order of unity [6] might be neglected. Using this value for K_3 gives agreement within a factor of two for most data shown in Table 4.1; however, the literature values shown for the narrow gap materials InAs and InSb are different from the theoretically estimated value by an order of magnitude. The data for InAs was taken using a picosecond OPA/OPG and free carrier absorption was considered in modeling the data. The data for InSb was taken using a 150ns CO2 laser and free carrier absorption and recombination were considered in modeling the data. These longer pulse width measurements have the disadvantage associated with free carrier effects, but there are also many difficulties that arise with femtosecond measurements in the mid infrared as discussed in CH.3. The values measured at 1064nm were obtained more than twenty years ago (tunable femtosecond systems like the one

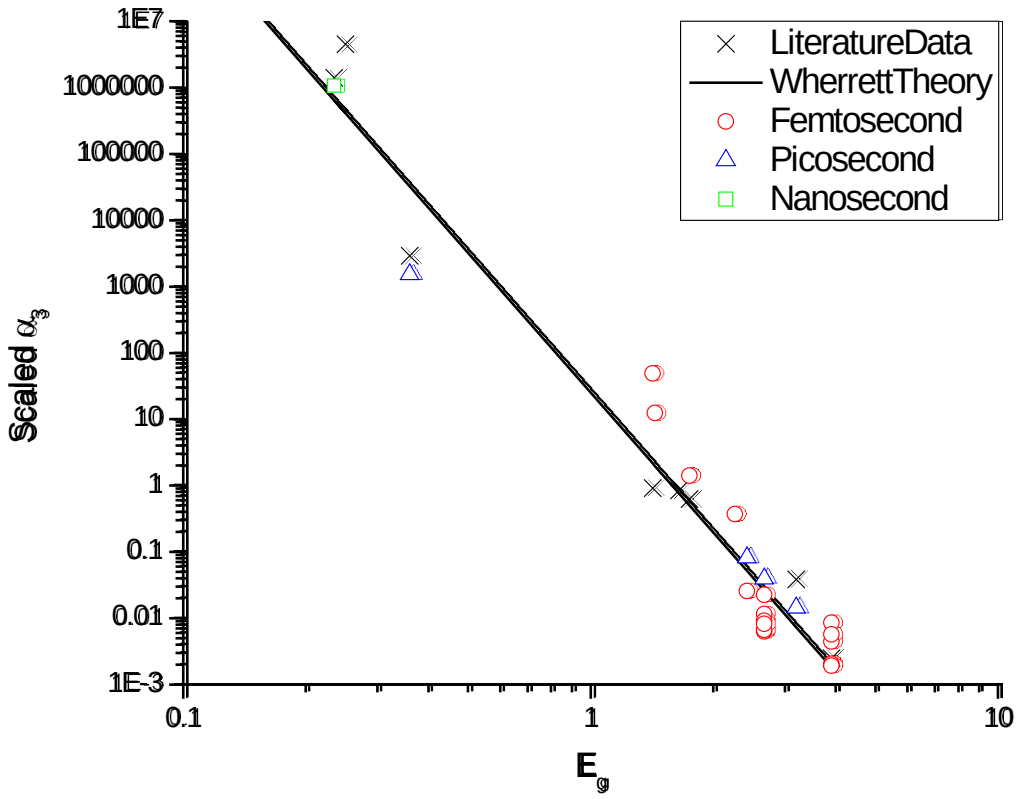
LiteratureData
WherrettTheory
Femtosecond
Picosecond
Nanosecond
Scaled α_3
E_g
1E7
1000000
100000
10000
1000
100
10
1
0.1
0.01
1E-3
0.1
1
10

Table 4.1 Important parameters and three-photon absorption coefficients.

Material	E_g[eV]	λ[μm]	n	E_p[eV]	Data α_3 [cm^3/GW^2]	Wherrett's Theory $K_3 = 25.1\ \alpha_3$ [cm^3/GW^2]
ZnS [10]	3.66	0.76	2.3	20.4	0.0019	0.0009
ZnS [10]	3.66	0.8	2.3	20.4	0.0017	0.0012
ZnS	**3.66**	**0.8**	**2.3**	**20.4**	**0.0014**	**0.0012**
ZnS	**3.66**	**0.85**	**2.3**	**20.4**	**0.0018**	**0.0017**
ZnO [10]	3.2	0.8	2.05	21	0.010	0.0019
ZnO [10]	3.2	0.9	2.05	21	0.0054	0.0044
ZnO	**3.2**	**1.05**	**2.05**	**21**	**0.0047**	**0.0106**
ZnO	**3.2**	**1.06**	**2.05**	**21**	**0.0220**	**0.0112**
ZnSe	**2.67**	**1.05**	**2.48**	**24.2**	**0.0078**	**0.0090**
ZnSe	**2.67**	**1.06**	**2.48**	**24.2**	**0.015**	**0.0099**
ZnSe	**2.67**	**1.2**	**2.48**	**24.2**	**0.0074**	**0.0211**
ZnSe	**2.67**	**1.3**	**2.48**	**24.2**	**0.0075**	**0.0290**
CdS	**2.42**	**1.06**	**2.34**	**21**	**0.015**	**0.009**
CdS	**2.42**	**1.2**	**2.34**	**21**	**0.011**	**0.022**
ZnTe	**2.26**	**1.3**	**2.8**	**19.1**	**0.02**	**0.028**
CdSe	**1.74**	**1.5**	**2.5**	**21**	**0.24**	**0.085**
CdSe [12]	1.74	1.54	2.5	21	0.13	0.103
AlGaAs[11]	1.648	1.55	3.34	21	0.055	0.045
CdTe	**1.44**	**1.75**	**2.7**	**20.7**	**1.2**	**0.19**
GaAs	**1.42**	**1.75**	**3.4**	**25.7**	**3**	**0.13**
GaAs [8]	1.42	2.3	3.4	25.7	0.35	0.82
InAs [9]	0.36	9.54	3.42	21	1000	11000
InAs	**0.36**	**8**	**3.42**	**21**	**200**	**4200**
InSb [5]	0.25	10.6	3.95	21	200000	18400
InSb [13]	0.235	10.6	3.95	21	40000	18000
InSb	0.235	10.6	3.95	21	30000	18000

The scaled 3PA value in Fig. 4.3 is $\alpha_3 n^3 / (E_P^{3/2} F3) = K_3/E_g^7$. The spectral function, F3 (given by the bracketed portion of Eq. 2) suggested by Wherrett is different from the F3 suggested by Brandi and de Araujo [2, 3]. Without data on the frequency dependence of 3PA, it is impossible to verify any particular theory. The vertical span of values shown in Fig. 4.3 for ZnSe and ZnS demonstrates that Wherrett's spectral function generally agrees with data taken at different wavelengths. The trend of the data for ZnSe and ZnS shown in Fig. 4.3, along with data for GaAs [8], suggests that the spectral dependence of 3PA is different than predicted by Wherrett. The agreement of data and theory depends on the wavelength for each calculated theoretical value.

It is important to note that although most of the literature on 3PA refers to Wherrett's theory, each study uses a different arbitrary scaling constant to obtain a theoretical value. Sometimes, a theoretical value is obtained by taking an experimental value and applying the scaling rules to estimate a value for another material, which is the justification for an arbitrary scaling factor [2]. For example, InAs was determined to have a theoretical 3PA value of α_3 = 1,800 cm^3/GW^2 [9], but the value predicted by the present work is 11,000 cm^3/GW^2. It was suggested recently that the spectral function of Brandi and de Araujo might show better agreement for the wide gap materials ZnO and ZnS [10]; however, for AlGaAs the trend of the data from 1500nm to 1650nm shows agreement with Wherrett's theory [11]. CdSe was determined to have a theoretical 3PA value of α_3 = 0.05 cm^3/GW^2 [12], but the value predicted by the present work is 0.10 cm^3/GW^2. It should also be noted that absorption observed in InSb was concluded not to be due to 3PA, partially based on the magnitude of the value obtained by fitting the data [13].

4.4. Spectral Dependence of Three Photon Absorption

The approach of this work was to use many materials to determine a reasonable empirical constant or average scaling factor for 3PA theory. We have measured 3PA in ten binary semiconductors including narrow band-gap and wide band-gap samples. To the best of the authors' knowledge this work includes the first reported experimental values for 3PA in bulk ZnSe, ZnTe, and CdTe [14]. The scaled 3PA coefficients obtained from experiment were plotted versus band-gap energy. The band-gap scaling of the 3PA coefficient was found to vary as Eg^{-7} as predicted by theory. The best fit for the data is found to be K_3=25.1 $eV^{11/2}cm^3/GW^2$. Using this value gives agreement within a factor of two for most data; however, the values obtained for the narrow gap materials are different than the theoretically estimated values by an order of magnitude. The 3PA spectra predicted by Wherrett peaks close to $E_g/3$ while the theory of Brandi and de Araujo peaks closer to $E_g/2$. This is not surprising since Wherrett assumed the allowed-allowed-allowed transitions between the light hole and the conduction band to be dominant while Brandi and de Araujo assumed path ways including self transitions dominated as shown in Fig 4.4.

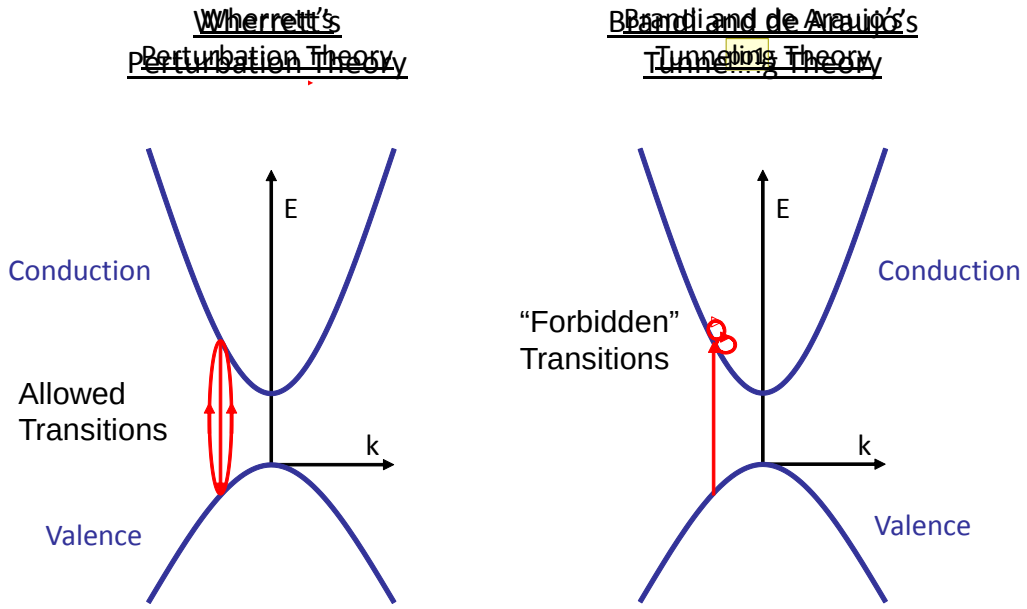

Figure 4.4 Wherrett's theory followed a perturbation approach and assumed allowed transitions dominated while Brandi and de Araujo used a tunneling theory which is equivalent to the assumption of forbidden transitions being dominant.

It is likely that transition schemes including other additional factors such as self transitions and additional bands could easily introduce a factor of four [3]. These additional factors could influence the wavelength dependence of 3PA. Indeed, the 3PA data for ZnS and ZnSe shown as vertical columns earlier in Fig. 4.3 appears in Fig 4.5 to be more flat on a log scale than the spectral scaling predicted by Wherrett with the biggest discrepancy near the 2PA edge, while the theory of Brandi and de Araujo has discrepancy near the 3PA edge.

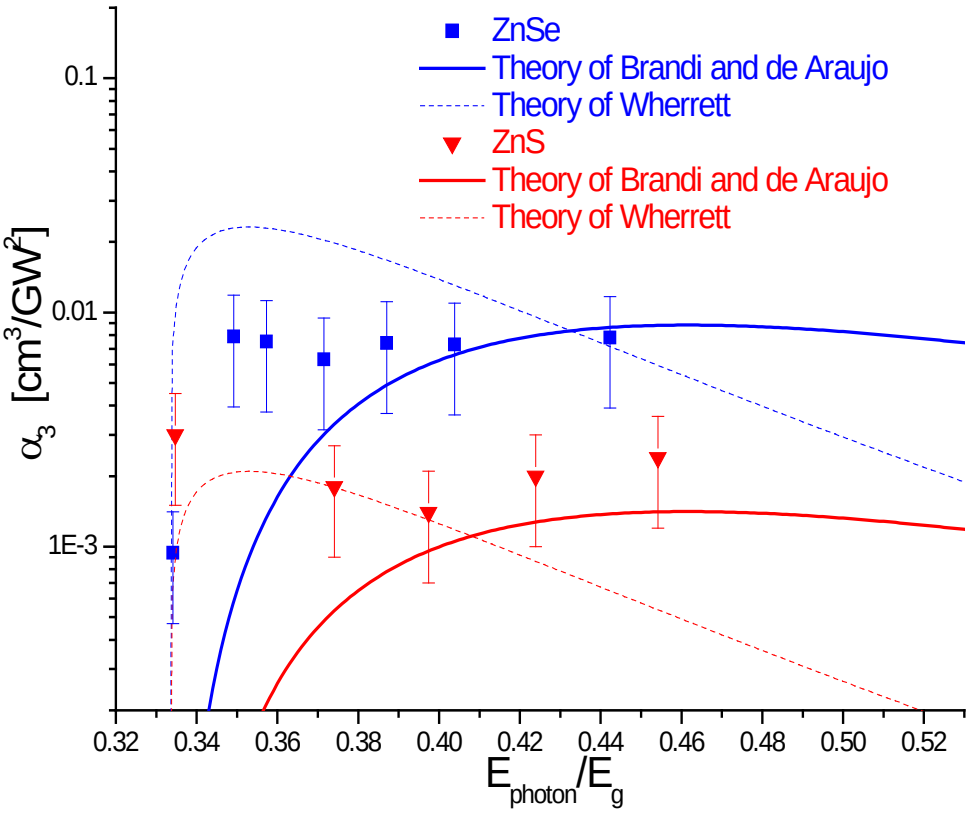

Figure 4.5 Plot of the scaled 3PA coefficient for ZnSe (Blue) and ZnS (Red) versus E_{photon}/E_g. The solid line is the theory of Brandi and de Araujo multiplied by an arbitrary factor of five, and the dashed line is the theory of Wherrett using the estimated scaling parameter K_3=25.1

A more detailed theoretical approach including all possible transitions for a four band model was then developed by our group and shown to agree with the measured spectral data for several zinc-blend semiconductors which is part of another dissertation (Claudiu Cirloganu's) from our research group. A comparison of the theoretically predicted 3PA spectrum for ZnSe from [15] is shown in Fig.4.6.

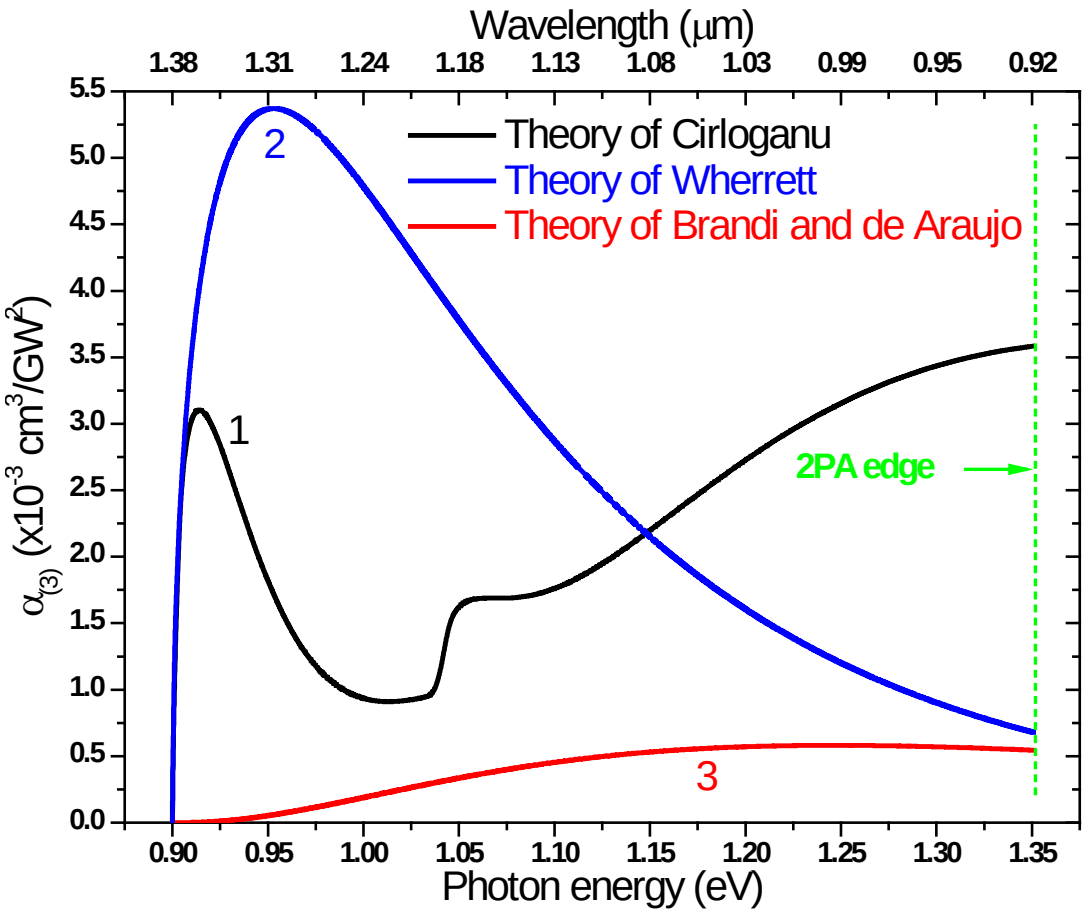

Figure 4.6 Comparison of 3PA spectrum predicted for ZnSe by different theories

The experiment for ZnSe was then repeated using more wavelengths and with attention to the photon energies where sharp spectral features were predicted for example near the split off edge in the middle of the 3PA spectrum. This data is consistent with the data shown earlier on a log scale, however small step sizes are deliberately used here where sharper features in the theory are expected. The relative error due to day to day variations in the laser system is reduced by taking the spectrum in a shorter time frame. In this repeated experiment all data shown was obtained in one continuous session. Results of these experiments compared to the four band theory scaled by an arbitrary factor of 3.2 are shown in Fig.4.7 from Ref [15].

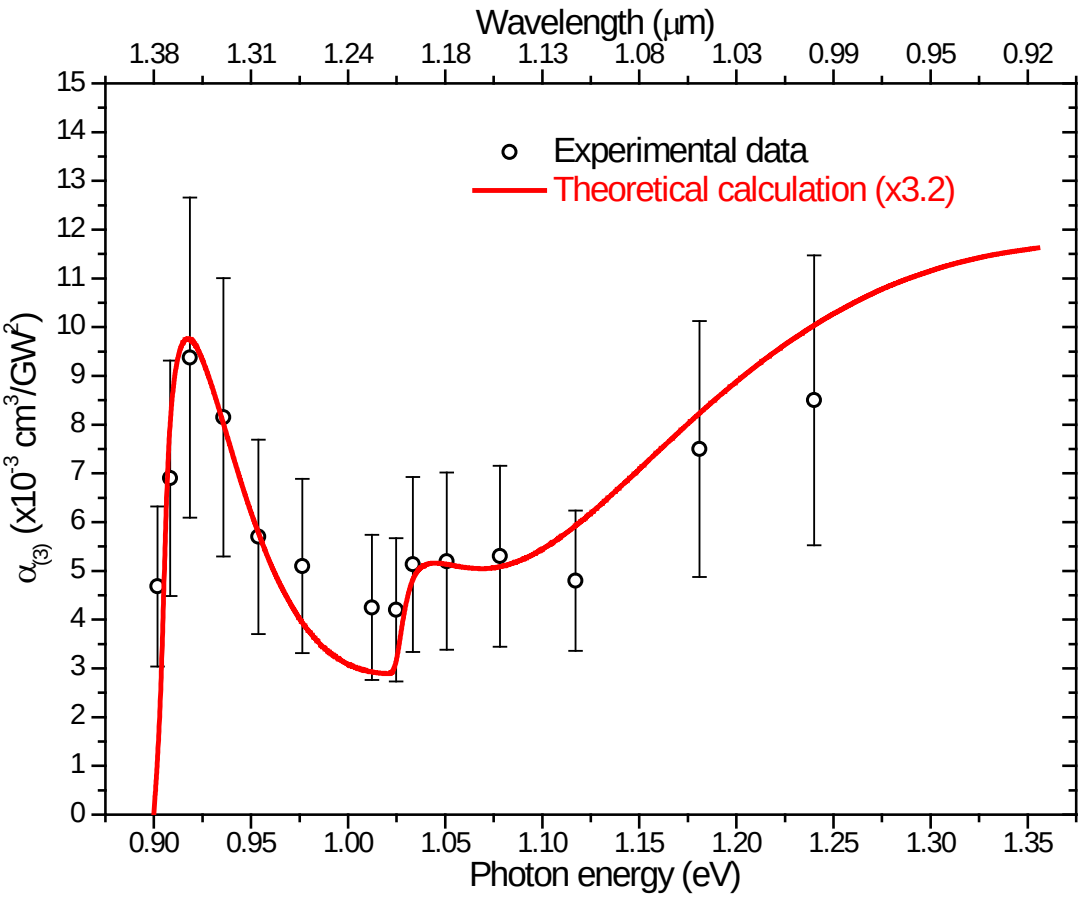

Figure 4.7 Data for 3PA in ZnSe obtained from fitting Z-scans compared to calculated value from four band model scaled by an arbitrary factor of 3.2.

This data shows agreement with all the salient features of the new theoretical 3PA spectrum. The location and width of the spectral peak coincide with the data and the location of the absorption edge due to the band gap energy is observed. The feature predicted and resolved in the middle of the spectrum due to the split off energy and this is the absorption edge near 1.2μm for transitions including that band. Multiphoton absorption is demonstrated here to be an alternative method of measuring the split off energy. For 3PA the split off band edge is observed in the spectrum if the split off energy is less than half the band gap energy. The split off energy

can be used as a fitting parameter for calculating the theoretical spectrum. Since 3PA edges are sharp spectrally, this could quite possibly be a more precise way of determining the band gap and split off energy than other standard methods which use one photon absorption data. The last and perhaps most important point about this 3PA theory that is confirmed by the data is that the magnitude of the absorption is just as large near the 2PA edge ($E_g/2$) as at the peak near the 3PA edge ($E_g/3$). This is extremely important for estimating (as was done in previous work [13]) the influence of 3PA near the 2PA edge where it was predicted by Wherrett's theory to be an order of magnitude smaller. If one underestimates the magnitude of 3PA then it is possible to mistakenly neglect the process or attribute the loss to another process thus distorting interpretation of experimental results.

Previously published experiments were compared to the theories of Brandi and De Araujo or Wherrett. The agreement found depended on whether data was taken closer to the 2PA edge or the 3PA edge. This work shows that neither theory correctly predicts the spectral shape of 3PA and explains why previous results tended to agree with one theory or another. For example published spectral data shown in Fig. 4.8 taken using ZnS and ZnO was thought to agree quite well with the theory of Brandi and De Araujo. However, this data did not include wavelengths close enough to the 3PA edge to show the 3PA peak.

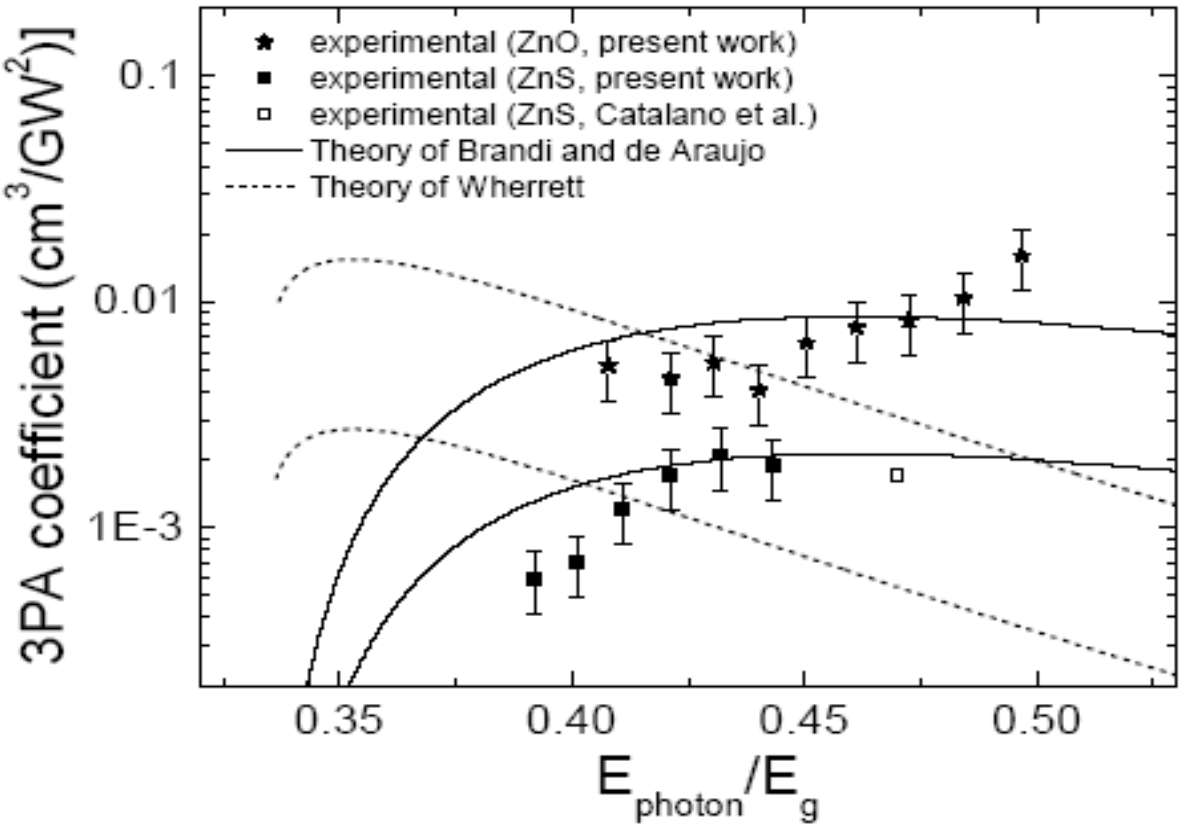

Figure 4.8 Literature data for 3PA in ZnS andZnO [10] showing an increasing trend toward $E_{photon}=E_g/2$consistent with the theoretical prediction of Brandi and de Araujo.

By taking Z-scan data over the entire spectrum we were able to confirm the four band theory used for ZnSe also explained the 3PA spectrum of ZnS. [15]. This data compared to theory along with previously published data for ZnS are shown in Fig. 4.9. This data shows the peak of the 3PA spectrum and agrees with the overall structure predicted by the four band theory. The previously published data also agrees reasonably well with the theoretical spectrum. [15].

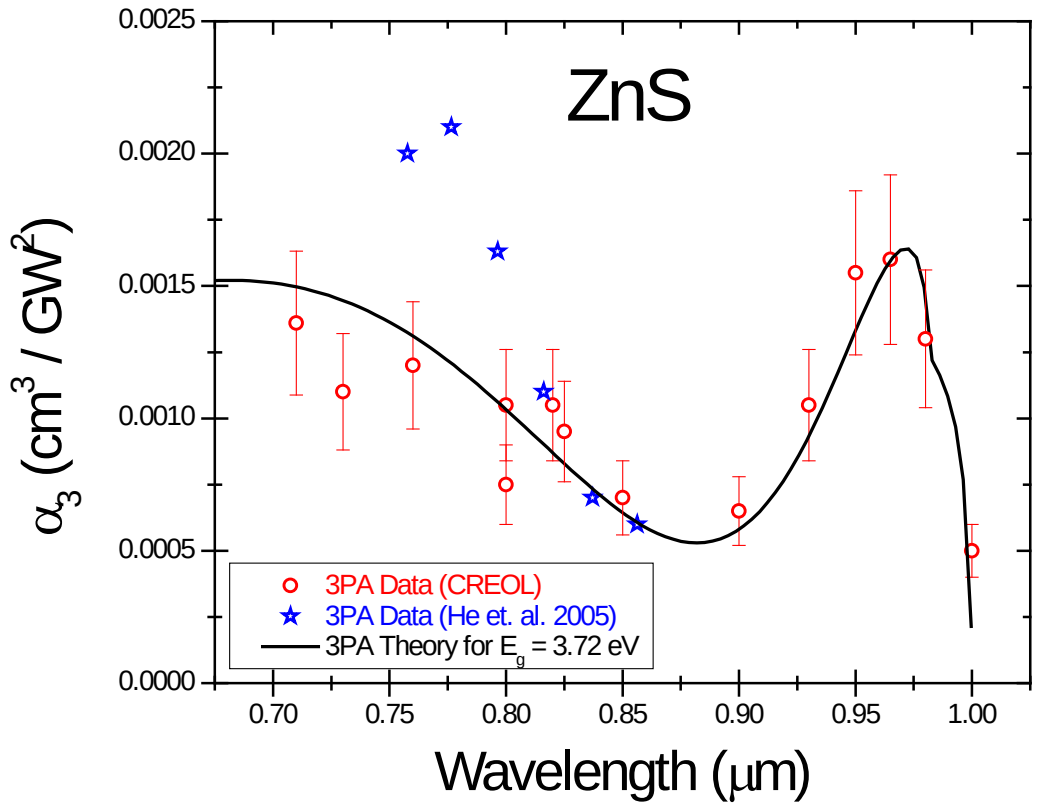

Figure 4.9 Theoretical curve for 3PA spectrum of ZnS (solid line) compared to literature data [11] (stars) and data from the present work (circles).

4.5. Three Photon Absorption Spectrum of GaAs

Now having obtained agreement for the wide gap semiconductor ZnS and the widely used semiconductor ZnSe, the narrower band gap and commonly used semiconductor GaAs was chosen as a sample for 3PA experiments. Data for the 3PA spectrum shown in Fig. 4.10 had been recently published [8]; however, only four wavelengths were shown making it difficult to confirm any theory.

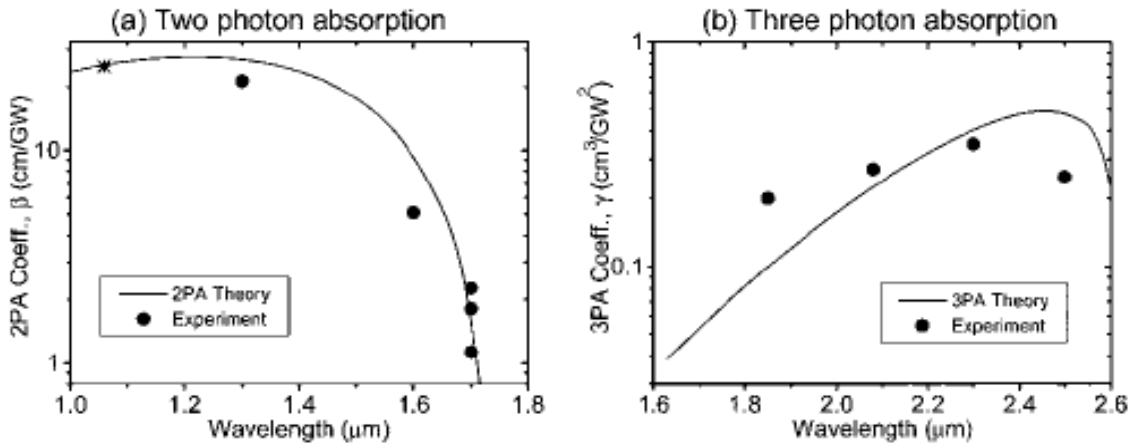

Figure 4.10 Previously published comparison of 2PA and 3PA data for GaAs to Wherrett's theory. [8]

The Z-scan data is fit using the measured pulse widths for each wavelength which ranged from 160fs to 430fs full width at half the maximum. The measured pulse width vs. wavelength fit with a linear function is shown in Fig. 4.11.

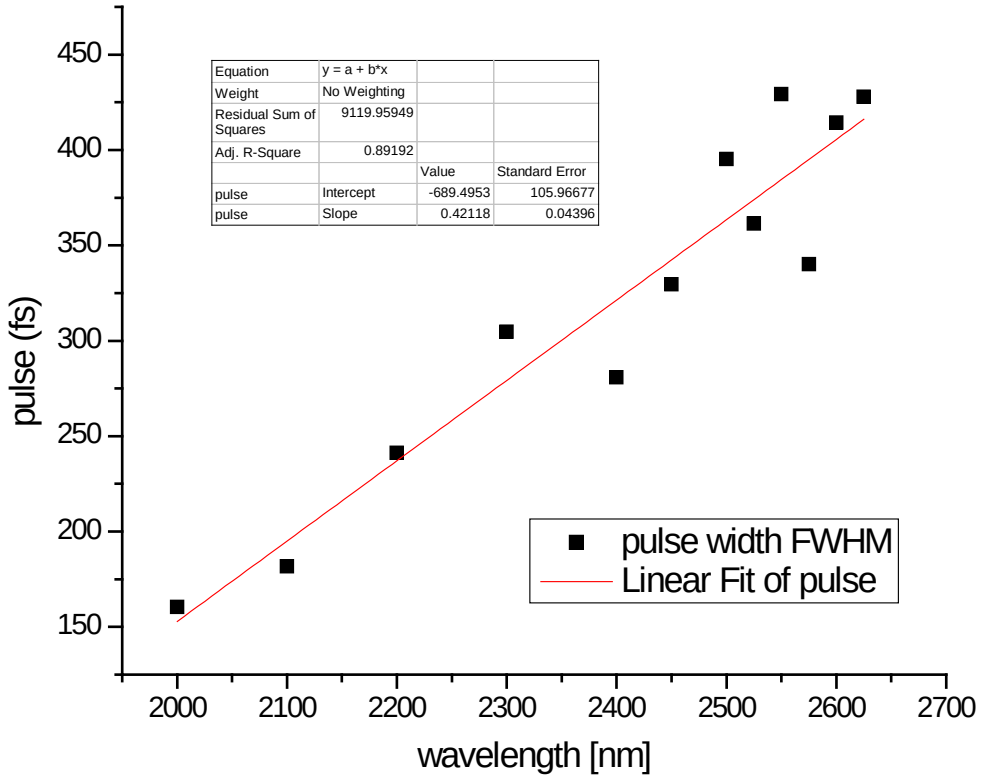

Figure 4.11 Pulse width measured by intensity autocorrelation using a Michelson interferometer built into the Z-scan setup so that the pulse width at the sample is the same measured. The pulse width gets larger toward longer wavelengths and the data is fit with a linear function.

An example of intensity autocorrelation data taken at 2575nm and fitting is shown in Fig. 4.12. A Gaussian pulse is assumed and therefore the autocorrelation width is divided by 1.414 to obtain the pulse width.

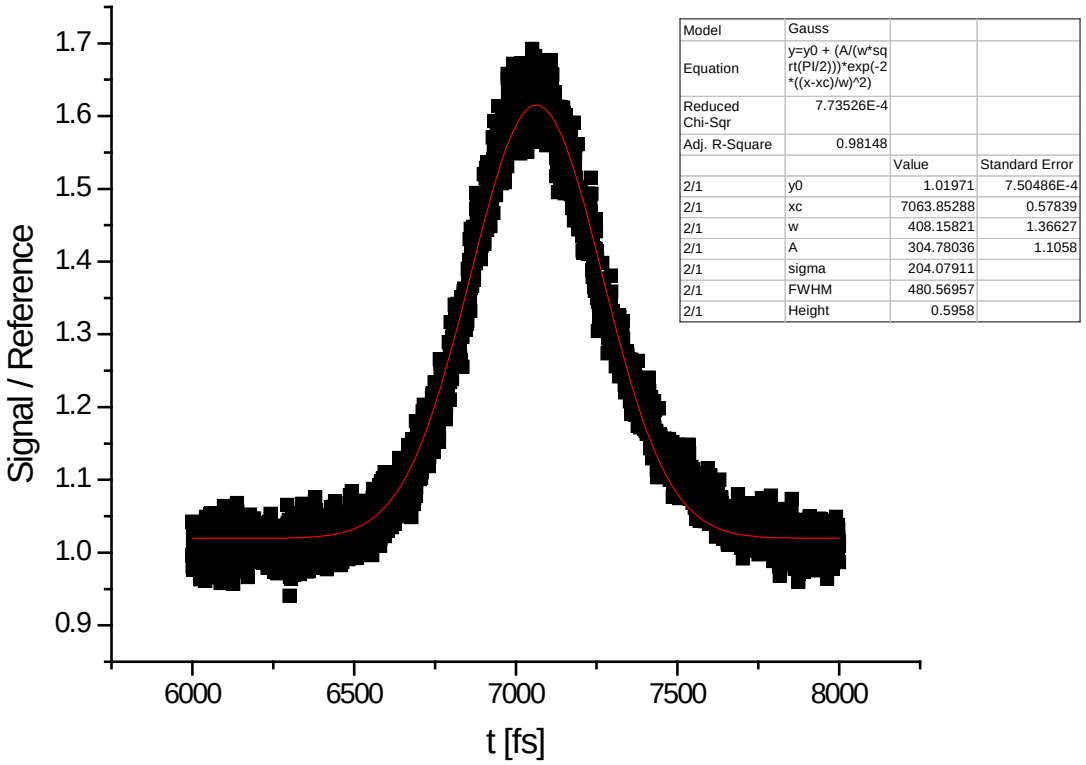

Figure 4.12 Intensity autocorrelation data taken at 2575nm fit to a Gaussian showing that the pulse width (FWHM) is 480fs divided by 1.414 for a Gaussian pulse.

Since the pulse width was nearly half a picosecond a transform limited pulse would have a bandwidth of about 25nm. The system is pumped by a 150fs Titanium Sapphire laser and it is more likely that the pulses used in this experiment were chirped. If the bandwidth of the pulse is too broad, then it is possible that the absorption spectrum measured is smoothed and distorted. A monochrometer and PbS detector were used to measure the spectrum of the pulse at the setup for each wavelength used. The measured pulse spectrum was corrected by the responsivity of the PbS detector shown in Fig 4.13.

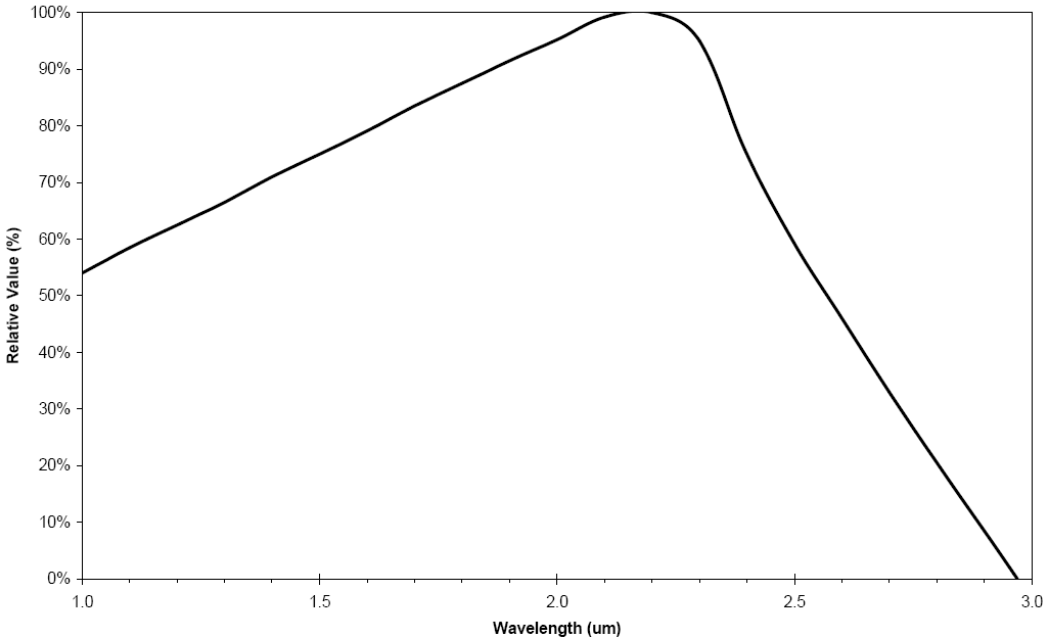

Figure 4.13 Responsivity spectrum of the Thor Labs PDA 30G PbS detector used in the 3PA Z-scan, autocorrelation, and pulse spectrum measurements. The pulse spectrum measurements must be corrected by the relative responsivity at each wavelength to obtain the corrected spectral intensity of the pulse.

Examples of the corrected pulse spectrum at 2.4μm and 2.6μm are shown in Fig. 4.14 and Fig 4.15.

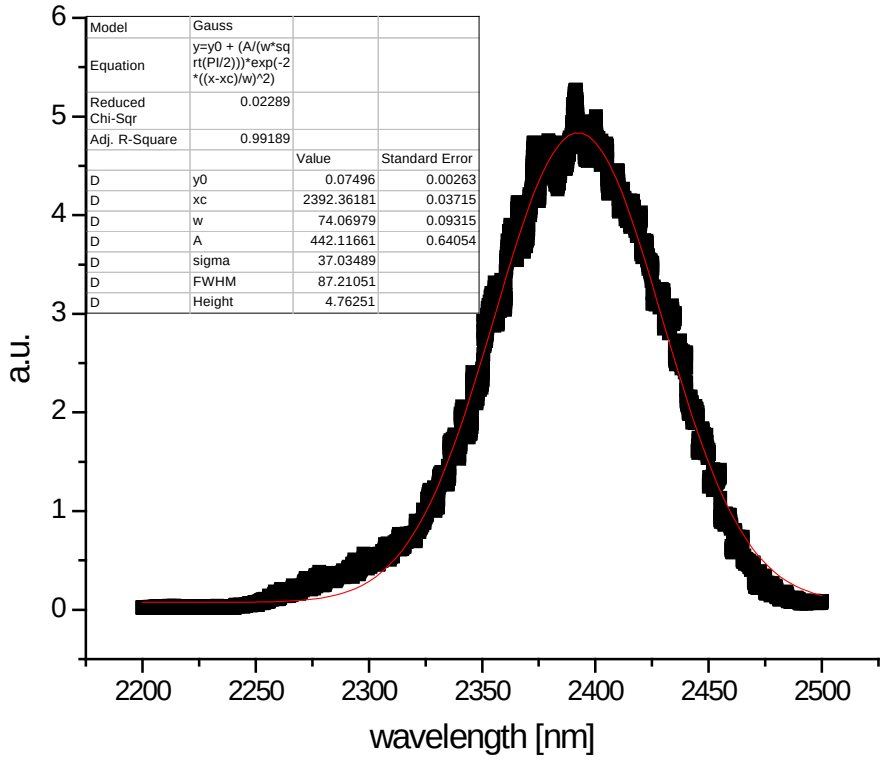

Figure 4.14 The spectral intensity of the pulse measured at 2400nm by scanning a monochrometer and then correcting for the responsivity of the PbS detector.

The bandwidth of the pulse between 2.4μm and 2.6μm was found to be approximately 100nm which is about 4 times larger than the bandwidth. Therefore at 2.55μm where the 3PA peak is expected to be observed some of the pulse energy is carried by photons with energies below the 3PA edge.

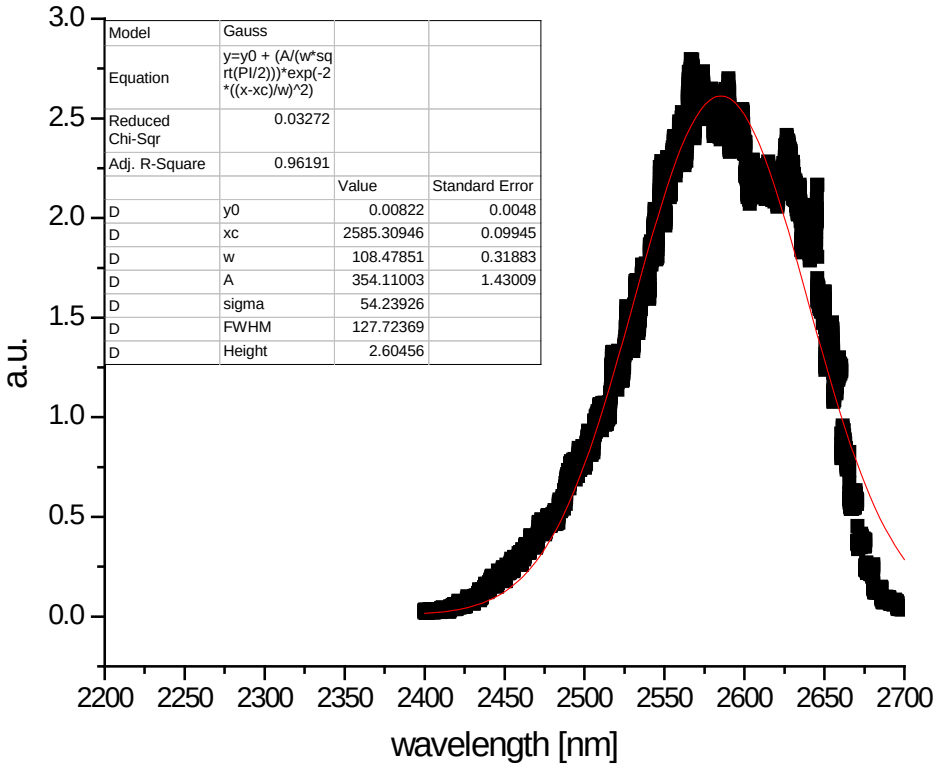

Figure 4.15 The spectral intensity of the pulse measured at 2575nm by scanning a monochrometer and then correcting for the responsivity of the PbS detector.

A comparison of 3PA theory convolved with different bandwidth pulses is shown in Fig. 4.16 to illustrate the problem described above and compare with measured data for small signals from the following equation,

$$1-\alpha_3^{raw} I_0^{\,2} L \approx \frac{1}{\Delta\omega}\int f(\omega)d\omega - \frac{1}{\Delta\omega}\int \alpha_3(\omega) I_0^{\,2} f^3(\omega) L d\omega \qquad [4\text{-}3]$$

As the bandwidth becomes large the assumption that the pulse is nearly monochromatic with a wavelength equal to the spectral peak of the source breaks down and it becomes more important to consider nondegenerate nonlinear absorption. The nondegenerate absorption should allow

some photons past the band edge to be absorbed when paired with higher energy photons within the pulse. All these effects serve to complicate the analysis and it is preferred that a narrower bandwidth source be used to measure the pulse. This can be achieved by using a spectral filter to limit the bandwidth of the source. A tunable band pass filter with a bandwidth of 25nm and a center wavelength range from 1.9μm to 2.7μm would be an ideal solution as long as there is enough energy. A throughput of 50% for such a filter should be sufficient with the system used in these experiments.

$$\text{Convolution}(a,b,x) := \sum_{i=1}^{N-1}\left[\alpha_i\cdot\left[\frac{a}{b\cdot\sqrt{\frac{\pi}{2}}}\cdot e^{\left[-2\left(\frac{x-\lambda_i}{b}\right)^2\right]}\right]\right]^3$$

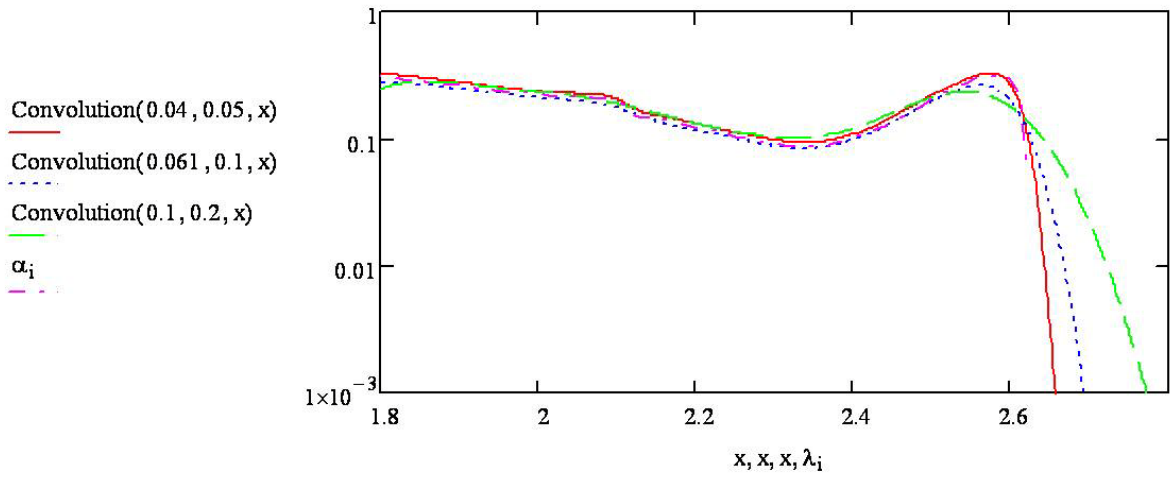

Figure 4.16 Convolution of 3PA theory for GaAs (x2.5) shown in Fig. 4.12 convolved with a Gaussian spectrum with a half width 1/e2 value of 50nm (red), 100nm (blue), and 200nm (green) illustrating the blurring effect a large bandwidth could have.

The 3PA spectral data of GaAs measured via Z-scan is as shown in Fig. 4.17. The magnitude of the absorption measured is similar to the values previously published and consistent with the values predicted by theory scaled by a factor of 2.5, but the spectral shape and structure predicted is not observed. The spectrum measured drops near 2.5μm and flattens at 2.55μm where the peak is expected then drops again as expected near 2.6μm at the edge of the 3PA absorption. Since the 3PA theory has already been confirmed in this work in two other Zinc Blende semiconductors it seems likely there was some problem with the experimental data at the longer wavelengths. This problem is identified by measuring the pulse spectrum which is larger than expected and prevents resolving any sharper features of the spectrum. A nonlinear convolution of the pulse spectrum with the absorption spectrum shows the blurring effect of using a pulse with too much bandwidth.

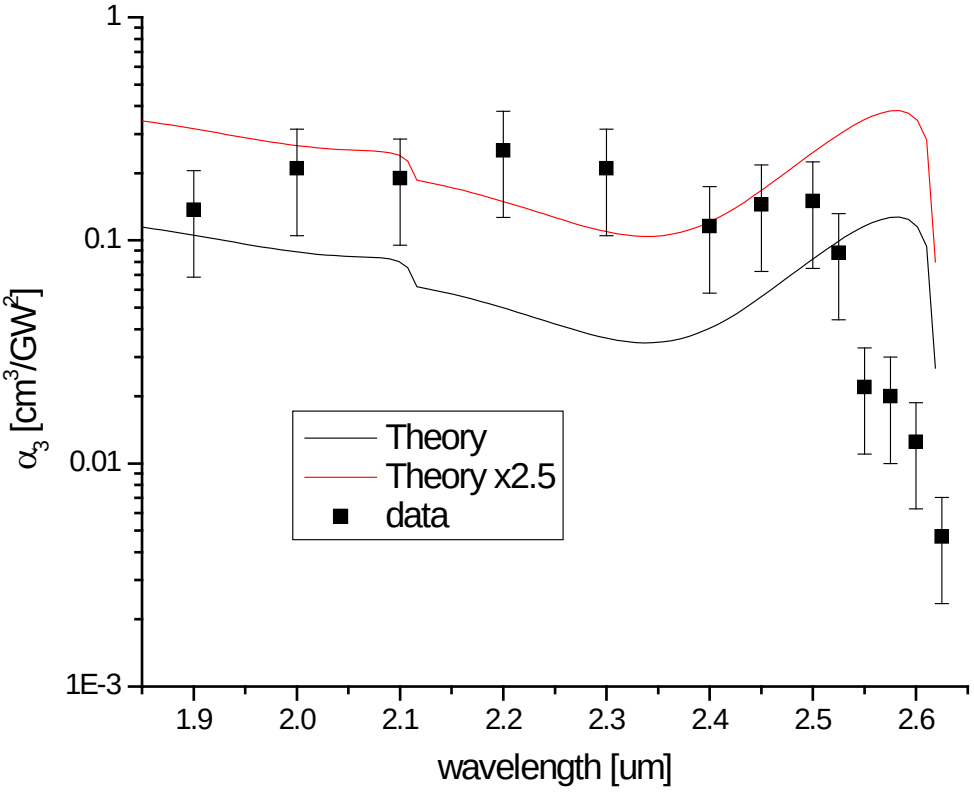

Figure 4.17 Z-scan results measured for 3PA in GaAs [squares] compared to the four band theory (black solid line) and the same theory scaled by a factor of 2.5 (red solid line).

4.6. Chapter Summary

Previous to this work the theoretical 3PA band gap and spectral scaling had not been satisfactorily confirmed and conflicting results existed in the literature. In this work 3PA was measured in ten semiconductors confirming the expected band gap scaling of E_g^{-7} as predicted by the simple two band theories of both Wherrett and Brandi & de Araujo. Using K_3=25eV$^{11/2}$cm^3/GW^2 gives agreement within a factor of two for most data; however, the values

obtained for the narrow gap materials are different than the theoretically estimated values by an order of magnitude. Extrapolation of the theory to InSb at 10K predicts 18,000 cm^3/GW^2 using K_3=25.1 $eV^{11/2}cm^3/GW^2$ and the measured value is 30,000 cm^3/GW^2 using a free carrier cross section of 40 x 10^{-16} cm^2. To the best of the authors' knowledge this work includes the first published experimental values for 3PA in bulk ZnSe, ZnTe, and CdTe.

For ZnS, ZnSe, the spectral dependence of the 3PA was measured and compared to existing theory showing a need for a different theoretical approach and as a result a 4-band theory was subsequently developed that explained the shape of 3PA spectrum [15]. The measured 3PA spectra for ZnS, ZnSe, confirms this new theory. The spectrum of GaAs was also measured but the unexpectedly large spectral width of the source was shown to be problematic to resolving the predicted spectral structure. Since the spectrum of the source was measured for each wavelength used in the experiment, a convolution of the data with the theory is performed; however, a more convincing conclusion could be made by measuring the 3PA spectrum of GaAs with a narrower bandwidth source.

Chapter References

1 J.H. Yee, “Three-photon absorption in semiconductors,” Phys. Rev. B, **5**, 449 (1972).

2 H.S. Brandi and C.B. de Araujo, “Multiphoton absorption coefficients in solids: a universal curve,” J. Phys. C, **16**, 5925-5936 (1983).

3 B.S. Wherrett, “Scaling rules for multiphoton interband absorption in semiconductors,” JOSAB **1**, 67 (1984).

4 E.W. Van Stryland, M.A. Woodall, H. Vanherzeele, and M. J. Soileau, “Energy band-gap dependence of two-photon absorption,” Opt. Lett., **10**, 490 (1985).

5 M. Sheik-bahaei, P. Mukherjee, H. Kwok, “Two-photon and three-photon absorption coefficients of InSb,” JOSAB **3**, 379 (1985).

6 M.A. Woodall, “Nonlinear absorption techniques and measurements in semiconductors,” North Texas State University Dissertation, Ch.4 pg.138 (1985).

7 M. Sheik-Bahae, A. A. Said, T.-H. Wei, D. J. Hagan, and E. W. Van Stryland, “Sensitive measurement of optical nonlinearities using a single beam,” IEEE J. Quantum Electron., **26**, 760 (1990).

8 W.C. Hurlbut, Y.-S. Lee, K. L. Vodopyanov, P. S. Kuo, and M. M. Fejer, “Multiphoton absorption and nonlinear refraction of GaAs in the mid-infrared,” Opt. Lett., **32**, 668 (2007).

9 M.P. Hasselbeck, A.A. Said, E.W. Van Stryland, M. Sheik-Bahae, “Three-photon absorption in InAs,” Opt. Quant. Electron., **30**, 193-200, (1998).

10 J. He, Y. Qu, H. Li, J. Mi, and W. Ji, “Three-photon absorption in ZnO and ZnS crystals,” Opt. Exp., **13**, 9235, (2005).

11 J.U. Kang, A. Villeneuve, M. Sheik-Bahae, G.I. Stegeman, K. Al-hemyari, J. Stewart Aitchison, C.N. Ironside, “Limitation due to three-photon absorption on the useful spectral range for nonlinear optics in AlGaAs below half band gap,” A.P.L., **65**, 147, (1994).

12 G.M. Schucan, R.G. Ispansoiu, A.M. Fox, J.F. Ryan, “ Ultrafast Two-Photon Nonlinearities in CdSe Near 1.5μm Studied by Interferometric Autocorrelation”, IEEE J.Q.E., **34**, 1374, (1998).

13 M.P. Hasselbeck, E.W. Van Stryland, M. Sheik-Bahae, “ Dynamic band unblocking and leakage two-photon absorption in InSb,” Phys. Rev. B, **56**, 7395, (1997).

14 P.D. Olszak, S. Webster, L. A. Padilha, C.M. Cirloganu, M. Woodall, D.J. Hagan, E.W. Van Stryland, “Energy band-gap dependence of three-photon absorption in semiconductors,” in *Nonlinear Optics: Materials, Fundamentals and Applications*, Topical Meeting (CD) (Optical Society of America, 2007), paper WC5.

15 Cirloganu, C.M., et al., “Three-photon absorption spectra of zinc blende semiconductors: theory and experiment.” Optics Letters, 2008. **33**(22): p. 2626-2628.

CHAPTER 5. CONCLUSION

5.1. Summary

In this work the temperature and spectral dependence of nonlinear absorption and recombination in InSb were investigated along with three-photon absorption in a series of semiconductors. Two-photon absorption and free carrier absorption in InSb have been the topic of research for many years, yet a study of the full 2PA spectrum at room temperature had not yet been presented, nor had the temperature dependence of 2PA been thoroughly investigated. Temperature dependent 2PA and FCA spectra of InSb were measured a combination of tunable ~160 femtosecond, ~10 picosecond, and ~150 nanosecond IR sources along with a cryostat for controlling the sample temperature to vary the band gap energy from 0.165 eV to 0.235 eV.

Measurements over a wide range of pulse widths gave results consistent with a recent theoretical model and the results for 2PA are also consistent with the band gap scaling (E_g^{-3}) as predicted by a simple two parabolic band model. The measured 2PA absorption spectrum agreed well with the spectral shape predicted by both theories for thermal variation (80 to 300 K) at fixed wavelengths and for spectral variation (8 to 12 μm) at fixed temperatures. Using 150 nanosecond pulses from a CO_2 laser required the recombination rates to be included for modeling the nonlinear transmittance experiments. The observation of a temperature dependence of the FCA as recently predicted is important in our analysis. By taking this into account, we found a quantitative agreement for the nonlinear response.

FCA cross section values are confirmed through modeling of 1PA, 2PA, and 3PA data. In order to obtain a consistent analysis of the 2PA spectra for nanosecond pulse widths, it is

necessary to consider that the FCA cross section as temperature dependent. FCA cross section values were measured at and above 200 K through 1PA via temperature controlled FTIR measurements and temperature controlled linear transmittance measurements of picosecond pulses. This along with FCA values used for the entire temperature range (80 K to 300 K) to fit picosecond Z-scans and nanosecond nonlinear transmittance measurements confirm that the FCA cross section is temperature dependent. Recombination rates are included for modeling nanosecond data and it is found through modeling this data that these rates change with sample temperature.

Three-photon absorption (coefficient of 0.025 cm^3/GW^2 at a wavelength of 12 μm) was also observed in InSb past the 2PA band edge at 80 K using picosecond pulses where 2PA is not allowed due to energy conservation. Confirmation of band gap and spectral scaling predicted by existing theories for 3PA had not yet been demonstrated satisfactorily. Also, there was disagreement between the theoretical results generated by different models in the published literature, primarily in the spectral behavior. This made useful comparison of 3PA data for InSb to the available theoretical models difficult. By studying three-photon absorption in a large range of band gaps, existing theories can be tested and properly extrapolated to InSb for comparison to experimental results. Therefore, the band gap and wavelength scaling of 3PA was studied in several semiconductors by the Z-scan technique. To the best of the authors' knowledge this work includes the first reported experimental values for 3PA in bulk ZnSe, ZnTe, and CdTe. Three photon absorption was also shown to be an accurate method of determining the band gap and sometimes the split off energy.

In this work 3PA was measured in ten semiconductors confirming the expected band gap scaling of E_g^{-7} as predicted by the simple two band theories of both Wherrett and Brandi & de Araujo. Using K_3=25 $eV^{11/2}cm^3/GW^2$ gave agreement within a factor of two for most data; however, the values obtained for the narrow gap materials are different than the theoretically estimated values by almost an order of magnitude. Extrapolation of the theory to InSb at 10K predicts 18,000 cm^3/GW^2 using K_3=25.1 $eV^{11/2}cm^3/GW^2$ and the measured value is 6x larger.

For ZnS and ZnSe, the spectral dependence of the 3PA was measured and compared to existing theory showing a need for a different theoretical approach. Claudiu Cirloganu in our group then calculated the degenerate 3PA spectrum of ZnSe using third-order perturbation theory based on a Kane 4-band structure consisting of three valence bands (heavy-hole, light-hole, and split-off) and a conduction band This model for zincblende structures accounts for the non-parabolicity of the bands and non-zone-center wave functions. Our experimental 3PA results for ZnSe matched the measured spectral shape although the predicted values were a factor of 3.2 smaller than the experimental data for ZnSe. The measured 3PA spectra for ZnS, was also compared to and found to agree well with a recently published theory based on a four band model. The spectrum of GaAs was also measured but the unexpectedly large spectral width of the source was shown to be problematic for resolving the predicted spectral structure Our theoretical value for InSb at 80 K using E_g=0.228 eV is $\alpha_3 \approx 0.012$ cm^3/MW^2 at 12 μm which is approximately a factor of 2 smaller than the experimental value.

5.2. Future Work

A complete model including laser heating requires accurate knowledge of the temperature dependent coefficients. Having confirmed recently published models for the temperature dependence of 2PA and FCA in InSb the carrier recombination processes are still in need of further research. Samples with various doping levels could be used in a temperature controlled pump probe experiment to study the carrier recombination rates and separately study the different Auger rates. Radiative recombination should be studied further using samples of various thicknesses through detecting the lifetime of photoluminescence and this should also be done in a temperature controlled experiment. Carrier diffusion should also be included in the model as it becomes important for longer pulses.

The 2PA and 3PA spectrum of other semiconductors of interest should be measured. The 3PA spectrum of GaAs should be remeasured with a tunable bandpass filter as suggested in Ch.4. Nonlinear absorption in GaAs, GaSb, InAs and other infrared materials should also be investigated using the same approach demonstrated in this work with InSb. Using temperature controlled experiments with tunable sources of various pulse widths would be useful in determining the nonlinear absorption parameters of these and other semiconductors

Another area of interest is measuring and modeling the nonlinear transmittance of ternary semiconductors such as InGaSb or InGaAs. By understanding the binary semiconductors first and studying how the material properties vary by mixture it is possible to engineer a semiconductor to have the optical properties that are desirable for a particular application. As was discussed in the introduction of this work, the properties desired for an optical limiter are high linear transmittance, high damage threshold, and large nonlinear loss through absorption,

refraction, or scattering. Future work should therefore be directed at both understanding the optical properties of specific materials like InSb or GaAs and also at developing materials or combinations of materials with the optical qualities required for devices.

In conclusion to this work, the author suggests a novel approach where a thick semiconductor limiter is used in a graded density modality by employing the thermal dependence of the nonlinear absorption. In other words, the graded density can be achieved through a thermal gradient within the limiter. It therefore becomes important to first fully characterize both the spectral dependence of the nonlinear absorption and its temperature dependence so that such a device could be designed and optimized. This work reports such a characterization for thin sample InSb; however, an effective model must be developed and tested for thick samples as well.

APPENDIX A: MATHCAD Z-SCAN MODEL FOR 3PA

Input Parameters:

FWHM to HW/e

$\lambda := 2600 \times 10^{-9}$ Wavelength [m] -

$wo := 22 \times 10^{-6}$ Beam size at the focus hw1/e2 [m] -

$2\sqrt{\ln(2)} = 1.665E+000$

$Energy := 208 \times 10^{-9}$ Energy per pulse [J] -

FWHM to HW/e^2

$to := \frac{160}{1.6651} \times 10^{-15}$ Laser pulse width HW1/e [s] -

$2 \times \sqrt{\ln(\sqrt{2})} = 1.177E+000$

$L := .4 \times 10^{-3}$ Sample thickness [m] -

$n := 3.3$ Refractive index -

$trans := .999$ linear transmittance

$\gamma := 2.1 \times 10^{-4}$ 3PA coefficient [cm^3/GW^2]

Data :=

$to = 9.609E-014$

$Tnorm := 1.000$ $Z\_Offset := -0.05$

Importing Data:

$N := rows(Data)$

$i := 1..N - 1$

$z_i := Data_{i,0}$

$Tdata_i := Data_{i,1}$

$z_1 = -4.950E+000$ $z_{10} = -4.500E+000$ $z_{21} = -3.950E+000$

$Tdata_1 = 9.950E-001$ $Tdata_{10} = 9.955E-001$ $Tdata_{21} = 9.952E-001$

Calculated parameters:

$z0 := \frac{\pi \times wo^2 \times 10^3}{\lambda}$ z0 = 5.848E-001 Rayleigh range [mm]

$\alpha := \frac{-\ln(trans)}{L}$ Input_Energy := Energy

$Leff := \frac{1 - e^{-\alpha \times L}}{\alpha}$ $Leff \times 10^3 = 0.3998$ Effective length [mm]

$R := \left(\frac{n-1}{n+1}\right)^2$ R = 2.861E-001 Reflectance

$I0 := \frac{2Energy}{\pi \times \sqrt{\pi} \times wo^2 \times to} \times (1 - R)$ Irradiance := $I0 \times 10^{-13}$

Irradiance = 1.147E+002 Effective Irradiance $[\frac{GW}{cm^2}]$

$\gamma 1 := \frac{\gamma \times 100^{-3}}{10^{18}}$ $\gamma 1 = 2.100E-028$

$In_i := \frac{I0}{1 + \frac{(z_i)^2}{z0^2}}$

$A_i := \frac{\gamma 1 \times (In_i)^2 \times \pi \times \left(1 - e^{-2 \times \alpha \times L}\right)}{\alpha}$

$c3_i := \sqrt{\frac{\gamma 1}{\alpha}} \times In_i \times \sqrt{1 - e^{-2 \times \alpha \times L}}$

$Tfit0_i := \frac{\int_0^1 \frac{\ln\left[c3_i \times x + \sqrt{(c3_i \times x)^2 + 1}\right]}{x \times \sqrt{-\ln(x)}} dx}{\sqrt{A_i}}$

$Tfit_i := \frac{Tfit0_i}{Tfit2(z10)}$

Normalization to 20 Zo:

$z10 := 20 \times z0$

$In2(z10) := \frac{I0}{1 + \frac{z10^2}{z0^2}}$

$A2(z10) := \frac{\gamma 1 \times In2(z10)^2 \times \pi \times \left(1 - e^{-2 \times \alpha \times L}\right)}{\alpha}$

$c32(z10) := \sqrt{\frac{\gamma 1}{\alpha}} \times In2(z10) \times \sqrt{1 - e^{-2 \times \alpha \times L}}$

$Tfit2(z10) := \frac{\int_0^1 \frac{\ln\left[c32(z10) \times x + \sqrt{(c32(z10) \times x)^2 + 1}\right]}{x \times \sqrt{-\ln(x)}} dx}{\sqrt{A2(z10)}}$

Tfit2(z10) = 1.000E+000

$Norm\_Data_i := \frac{Tdata_i}{Tnorm}$ $OffsetZ_i := Z\_Offset + z_i$

OutputData0 := augment(z, Tfit, OffsetZ, Norm_Data) r1 := rows(OutputData0) − 1

OutputData := submatrix(OutputData0, 1, r1, 0, 3) $minTrans := \min\left(OutputData^{\langle 1 \rangle}\right)$

APPENDIX B: FREE CARRIER POPULATION CALCULATION

InSb

$Egap(Temp) := 0.235 - \frac{6\cdot10^{-4}\cdot Temp^2}{Temp + 500}$ $Egap(300) = 0.167$

$Eg := 0.167\cdot\left(1.609\cdot10^{-19}\right)J$ $Temp := 300K$ $\lambda g := \frac{h\cdot c}{Eg}$ $h := 6.6260755\cdot10^{-34}J\cdot s$

$mv := 0.43\cdot m0$ $Ev := 0$ $m0 := 9.109\cdot10^{-31}kg$

$mc := 0.014\cdot m0$ $Ec := Eg$ $\lambda g = 7.393\times10^{-6}m$ $kB := 1.380658\cdot10^{-23}\frac{J}{K}$

$$Nc := 2\cdot\left[\frac{mc\cdot kB\cdot Temp}{2\cdot\pi\cdot\left(\frac{h}{2\cdot\pi}\right)^2}\right]^{\frac{3}{2}} \qquad Nv := 2\cdot\left[\frac{mv\cdot kB\cdot Temp}{2\cdot\pi\cdot\left(\frac{h}{2\cdot\pi}\right)^2}\right]^{\frac{3}{2}}$$

$Nc = 4.157\times10^{22}m^{-3}$

$Nv = 7.075\times10^{24}m^{-3}$

$$nB(EF) := Nc\cdot e^{\left(\frac{EF-Ec}{kB\cdot Temp}\right)} \qquad pB(EF) := Nv\cdot e^{\left(\frac{Ev-EF}{kB\cdot Temp}\right)} \qquad niB := \sqrt{Nc\cdot Nv}\cdot e^{\left(\frac{-Eg}{2\cdot kB\cdot Temp}\right)}$$

$nB(0.89589Eg) = 2.116\times10^{22}m^{-3}$ $niB = 2.116\times10^{22}m^{-3}$ $\frac{niB}{Nc} = 0.509$

$$F12n(EF) := \left[e^{-\frac{EF-Ec}{kB\cdot Temp}} + \frac{3}{4}\cdot\sqrt{\pi}\cdot\left[\left(\frac{EF-Ec}{kB\cdot Temp}\right)^4 + 50 + 33.6\cdot\frac{EF-Ec}{kB\cdot Temp}\cdot\left[1-0.68\cdot e^{-0.17\cdot\left(\frac{EF-Ec}{kB\cdot Temp}+1\right)^2}\right]\right]^{-\frac{3}{8}}\right]^{-1}$$

$$F12p(EF) := \left[e^{-\frac{Ev-EF}{kB\cdot Temp}} + \frac{3}{4}\cdot\sqrt{\pi}\cdot\left[\left(\frac{Ev-EF}{kB\cdot Temp}\right)^4 + 50 + 33.6\cdot\frac{Ev-EF}{kB\cdot Temp}\cdot\left[1-0.68\cdot e^{-0.17\cdot\left(\frac{Ev-EF}{kB\cdot Temp}+1\right)^2}\right]\right]^{-\frac{3}{8}}\right]^{-1}$$

$n(EF) := Nc\cdot F12n(EF)$ $p(EF) := Nv\cdot F12p(EF)$

$n(0.9086Eg) = 1.949\times10^{22}m^{-3}$ $p(0.9086Eg) = 1.949\times10^{22}m^{-3}$

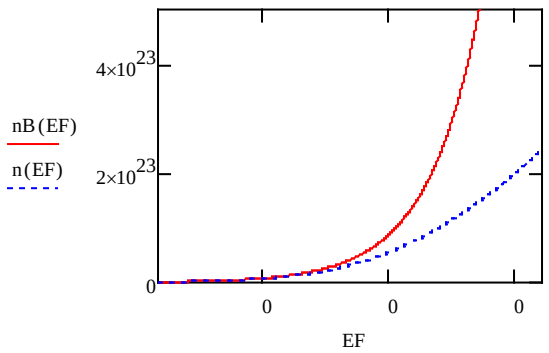

EF-Eg [-100 to100 meV]

$error := \frac{nB(0.89589Eg) - n(0.9086Eg)}{n(0.9086Eg)}$

$error = 0.085$

$error := \frac{pB(0.89589Eg) - p(0.9086Eg)}{p(0.9086Eg)}$

$error = 0.086$

APPENDIX C: MODEL FOR 2PA AND FCA Z-SCAN

```
%   Scott Webster - 6-27-2006 ver1
%
%   This program models thin sample open apeture Z-scan with ESA (or FCA)
%   accessed by 2PA and/or 3PA.   Saturable absorption can be added by
%   replacing alpha in dIdz with Homogeneous and Inhomogeneous broadening
%   terms.  Program assumes temporal and spatial guassian distributions.

tic
clear all
clear global variable
format short
format compact
delete temporal.txt
%************************ Input Parameters
************************************************


Energy=1.3*20*10^-9;                %Energy in Joules
lambda=8*10^-6;                 %Wavelength in meters
wo=120*10^-6;                    %Spot size radius in meters - HW/e^2
to=6*10^-12;                    %Temporal width in seconds - HW/e
L=0.65*10^-3;                      %Sample length in meters
n=1.4;                          %Linear index of refraction of material
LinTrans=.501;                    %Linear transmittance at wavelength

beta=2.5*10^-8;                  %2PA in m/W
sigma_ex=8.073*10^-20;                %2PA accessed excited state cross section
m^2
tau=143*10^-9;                       %Lifetime of 2PA excited state
N0=1.588*10^22;                    %1/m^3
Caug=0*2*10^-38;
gamma=0*0.12*10^-18;                 %3PA in m/W

%Isat=1*10^12                       %W/m^2

Zpoints=50;                         %Number of Zscan positions
ZscanMinMax=50;                    %Zscan position min and max in mm

Rpoints=50;                        %Number of spatial slices ********min 50
Tpoints=50;                        %Number of temporal slices********min 50
Spoints=50;                        %Number of sample slices  ********min 50

Nr=3;                              %width of spatial to integrate over - (Nr*wo)
Nt=3;                              %width of temporal to integrate over -
(Nr*to)

File_name_in=['InSb650um ps 8um 26nJ.txt'];     %Input Filename to be modeled
```

```
%************************** Initialization and
Calculations*********************************

Zo=((pi*wo^2)/lambda)*10^3;                          %Rayliegh range in mm
alpha=-log(LinTrans)/L;                              %Alpha from linear
transmittance
R=((n-1)/(n+1))^2;                                   %Fresnel reflection from
front surface of sample
eV=1239.842*10^-9/lambda;                            %Conversion of nm to eV
eV_to_J=1.60219*10^-19;                              %Conversion of eV to J

Data_in=load(File_name_in);                                  %Loads
experimental data
zdata=Data_in(:,1);                                          %Experimental
data Z-scan position
Tdata=Data_in(:,2);                                          %Experimental
data Transmittance
zmodel=[-ZscanMinMax:2*ZscanMinMax/(Zpoints):ZscanMinMax]'; %Creates Zscan
positions used in model
zmodel(1)=-20*Zo;                                            %Replaces first
value of zmodel with value very far from focus for Normalization
NZ=length(zmodel);                                           %Length of zmodel

File_name_out=strrep(File_name_in, '.txt', '-fit.txt');
delete(strrep(File_name_in, '.txt', '-fit.txt'));

%%%%%%%%%%%%%%%%%%%%%%%%%%%%
t_length=Nt*to;                                  %Length of time to integrate
over
tx=[-t_length:t_length/(Tpoints/2):t_length]';   %Time vector
ty=exp(-(tx./to).^2);                            %Input temporal pulse
distribution (HW/e)
NT=size(tx);                                     %Number of elements in time
vector
temporal=[tx,ty];
save temporal.txt temporal -ASCII -append



Sample_Length=[0:L/Spoints:L]';                  %Sample position vector
NL=length(Sample_Length);                        %Number of elements in
position vector

dt=abs(tx(1)-tx(2));                            %Width of time slice
dz=abs(Sample_Length(2)-Sample_Length(1));       %Width of sample slice

%************************************************************************
********************
%Calculate I(r,t,z)
Zscan_fit=zeros(NZ,2);                       %Initialization of Zscan position
vs. Transmittance
```

```
Trans=zeros(NZ);
for i=[1:NZ]                                %Loop for Zscan positions
    wz=wo.*(1.+(zmodel(i)./Zo).^2).^(1/2);      %Beam waist at Zscan
positions

    r_length=Nr*wz;                         %Length in space to integrate wz
over
    rx=[0:r_length/(Rpoints/2):r_length]';  %Space vector
    ry=exp(-2.*(rx./wo).^2);                %Input spatial pulse distribution
    NR=size(rx);                            %Number of elements in space
vector

    Fluence_r_x=zeros(NR);                  %Initialization of Fluence vector
(x-axis)
    Fluence_r_y1=zeros(NR);                 %Initialization of Fluence vector
with NLA (y-axis)
    Fluence_r_y2=zeros(NR);                 %Initialization of Fluence vector
without NLA (y-axis)

    for j=[1:NR]                            %Loop for spatial slices

        Output_Irradiance_t_x=zeros(NT);    %Initialization of Irradiance
vector (x-axis)
        Output_Irradiance_t_y1=zeros(NT);   %Initialization of Irradiance
vector with NLA (y-axis)
        Output_Irradiance_t_y2=zeros(NT);   %Initialization of Irradiance
vector without NLA (y-axis)

        Nsum=zeros(NL+1);                   %Initialization of Population
vector corresponding to sample slices

        for k=[1:NT]                        %Loop for temporal slices

            Irradiance=zeros(NL);
%Initialization of Irradiance vector (y-axis)
            Irradiance(1)=((2.*Energy.*(1.-
R)./(pi.^(3./2).*wz.^2.*to)).*ry(j).*ty(k); %Irradiance at each temporal and
spatial position

            for LL=[1:NL]



                %Homogeneous broadening -> -
(alpha*Irradiance(LL))/(1+Irradiance(LL)/Isat)
                %Inhomogeneous broadening -> -
(alpha*Irradiance(LL))/sqrt((1+Irradiance(LL)/Isat))

                dIdz(LL)=(-alpha*Irradiance(LL)-beta*Irradiance(LL)^2-
gamma*Irradiance(LL)^3-sigma_ex*Nsum(LL)*Irradiance(LL))*dz;
```

```
                Irradiance(LL+1)=Irradiance(LL)+dIdz(LL);   %Stores
Irradiance after each sample slice to update dNdt


A=((beta*Irradiance(LL)^2)/(2*eV*eV_to_J)+(gamma*Irradiance(LL)^3)/(3*eV*eV_t
o_J));
                dN=(A-Nsum(LL)/tau-Caug*Nsum(LL)^3)*dt;
                Nsum(LL)=dN+Nsum(LL);



            end

            Output_Irradiance_t_x(k)=tx(k);             %Stores position in
time for Irradiance
            Output_Irradiance_t_y1(k)=Irradiance(NL+1);   %Stores Irradiance
after dIdz and dNdt
            Output_Irradiance_t_y2(k)=Irradiance(1);    %Stores Input
Irradiance

        end

        Fluence_r_x(j)=rx(j);
%Stores spatial position for Fluence
        Fluence_r_y1(j)=trapz(Output_Irradiance_t_x,Output_Irradiance_t_y1);
%Integrates Irradiance with NLA to give Fluence
        Fluence_r_y2(j)=trapz(Output_Irradiance_t_x,Output_Irradiance_t_y2);
%Integrates Irradiance without NLA to give input Fluence

    end

    Energy_out=trapz(Fluence_r_x,Fluence_r_y1.*Fluence_r_x)*2*pi;
%Integrates Fluence with NLA to give Energy
    Energy_in=trapz(Fluence_r_x,Fluence_r_y2.*Fluence_r_x)*2*pi;
%Integrates Fluence without NLA to give input Energy

    Trans(i)=Energy_out/Energy_in;
%Transmittance
    Zscan_fit(i,1)=zmodel(i);
    Zscan_fit(i,2)=Trans(i)/Trans(1);

    percent_done=i/NZ*100

end
Zscan_fit(1,1)=Zscan_fit(2,1);
Zscan_fit(1,2)=Zscan_fit(2,2);
```

```
plot(Zscan_fit(:,1),Zscan_fit(:,2),'-b')
xlabel('Z-scan Position (mm)')
ylabel('Normalized Transmittance')
title(File_name_in,'FontSize',12)
hold on
plot(zdata,Tdata,'or')

save(File_name_out, 'Zscan_fit', '-ASCII', '-append', '-double')

alpha_ex=N0*sigma_ex*(100)^2

beep
toc
```

APPENDIX D: EXCITON ENHANCEMENT FACTOR CALCULATION

exciton binding energy $Eb := 0.00057$

band gap energy $Eg := 0.115, 0.116 .. 0.235$

photon energy $Ev := 0.11709$

$$X(Eg) := \left(\frac{Eb}{2Ev - Eg}\right)^{\frac{1}{2}} \qquad Y(Eg) := \left(\frac{Eb}{Eg - Ev}\right)^{\frac{1}{2}} \qquad \alpha(Eg) := \frac{Ev}{Eg}$$

$$J(Eg) := 2 \cdot Y(Eg)^2 \cdot \int_0^1 \frac{t \cdot \left(\frac{1+t}{1-t}\right)^{Y(Eg)}}{\left[1 + \left(\frac{t \cdot Y(Eg)}{X(Eg)}\right)^2\right]^2} \, t$$

exciton enhancement factor $$gex(Eg) := \left[\left(1 + X(Eg)^2\right) \cdot \frac{\pi \cdot X(Eg) \cdot e^{\pi X(Eg)}}{\sinh(\pi \cdot X(Eg))}\right] \cdot \left(\frac{Ev}{Eb} \cdot J(Eg)\right)^2$$

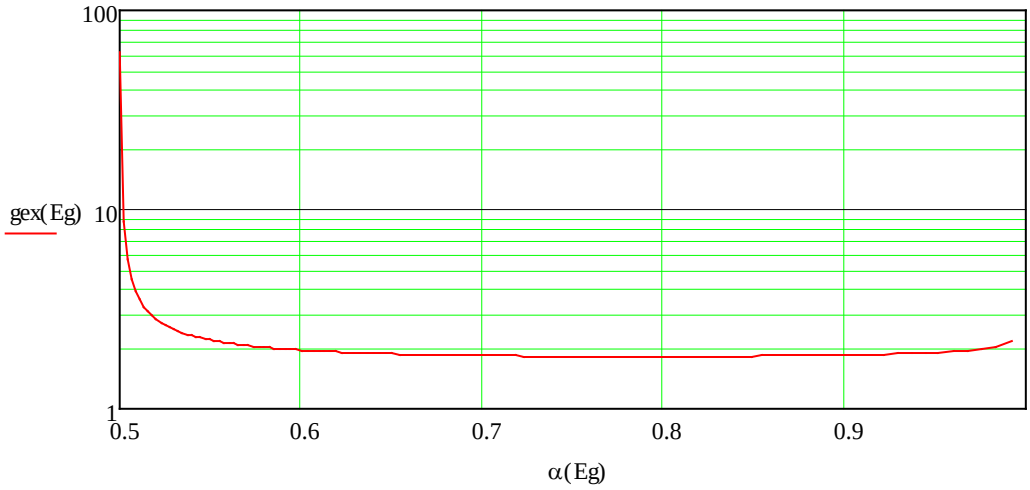

APPENDIX E: NONLINEAR TRANSMITTANCE MODEL

```
%   Scott Webster - 6-16-06 ver1
%   modified by Peter Olszak 08-06
%   This program models thin sample open apeture Z-scan with ESA (or FCA)
%   accessed by 2PA and/or 3PA.   Saturable absorption can be added by
%   replacing alpha in dIdz with Homogeneous and Inhomogeneous broadening
%   terms.  Program assumes temporal and spatial guassian distributions.

tic
clear all
clear global variable
format short
format compact

%************************ Input Parameters
%************************************************
lambda=10.59*10^-6;              %Wavelength in meters
wo=180*10^-6;                    %Spot size radius in meters - HW/e^2
% to = User defined below        %Temporal width in meters - HW/e
L=.55*10^-3;                     %Sample length in meters
n=1.33;                          %Linear index of refraction of material
%LinTrans=0.4;                  %Linear transmittance at wavelength
Isat=1000*10^10;                 %Saturation Intensity W/m^2
beta=0.0*10^-8;                  %2PA in m/W
sigma_ex=32*10^-20;               %2PA accessed excited state cross section
m^2
tau=143*10^-9;                   %Lifetime of 2PA excited state
C_Auger=10*10^-38;                %Auger recombination
No=3.183*10^15;                  %Number of initial carriers
gamma=12.*10^-18;                %3PA in m^3/W^2

OLpoints=20;                     %Number of OL Energies
OLminE=1*10^-6;                  %Starting Energy for OL
OLmaxE=1*10^-3;                 %Ending Energy for OL

Rpoints=200;                      %Number of spatial slices
Spoints=200;                      %Number of sample slices
Nr=3;                            %width of spatial to integrate over -
(Nr*wo)
Nt=3;                            %width of temporal to integrate over -
(Nr*to)

File_name_in=['InSb_10K_12_12_2006.txt'];      %Input Filename to be modeled
Temporal_in=['temporal_Dec112006.txt'];    %Input temporal profile to fit
with .txt
%************************** Initialization and
Calculations*********************************

Zo=((pi*wo^2)/lambda)*10^3;                          %Rayliegh range in mm
%No=-log(LinTrans)/(sigma_ex*L);
```

```
%alpha=-log(LinTrans)/L;                                  %Alpha from linear
transmittance
R=((n-1)/(n+1))^2;                                       %Fresnel reflection from
front surface of sample
eV=1239.842*10^-9/lambda;                                %Conversion of nm to eV
eV_to_J=1.60219*10^-19;                                  %Conversion of eV to J

Data_in=load(File_name_in);                                      %Loads
experimental data
Edata=Data_in(:,1);                                              %Experimental
data Input Energies
Tdata=Data_in(:,2);                                              %Experimental
data Transmittance

%OLmodel=[OLminE:OLmaxE/(OLpoints):OLmaxE]';                 %Creates
Energies used in model
%OLmodel=Edata;

OLmodel(1)=OLmaxE*10^-6;                                         %Replaces first
value of OLmodel with very small Energy for Normalization
OLmodel(2)=3*OLmaxE*10^-6;
OLmodel(3)=7*OLmaxE*10^-6;
OLmodel(4)=OLmaxE*10^-5;
OLmodel(5)=3*OLmaxE*10^-5;
OLmodel(6)=7*OLmaxE*10^-5;
OLmodel(7)=OLmaxE*10^-4;
OLmodel(8)=3*OLmaxE*10^-4;
OLmodel(9)=7*OLmaxE*10^-4;
OLmodel(10)=1*OLmaxE*10^-3;
OLmodel(11)=3*OLmaxE*10^-3;
OLmodel(12)=7*OLmaxE*10^-3;
OLmodel(13)=OLmaxE*10^-2;
OLmodel(14)=3*OLmaxE*10^-2;
OLmodel(15)=7*OLmaxE*10^-2;
OLmodel(16)=OLmaxE*10^-1;
OLmodel(17)=3*OLmaxE*10^-1;
OLmodel(18)=5*OLmaxE*10^-1;
OLmodel(19)=7*OLmaxE*10^-1;
OLmodel(20)=OLmaxE;

NE=length(OLmodel);                                              %Length of zmodel
File_name_out_Energy=strrep(File_name_in, '.txt', '-  -Energy-fit.txt');
delete(strrep(File_name_in, '.txt', '-  -Energy-fit.txt'));

File_name_out_Fluence=strrep(File_name_in, '.txt', '-  -Fluence-fit.txt');
delete(strrep(File_name_in, '.txt', '-  -Fluence-fit.txt'));

File_name_out_Irradiance=strrep(File_name_in, '.txt', '-  -Irradiance-
fit.txt');
delete(strrep(File_name_in, '.txt', '-  -Irradiance-fit.txt'));
```

```
%%%%%%%%%%%%%%%%%%%%%%%%%%%%%
T_in=load(Temporal_in);                                  %Loads temporal profile
tx=T_in(:,1);                                            %Experimental data
Input Energies
ty0=T_in(:,2);                                           %Experimental data
Transmittance

%t_length=;

Norm=max(ty0);

ty=(1/Norm).*ty0;
Area_to=trapz(tx,ty);

temp=[tx,ty];
%save temporal.txt temp -ASCII
NT=size(tx);                                          %Number of elements in time
vector


Sample_Length=[0:L/Spoints:L]';                          %Sample position vector
NL=length(Sample_Length);                                %Number of elements in
position vector
dt=abs(tx(1)-tx(2));                                     %Width of time slice
dz=abs(Sample_Length(2)-Sample_Length(1));               %Width of sample slice

r_length=Nr*wo;                             %Length in space to integrate wz over
rx=[0:r_length/(Rpoints/2):r_length]';      %Space vector
ry=exp(-2.*(rx./wo).^2);                    %Input spatial pulse distribution

NR=size(rx);                                %Number of elements in space vector


%*************************************************************************
*********************
%Calculate I(r,t,z)
OL_fit=zeros(NE,3);                          %Initialization of OL energies vs.
Transmittance
Trans=zeros(NE);
for i=[1:NE]                                    %Loop for Input Energies

    Fluence_r_x=zeros(NR);                      %Initialization of Fluence vector
(x-axis)
    Fluence_r_y1=zeros(NR);                     %Initialization of Fluence vector
with NLA (y-axis)
    Fluence_r_y2=zeros(NR);                     %Initialization of Fluence vector
without NLA (y-axis)

    for j=[1:NR]                                %Loop for spatial slices
```

```
        Output_Irradiance_t_x=zeros(NT);    %Initialization of Irradiance
vector (x-axis)
        Output_Irradiance_t_y1=zeros(NT);   %Initialization of Irradiance
vector with NLA (y-axis)
        Output_Irradiance_t_y2=zeros(NT);   %Initialization of Irradiance
vector without NLA (y-axis)

        Nsum=zeros(NL+1);                   %Initialization of Population
vector corresponding to sample slices

        for k=[1:NT]                        %Loop for temporal slices
            %k
            Irradiance=zeros(NL);
%Initialization of Irradiance vector (y-axis)
            Irradiance(1)=((2.*OLmodel(i).*(1.-
R))./(pi.*wo.^2.*Area_to)).*ry(j).*ty(k); %Irradiance at each temporal and
spatial position

            for LL=[1:NL]
%Loop for sample slices

                %dIdz(LL)=(-alpha*Irradiance(LL)-beta*Irradiance(LL)^2-
gamma*Irradiance(LL)^3-sigma_ex*Nsum(LL)*Irradiance(LL))*dz';
                dIdz(LL)=(-
sigma_ex*No*Irradiance(LL)/(sqrt(1+(Irradiance(LL)/Isat)))-
beta*Irradiance(LL)^2-gamma*Irradiance(LL)^3-
sigma_ex*Nsum(LL)*Irradiance(LL)/(sqrt(1+(Irradiance(LL)/Isat))))*dz';
                Irradiance(LL+1)=Irradiance(LL)+dIdz(LL);   %Stores
Irradiance after each sample slice to update dNdt
                %popdensity=[OLmodel(i),rx(j),tx(k),Nsum(NL)]
                %save popdensity.txt popdensity -ASCII -append
                %C_Auger*Nsum(LL)*(No+Nsum(LL))*(2*No+Nsum(LL))


A=((beta*Irradiance(LL)^2)/(2*eV*eV_to_J))+((gamma*Irradiance(LL)^3)/(3*eV*eV
_to_J));
                dN=((A-Nsum(LL)/tau)-
C_Auger*(Nsum(LL))*(Nsum(LL)+No)*(Nsum(LL)+2*No))*dt;
                Nsum(LL)=dN+Nsum(LL);
                Carrier_Population=Nsum(LL)

            end

            Output_Irradiance_t_x(k)=tx(k);             %Stores position in
time for Irradiance
            Output_Irradiance_t_y1(k)=Irradiance(NL);   %Stores Irradiance
after dIdz and dNdt
            Output_Irradiance_t_y2(k)=Irradiance(1);    %Stores Input
Irradiance
```

```
            %photo_carrier_density=Nsum(LL)
        end

        Fluence_r_x(j)=rx(j);
%Stores spatial position for Fluence
        Fluence_r_y1(j)=trapz(Output_Irradiance_t_x,Output_Irradiance_t_y1);
%Integrates Irradiance with NLA to give Fluence
        Fluence_r_y2(j)=trapz(Output_Irradiance_t_x,Output_Irradiance_t_y2);
%Integrates Irradiance without NLA to give input Fluence

    end

    Energy_out=trapz(Fluence_r_x,Fluence_r_y1.*Fluence_r_x)*2*pi;
%Integrates Fluence with NLA to give Energy
    Energy_in=trapz(Fluence_r_x,Fluence_r_y2.*Fluence_r_x)*2*pi;
%Integrates Fluence without NLA to give input Energy

    %Energy_out/OLmodel(i)

    Trans(i)=Energy_out/Energy_in;          %Transmittance
    %Trans2(i)=Energy_out/Edata
    OL_fit(i,1)=OLmodel(i);
    OL_fit(i,2)=Trans(i)/Trans(1);

    percent_done=i/NE*100


end

%%%%%%%%%%%%%%%%%%%%%%%%%%%%%%%%%%%%%%%%%%%%%%%%%%%%%%%%%%%%%%%%%%%%%%%%%%%
%Plot Input Energy vs. Normalized Transmittance

OL_fit(1,1)=OL_fit(2,1);
OL_fit(1,2)=OL_fit(2,2);
OL_fit(:,3)=OL_fit(:,1).*OL_fit(:,2);

subplot(2,2,1,'replace');semilogx(OL_fit(:,1),OL_fit(:,2),'-b')
xlabel('Input Energy (J)')
ylabel('Normalized Transmittance')
title(File_name_in,'FontSize',12)
hold on
subplot(2,2,1);semilogx(Edata,Tdata,'or')

%%%%%%%%%%%%%%%%%%%%%%%%%%%%%%%%%%%%%%%%%%%%%%%%%%%%%%%%%%%%%%%%%%%%%%%%%%%
%Input vs. Output Energy

Output_Data=Edata.*Tdata;
subplot(2,2,2,'replace');loglog(OL_fit(:,1),OL_fit(:,3),'-b')
hold on
subplot(2,2,2);loglog(Edata,Output_Data,'or')
```

```
xlabel('Input Energy (J)')
ylabel('Output Energy')
title(File_name_in,'FontSize',12)

save(File_name_out_Energy, 'OL_fit', '-ASCII', '-append', '-double')


%%%%%%%%%%%%%%%%%%%%%%%%%%%%%%%%%%%%%%%%%%%%%%%%%%%%%%%%%%%%%%%%%%%%%%%%%%%%
% Fluence vs. Normalized Transmittance
OL_fit_Fluence=zeros(NE,2);
OL_fit_Fluence(:,1)=OL_fit(:,1).*(2/(pi*(wo)^2)/1000);
OL_fit_Fluence(:,2)=OL_fit(:,2);

subplot(2,2,3,'replace');semilogx(OL_fit_Fluence(:,1),OL_fit_Fluence(:,2),'-
b')
xlabel('Input Fluence (J/cm^2)')
ylabel('Normalized Transmittance')
hold on
subplot(2,2,3);semilogx(Edata.*(2/(pi*(wo)^2)/1000),Tdata,'or')

save(File_name_out_Fluence, 'OL_fit_Fluence', '-ASCII', '-append', '-double')


%%%%%%%%%%%%%%%%%%%%%%%%%%%%%%%%%%%%%%%%%%%%%%%%%%%%%%%%%%%%%%%%%%%%%%%%%%%%
%Irradiance vs. Transmittance

OL_fit_Irradiance=zeros(NE,2);
OL_fit_Irradiance(:,1)=OL_fit(:,1).*(2/(pi*(wo)^2*Area_to)/1000*10^-9);
OL_fit_Irradiance(:,2)=OL_fit(:,2);

subplot(2,2,4,'replace');semilogx(OL_fit_Irradiance(:,1),OL_fit_Irradiance(:,
2),'-b')
xlabel('Input Irradiance (GW/cm^2)')
ylabel('Normalized Transmittance')
hold on
subplot(2,2,4);semilogx(Edata.*(2/(pi*(wo)^2*Area_to)/1000*10^-9),Tdata,'or')

save(File_name_out_Irradiance, 'OL_fit_Irradiance', '-ASCII', '-append', '-
double')

 beep
toc
```

APPENDIX F: 3PA SPECTRUM CONVOLUTION

SpectralTheory :=

$N := \text{rows}(\text{SpectralTheory})$

$i := 1 .. N - 1$ $\quad N = 100$

$\lambda_i := \text{SpectralTheory}_{i,0}$ $\quad \alpha_i := (2.5\text{SpectralTheory})_{i,1}$

$a := 1$ $\quad b := 0.2$

$$g_i := a \cdot \left[\left[-2 \left(\frac{\lambda_i - 2.5}{b} \right)^2 \right] \right]^3$$

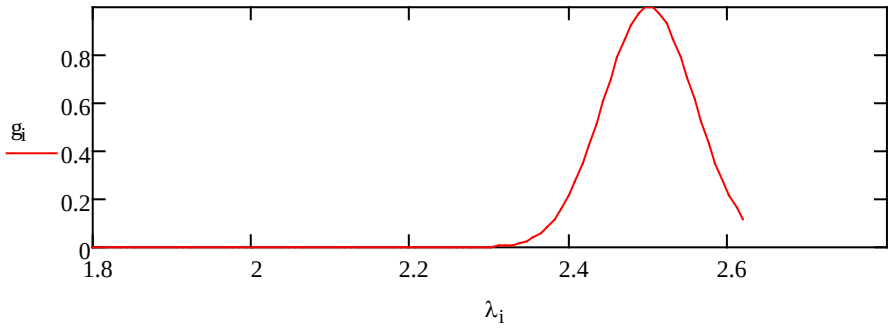

$$\text{Convolution}(a, b, x) := \sum_{i=1}^{N-1} \left[\alpha_i \cdot \left[\frac{a}{b \cdot \sqrt{\frac{\pi}{2}}} \cdot e^{\left[-2 \left(\frac{x - \lambda_i}{b} \right)^2 \right]} \right]^3 \right]$$